# Development and Applications of Fluoroalkyl End-capped Sulfobetaine-type Oligomeric Nanocomposites

Doctral Course
Graduate School of Materials Science and Technology
Hirosaki University

Doctoral Thesis

March 2014

Tetsushi Kijima

# Contents

## General Introduction

### 1. Fluorine and organofluorine compounds

The unique characteristics which fluorinated compounds possess are derived from the fact as follows: (1) Fluorine is the most electronegative of all the elements. The high electronegativity is conducive to high oxidation potential, high ionization energy and high electron affinity. (2) Fluorine has the second smallest atomic radius following hydrogen. (3) $F_2$ is the most reactive due to the very weak F-F bond (155 $kJmol^{-1}$) and can form the very strong bond with other atoms. For example, the strength of the carbon - fluorine bond (441 $kJmol^{-1}$) exceeds that of the carbon - hydrogen bond (414 $kJmol^{-1}$) as shown in Table 1. [1, 2] Such strength of bonds formed by fluorine gives the extraordinary thermal and oxidative stability to fluorinated compounds.

Table 1 Electronic properties of hydrogen, fluorine, chlorine and bromine

| | H | F | Cl | Br |
|---|---|---|---|---|
| Electronegativity (Pauling) | 2.1 | 4.0 | 3.0 | 2.8 |
| A van der Waals radius (Å) | 1.20 | 1.35 | 1.80 | 1.95 |
| Ionization energy (kJ/mol) | 1312 | 1681 | 1256 | 1142 |
| Electron affinity (kJ/mol) | 75 | 350 | 365 | 343 |
| Bond energies of X-X (kJ/mol) | 435 | 155 | 243 | 193 |
| Bond energies of C-X (kJ/mol) | 414 | 441 | 329 | 276 |
| Bond lengths of C-X (Å) | 1.100 | 1.271 | 1.767 | 1.937 |

Organofluorine compounds in particular plays a significant role in the field of medicinal chemistry. The small size of the fluorine substituent, combined with its high electronegativity gives the important biologically effects such as mimic effect, block effect and polarity effect. [2] Thus, the introduction of fluorine atoms and fluoroalkyl groups into organic molecules is very important from the developmental viewpoints of new functional materials.

## 2. Fluoropolymers

There have been a variety of technological applications in fluorinated organic polymers due to exhibiting distinctive properties such as high thermal and oxidative stability, low dielectric constant, low moisture absorption, low flammability, low surface energy, excellent biocompatibility, marked gas permeability and excellent resistance.[3] In these fluorinated organic polymers, poly(tetrafluoroethylene) [PTFE (Teflon$^{TR}$): -($CF_2$-$CF_2$)$_n$-] is the most widely used polymeric material owing to its extremely high thermal stability and chemical resistance. [4] Recent developments in the field of fluoropolymers serve to illustrate the distinctive role of fluorine in material science. CYTOP$^{TR}$ and Teflon$^{TR}$ AF (see Fig. 1) were developed as new amorphous fluorinated resins which play a crucial role in the production of new materials for microchip manufacture, microlithography and fiber optics. [5]

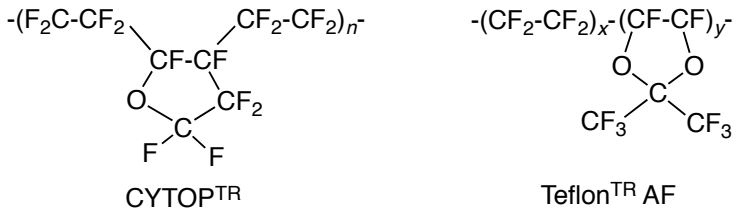


Fig. 1 Chemical structures of new amorphous fluorinated resins

It is well-known that perfluoropolymers such as PTFE exhibit excellent chemical and thermal stability, low surface energy and low refractive index and dielectric constant; however, these compounds, in general, exhibit extremely low solubility in organic solvents. [6] In contrast, it has been reported that cyclic fluoropolymers are soluble in some fluorinated solvents. [7] In fact, partially protonated ring containing fluoropolymers (see Fig. 2) have been reported as exhibiting a good solubility in polar aprotic solvent such as *N*,*N*-dimethylformamide (DMF), tetrahydrofuran (THF), acetone and acetonitrile, though such polymers were insoluble in benzene, chloroform and methanol. [8]

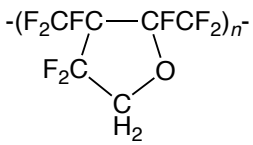


Fig. 2 Chemical structure of partially protonated fluoropolymers

On the other hand, acrylated and methacrylated polymers containing longer perfluoroalkyl

groups can exhibit the excellent properties imparted by fluorine, including their good solubility in fluorinated solvents and in polar solvents such as acetone and chloroform. However, these polymers are unstable under acidic or alkaline conditions since the perfluoroalkyl groups are introduced into such polymers through the ester or the amide bonds. [9]

In general, the introduction of perfluoroalkyl groups is not easy, because the usual synthetic methods for alkylation cannot be applied to the perfluoroalkylation due to the high electronegativity of perfluoroalkyl groups. [10] Hence, the development of efficient synthetic methodology for the direct introduction of perfluoroalkyl groups into polymeric materials has been deeply desirable. The exploration of fluoroalkylated polymeric compounds leading to relatively high solubility in both water and common organic solvents will open a new route to the development of the field of new functional fluorinated materials, in particular new fluorinated polysoaps.

**3. Fluoroalkylated surfactants**

In general, there has been a great interest in longer fluoroalkylated low molecular weight compounds containing hydrophilic groups such as carboxyl, sulfo and hydroxyl segments due

to exhibiting their good surface-active characteristics. [11] For example, it is well known that perfluorooctanesulfonic acid (PFOS) and perfluorooctanoic acid (PFOA) (see Fig. 3) possess the excellent surface-active properties, high thermal and chemical stability, and hydrophobic and lipophobic characteristics. [12]

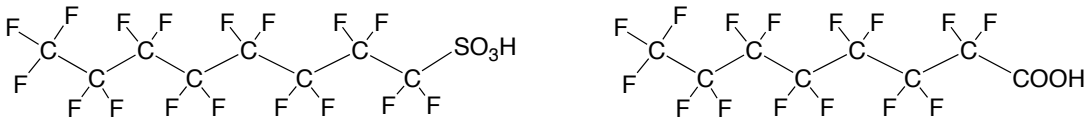


Perfluorooctane sulfonate [PFOS] Perfluorooctanoic acid [PFOA]

Fig. 3 Fluoroalkylated low molecular surfactants

These compounds have been widely used in commercial and industrial applications such as fire-fighting foams, soil- and stain-resistant coating for carpets and leather, lubricants, floor polishes, photographic film, denture cleaners, pharmaceuticals, and insecticides. [13] However, these fluorinated surfactants are toxic, resistant to degradation, persistent, and bioaccumulate in food chains because of the extremely stable perfluorinated chain. [12, 14] Thus, there have been a variety of reports on the synthesis of non-bioaccumulate fluorinated surfactants possessing a good surface-active characteristic which can be alternative to PFOA and PFOS as illustrated in Fig. 4. [15]


Fig. 4 Alternative fluorinated surfactants to PFOS and PFOA

On the other hand, polymeric surfactants (polysoaps) are well-known to possess a wide variety of unique properties such as high dispersibility and emulsion properties, which cannot be achieved by the low molecular weight surfactants.[16] However, polysoaps have in general a poor surface-active property, compared with that of the low molecular weight surfactants.[17] Therefore, it is in particular interest to introduce longer fluoroalkyl groups into these polysoaps from the developmental viewpoints of novel polysoaps possessing good surface-active properties. In fact, there have hitherto been numerous studies on the synthesis and surfactant properties of fluorinated polysoaps.[18, 19] These fluorinated polysoaps in general can be classified into three types such as randomly fluoroalkylated polysoaps, A-B block-type fluoroalkylated polysoaps, and A-B-A triblock-type fluoroalkyl end-capped polysoaps as shown in Fig. 5.[18, 19]

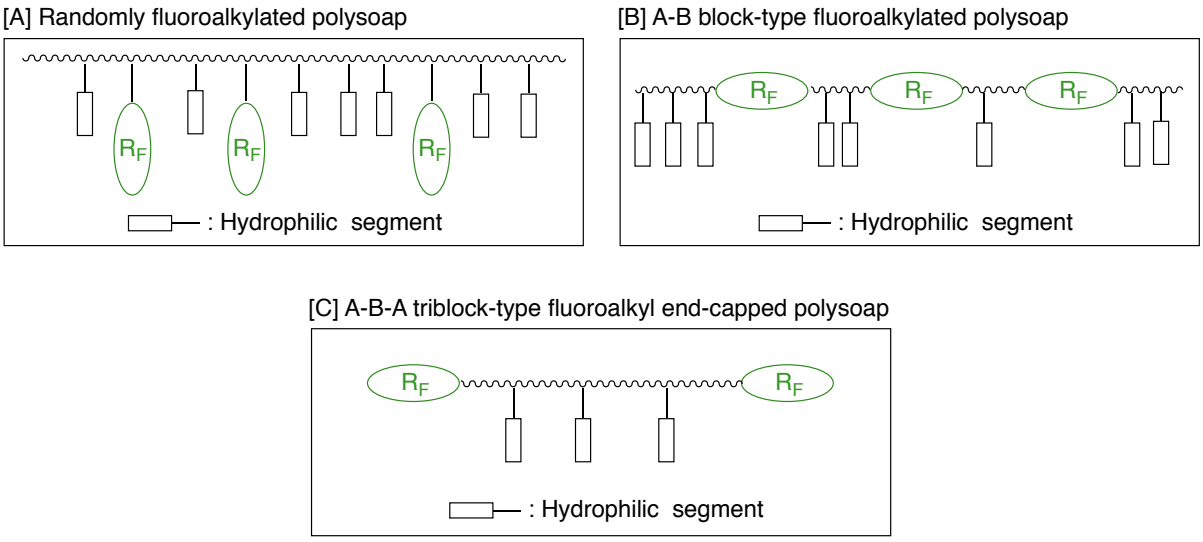


Fig. 5 Fluorinated polysoaps

In these fluorinated polysoaps, the syntheses and applications of randomly fluoroalkylated polysoaps have been studied in detail, so far. For example, Laschewsky et al. reported on the synthesis of fluorinated polysoaps in which fluoroalkyl segments have been randomly introduced into polymeric molecules as shown in Scheme 1. [19] However, in general, these fluorinated polysoaps possess a low solubility in various solvents and are not effective for reducing the surface tension of water effectively. [19]

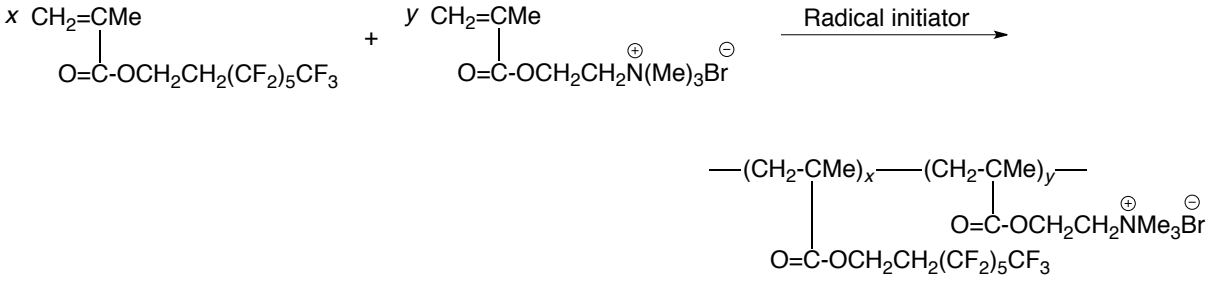


Scheme 1

This suggests that fluoroalkyl groups in these fluoroalkylated polysoaps are not likely to be arranged regularly above the water surface owing to the entanglement of fluoroalkyl groups in polysoaps as shown in Fig. 6.[19)]

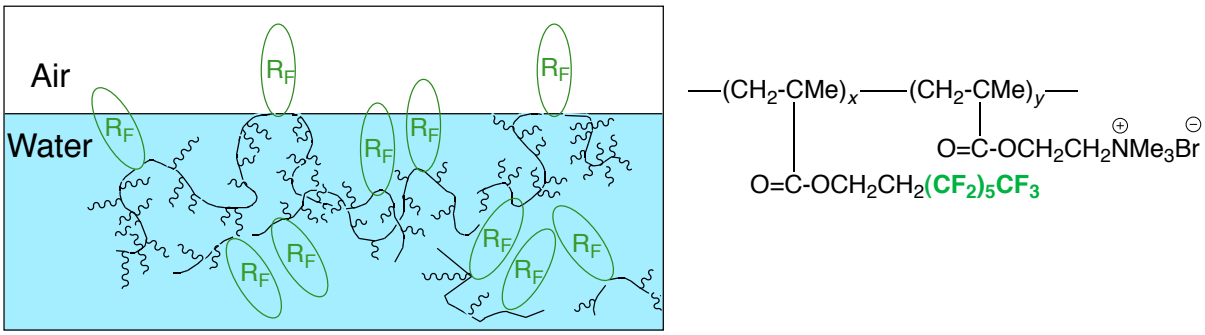


Fig. 6 Surface arrangements of randomly fluoroalkylated polysoaps in water

Therefore, it is very important to develop A-B block-type fluoroalkylated polysoaps possessing good stability and surface-active characteristic. In fact, acrylic acid oligomers containing perfluorooxaalkylene units as novel fluorinated A-B block-type polysoaps were prepared by using a fluorinated polymeric peroxide as shown in Scheme 2.[20, 21)]

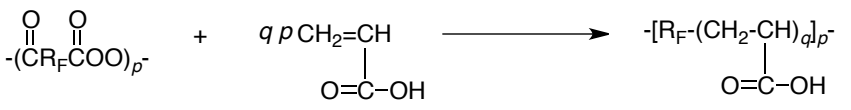


$R_F = -CF(CF_3)[OCF_2CF(CF_3)]_nO(CF_2)_5O\text{-}[CF(CF_3)CF_2O]_mCF(CF_3)-$ ;
$(n + m = 3)$

Scheme 2

In addition, as a new fluorinated polysoaps, A-B-A triblock-type fluoroalkyl end-capped acrylic acid oligomers have been already prepared by reaction of fluoroalkanoyl peroxide with acrylic acid via a radical process as shown in Scheme 3.

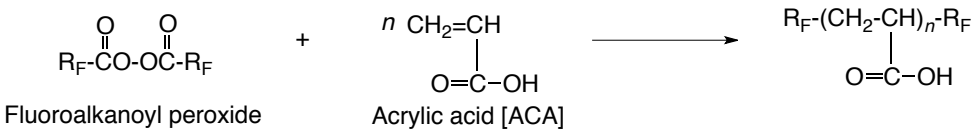


$R_F$ = $C_3F_7$, $C_6F_{13}$,
$CF(CF_3)[OCF_2CF(CF_3)]_mOC_3F_7$; $m$ = 0, 1, 2

Scheme 3

Mainly acrylic acid oligomers with two fluoroalkyl end groups are obtained by primary radical termination or radical chain transfer to the peroxide under the oligomeric conditions, in which the concentration of the peroxide was almost the same as that of acrylic acid as shown in Scheme 4. [22)]

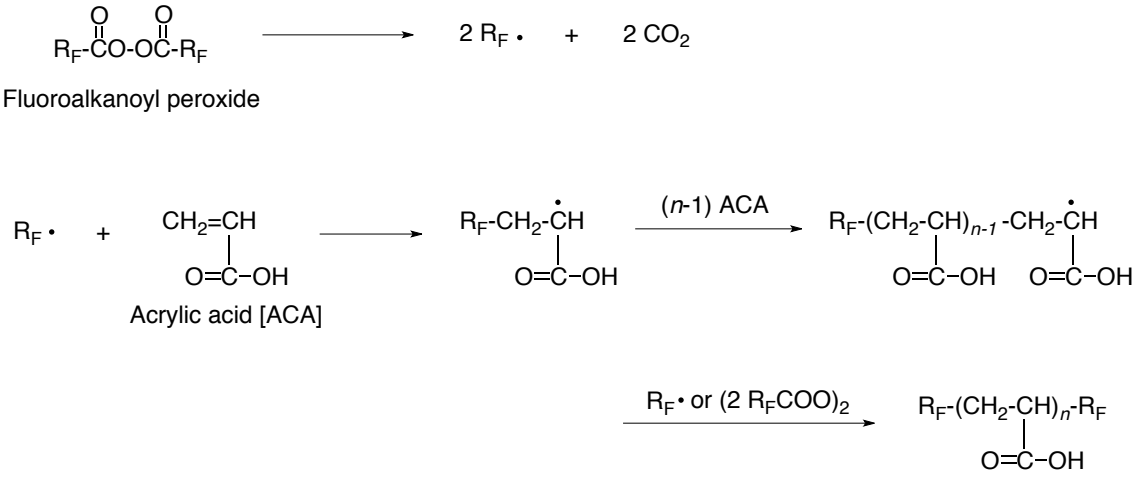


Scheme 4

A-B block-type fluorinated acrylic acid oligomers shown in Scheme 2 are effective for reducing the surface tension of water, compared with that of randomly fluoroalkylated polysoaps. [21] More interestingly, it was demonstrated that A-B-A triblock-type fluoroalkyl end-capped oligomers were more effective for reducing the surface tension of water, compared with that of A-B block-type fluoroalkylated polysoaps as illustrated in Fig. 7-(a) and -(b). [23]

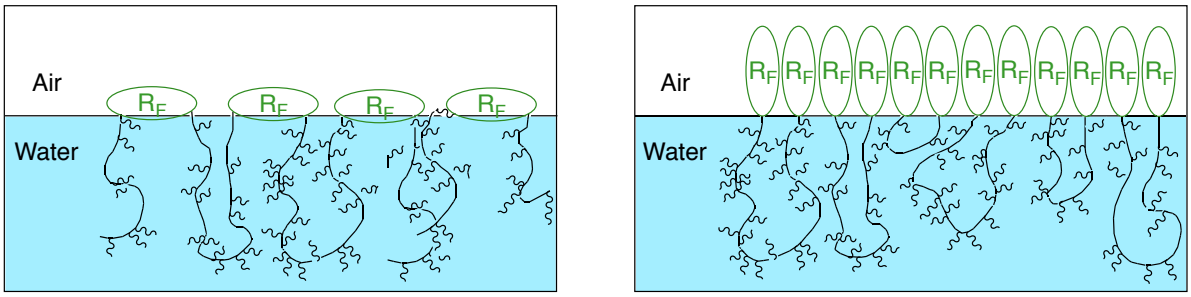


(a) $-[R_F-(CH_2-CH)_q]_p-$ with $O=C-OH$

(b) $R_F-(CH_2-CH)_n-R_F$ with $O=C-OH$

Fig. 7 Surface arrangements of A-B block-type fluoroalkylated polysoaps (a) and A-B-A triblock-type fluoroalkyl end-capped acrylic acid oligomers (b) in water

As shown in Fig. 7-(b), fluoroalkyl groups in fluoroalkyl end-capped oligomers are likely to be arranged regularly above the water surface, where all the fluoroalkyl groups are parallel to each other, quite similar to the general low molecular fluorinated surfactants. [23] In contrast, blocked fluoroalkyl groups are not likely to be arranged regularly above the water surface, compared with those of fluoroalkyl end-capped oligomers as shown in Fig. 7-(a). Thus,

fluoroalkyl end-capped acrylic acid oligomers are suggested to form the molecular assemblies in water. [23] Fluoroalkyl end-capped acrylic acid - vinyltrimethylsilane cooligomers, which were prepared by the reaction of fluoroalkanoyl peroxide with acrylic acid and vinyltrimethylsilane (see Scheme 5), could form the self-assembled molecular aggregates with the aggregations of terminal fluoroalkyl groups in cooligomers in aqueous and organic media as shown in Fig. 8. [24]

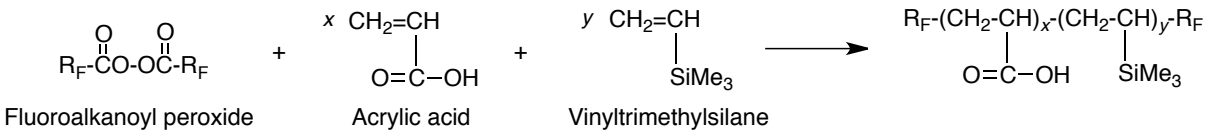


$R_F$ = $C_3F_7$,
$CF(CF_3)[(OCF_2CF(CF_3)]_mOC_3F_7$; $m$ = 0, 1, 2

Scheme 5

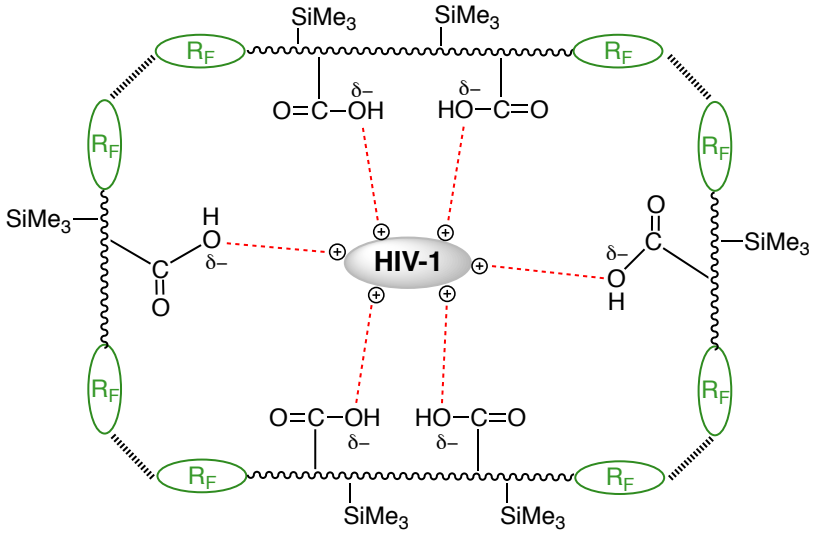


Fig. 8 Schematic illustration for the interaction of HIV-1 and the intermolecular aggregates of $R_F$-($CH_2$-$CHCO_2H$)$_x$-($CH_2$-$CHSiMe_3$)$_y$-$R_F$

In particular, these fluorinated molecular aggregates could interact with positively charged Human immunodeficiency virus type 1 (HIV-1) to exhibit a potent and selective anti-HIV-1 activity through the electrostatic interaction (see Fig. 8). [24] In this way, fluoroalkyl end-capped oligomers can exhibit various unique properties, which cannot be achieved by the corresponding randomly or A-B block-type fluoroalkylated polymers. [24]

## 4. Organic polymer/inorganic hybrid materials

Hitherto, considerable effort has been devoted to the design and controlled fabrication of nanostructured materials with a wide variety of unique properties, which can result from a function of nanoscale materials' size, composition and structure order. [25] Of these, organic polymeric nanoparticles have a higher potential for practical applications to a wide variety of fields such as nanocoatings, nanostructure-supported catalysts, and biomedical and pharmaceutical materials. [26] Surface modification and immobilization of inorganic particles by the use of organic polymers possessing some functional moieties is expected to improve the functionality of the parent particles. [27] Recently, there have been numerous studies on the nanometer size-controlled organic compound/inorganic particles hybrids which were

combined with organic polymer and inorganic particles such as $TiO_2$, ZnO, $SiO_2$, $Al_2O_3$, $Fe_3O_4$, Ag, Au, and Pd.[28 ~ 35] These hybrids can exhibit unique characteristics related to not only the organic compounds but also inorganic materials, and these hybrids are also expected to control their structures.[28 ~ 35] In these organic polymer/inorganic hybrid materials, for example, surface modification of silica nanoparticles by chemically bound-polymers is of great interest due to their potential applications in a variety of fields such as coatings, electronics, catalysts, optics and diagnosis.[36] In general, preparation of polymer grafted silica nanoparticles can be classified according to their preparative methods into the following:

a) Free radical polymerization (FRP)[37]

b) Cationic and anionic polymerization (CA and AP)[38]

c) Miniemulsion polymerization (MEP)[39]

d) Living radical polymerization (LRP) such as reversible addition-fragmentation chain transfer polymerization (RAFTP) with click reaction[40]

e) Nitroxide-mediated polymerization (NMP)[41]

f) Atom-transfer radical polymerization (ATRP)[42]

Inorganic nanoparticles are usually utilized as the cores of grafted polymers to combine the superior properties of the organic and inorganic materials. For example, silica nanoparticles containing methacryoyloxypropyl groups can copolymerize with styrene as a comonomer

catalyzed by potassium persulfate to afford polystyrene grafted silica nanoparticles as shown in Scheme 6. [39] Similarly, a diblock copolymer brush consisting of poly(methylmethacrylate)-*block*-poly(pentafluoropropyl acrylate) was prepared on a porous silica substrate. [43] Ober et al. reported the preparation of planar silicon oxide surface-grafted styrene-based diblock copolymer brushes bearing semifluorinated alkyl side groups by nitroxide-mediated controlled radical polymerization. [44]

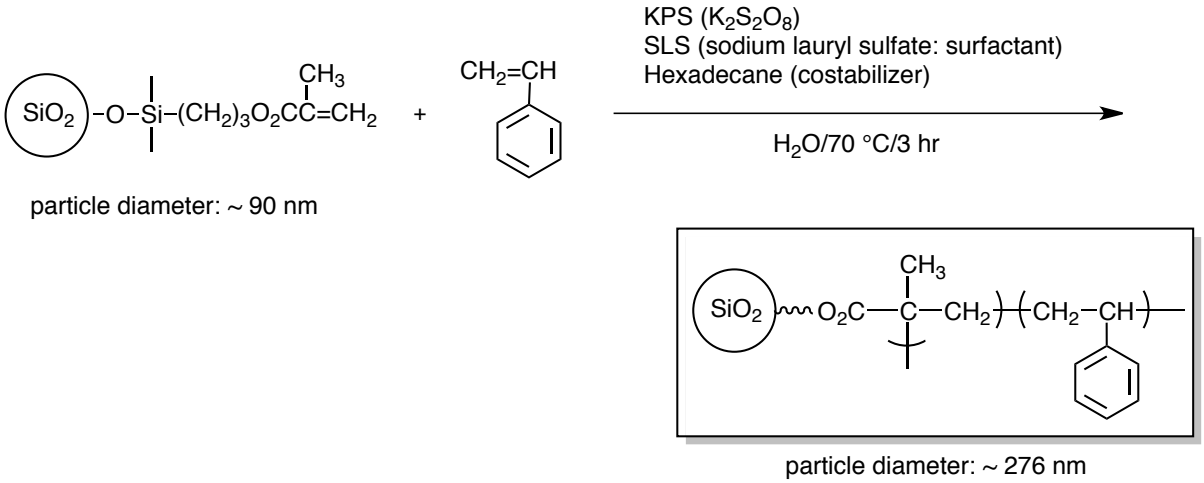


Scheme 6

Methacrylate polymer/$TiO_2$ particle hybrid was also prepared by emulsion polymerization of methacrylate monomer with titanate-modified $TiO_2$ in the presence of sodium dodecyl sulfate (SDS) as a surfactant as shown in Scheme 7. [28]

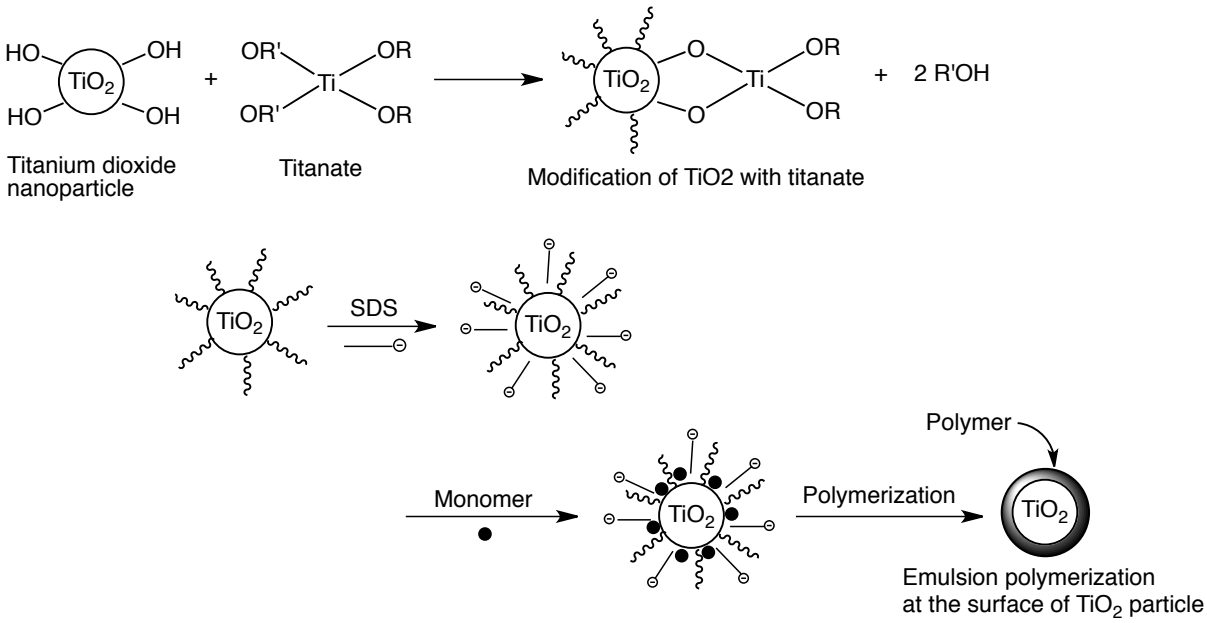


Scheme 7

Polymer-grafted magnetite nanoparticles have been already prepared through the surface-initiated nitroxide-mediated radical polymerization as shown in Scheme 8. [32)]

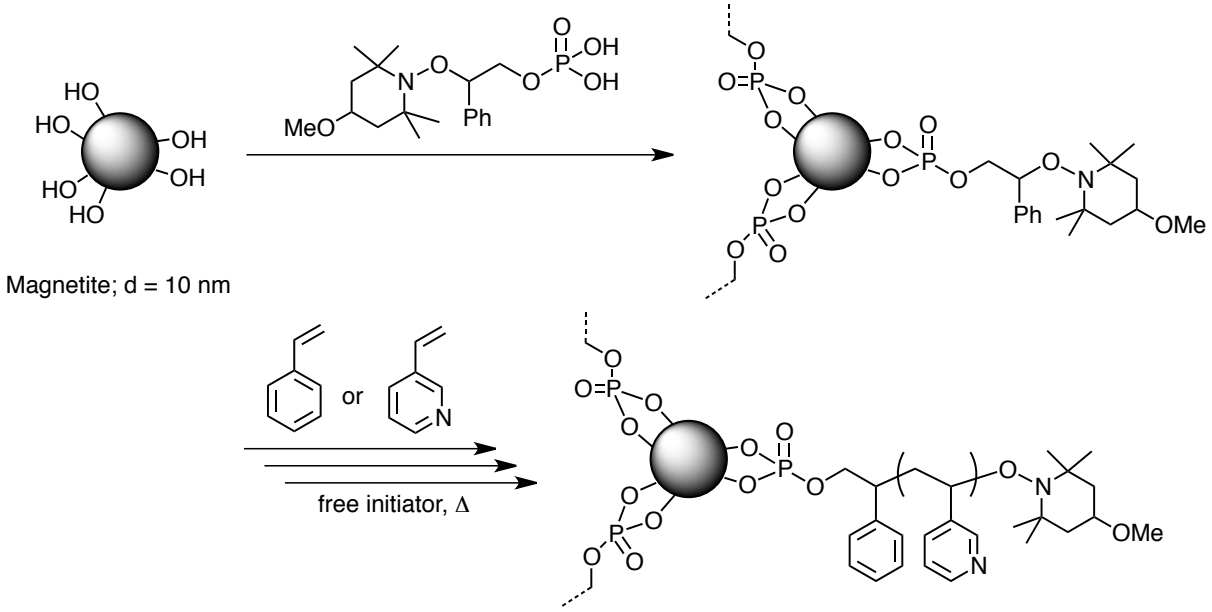


Scheme 8

In this way, the preparation of nanometer size-controlled organic polymer/inorganic hybrid materials is in particular interest from the developmental viewpoints of new functional materials.

## 5. Sulfonic acid group-containing materials

Sulfonic acid groups-containing polymers such as Nafion$^{TR}$ (see Fig. 9) have attracted much attention due to their applications in a wide variety of fields such as catalyst, hydrogel and fuel cell. [45 - 47)]

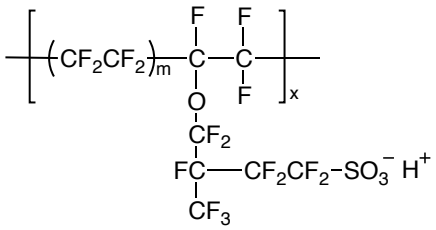

Nafion$^{TR}$

Fig. 9 Chemical structure of perfluorinated sulfonic acid resin

For example, as shown in Scheme 9, Kobayashi et al. reported on the preparation of sulfonic acid-functionalized polystyrene and their catalytic activity for the dehydration reaction of carboxylic acid with alcohol in water. [46)]

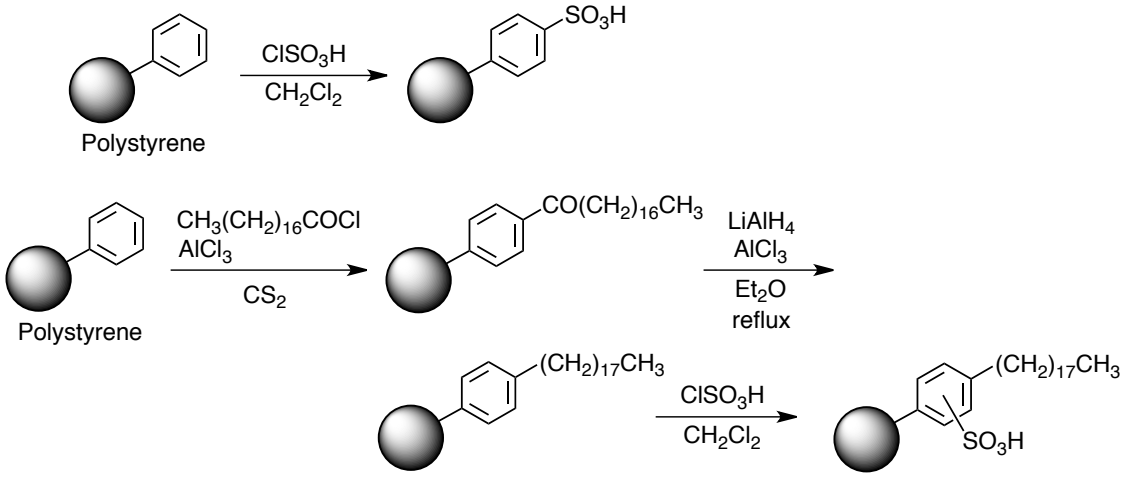


Scheme 9

Sulfonic acid-functionalized ordered nanoporous silica can be prepared by the sol-gel reaction of alkoxysilanes under alkaline conditions in the presence of cetyl trimethoxy ammonium bromide (CTAB) as shown in Scheme 10. [47)]

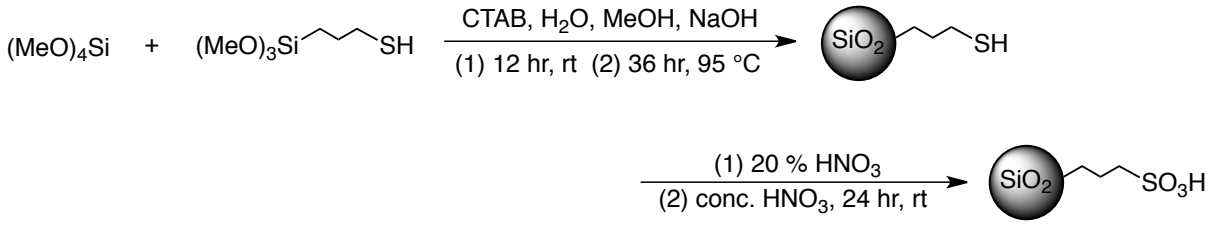


Scheme 10

However, studies on the fluorinated polymers containing sulfo groups have been hitherto very limited except for Nafion[TR], though there have been some reports on the preparation of

fluorinated polymeric materials possessing sulfo groups (see Scheme 11). [48)]

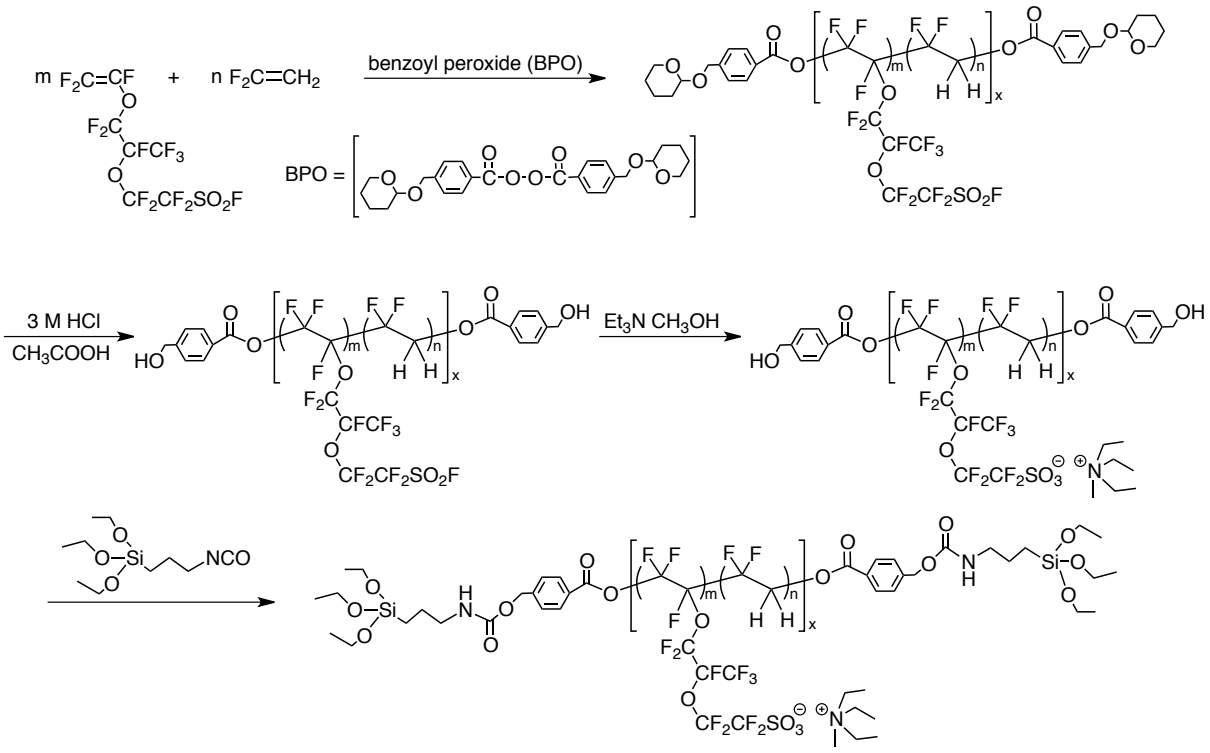


Scheme 11

Therfore, from the developmental viewpoints of novel fluorinated functional polymeric materials, it is of particular interest to study the fluorinated polymers-containing sulfo groups possessing not only a surface-active characteristic imparted by fluorine but also a unique property related to sulfonic acid moieties.

## 6. Thesis outline

As mentioned above, fluoroalkyl end-capped oligomers are attractive materials due to their various unique properties such as high solubility, surface-active properties, anti-HIV-1 activity and the ability to form the nanometer size-controlled self-assembled molecular aggregates, which cannot be achieved in the corresponding randomly fluoroalkylated polymers and fluoroalkylated block polymers. [24, 49] Thus, the preparation of fluoroalkyl end-capped oligomer/inorganic composites is in particular interest from the viewpoint of fabrication of new fluorinated functional materials. In fact, various fluoroalkyl end-capped oligomers/inorganic nanocomposites (Au, Ag, Cu and $SiO_2$) have been already prepared to exhibit a variety of unique characteristics. [50]

In these fluoroalkyl end-capped oligomers, fluoroalkyl end-capped sulfobetaine-type oligomers are in particular interest, due to exhibiting quite different characteristics such as a biological activity and a gelling ability from the other fluoroalkyl end-capped oligomers. [51] Therefore, from the developmental view point of new fluorinated functional materials, it is very important to develop fluoroalkyl end-capped sulfobetaine-type oligomeric nanocomposite-encapsulated not only inorganic nanoparticles but also low molecular organic compounds possessing a variety of functional units such as carbonyl groups.

In this study, preparation and applications of fluoroalkyl end-capped sulfobetaine-type oligomeric nanocomposites-encapsulated not only inorganic nanoparticles such as magnetic nanoparticles and palladium nanoparticles but also low molecular weight ketones such as acetone and acetophenones. In chapter 1, selective preparation and applications of fluoroalkyl end-capped sulfobetaine-type cooligomeric nanocomposites-encapsulated magnetitic nanoparticles are described (see Scheme 12 and 13), in this study, preparation and applications of fluoroalkyl end-capped block isocyanate cooligomeric nanocomposites and described, for comparison.

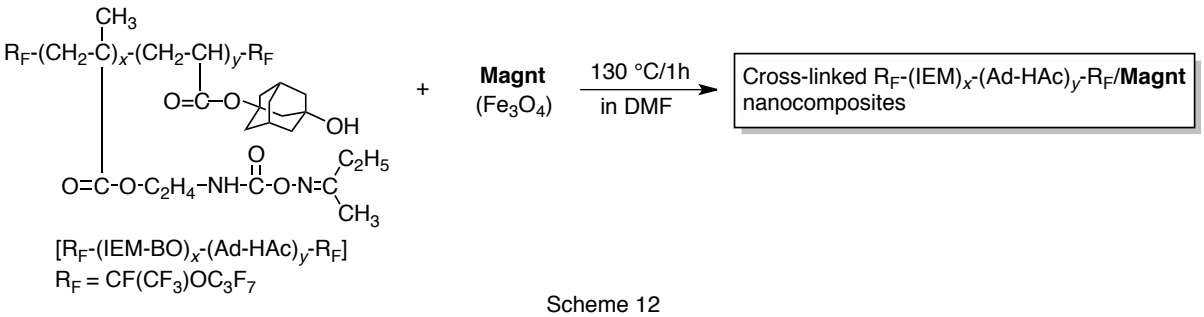


Scheme 12

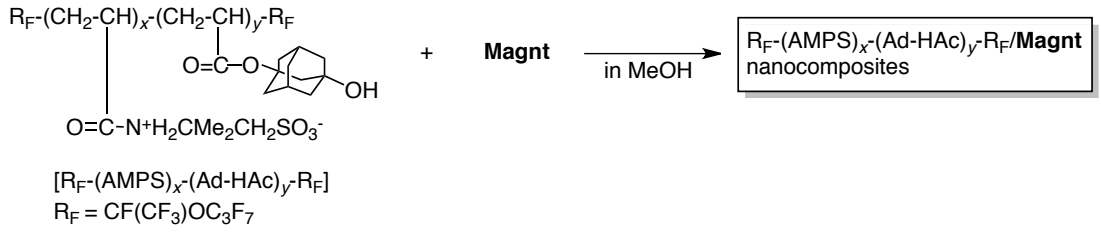


Scheme 13

In chapter 2, controlled immobilization of palladium nanoparticles in two different fluorinated

polymeric aggregate cores is described (see Scheme 14 and 15), and applications to the catalyst for Suzuki-Miyaura cross-coupling reaction are also described.

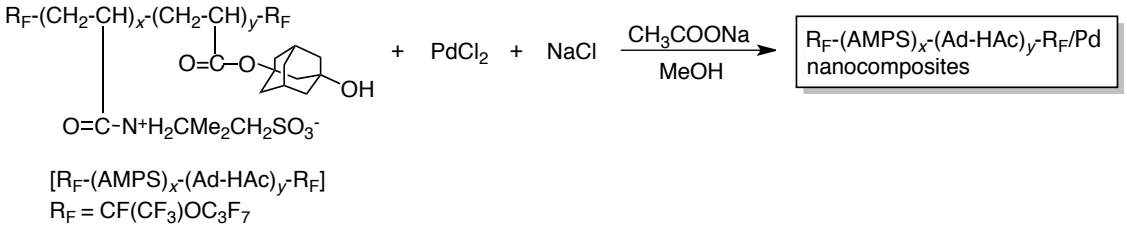


Scheme 14

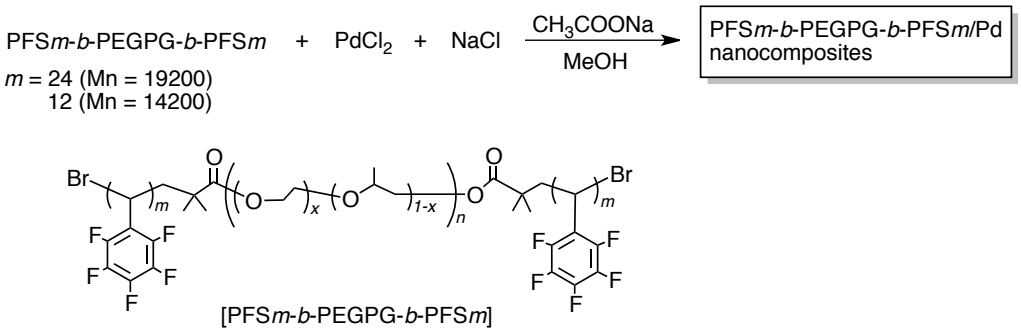


Scheme 15

In chapter 3, coloring-decoloring behavior of fluoroalkyl end-capped sulfobetaine-type oligomer/acetone composites in methanol is described. In chapter 4, homoaldol condensation of acetophenones in fluoroalkyl end-capped sulfobetaine-type oligomeric gel network cores is described.

**References**


1) L. Pauling, "*The Nature of the Chemical Bond and the Structure of Molecules and Crystals: An Introduction to Modern Structural Chemistry*", Cornell University Press, New York (1960).

2) W. R. Dolbier Jr., *J. Fluorine Chem.*, **126**, 157 (2005).

3) a) G. G. Hougham, P. E. Cassidy, K. Johns, and T. Davidson, Ed., "*Fluoropolymers 2: Properties*", Kluwer Academic/ Plenum Publishers, New York (1999);

b) K. M. Choi and J. W. Stansbury, *Chem. Mater.*, **8**, 2704 (1996);

c) E. T. Kang and Y. Zhang, *Adv. Mater.*, **12**, 1481 (2000).

4) a) K. Johns, and G. Stead, *J. Fluorine Chem.*, **104**, 5 (2000);

b) C. Rehwinkel, D. F. Gronarz, P. Fischer, R.-D. Hund, and V. Rossbach, *J. Fluorine Chem.*, **104**, 19 (2000).

5) M. Nakamura, *Kobunshi*, **38**, 364 (1989).

6) L.A.Wall, Ed., "*Fluoropolymers*", Wiley-Interscience, New York (1972).

7) a) N. Nakamura, T. Kawasaki, M. Unoki, K. Oharu, N.Sugiyama, I. Kaneko, and G. Kojima, *Prepr.1st Pacific Polym. Conf.*, Maui, HI, Dec. 369 (1989);

b) P. R. Resnick, *Polym, Prepr*., *Am. Chem. Soc., Div. Polym. Chem.*, **31**, 312 (1990).

8) Z.-Y. Yang, A. E. Feiring, and B. E. Smart, *J. Am. Chem. Soc.*, **116**, 4135 (1994).

9) S. Koizumi, A. Ohmori, T. Shimizu, and M. Iwatani, *Hyomen Kagaku*, **13**, 428 (1992).

10) H. Sawada, *Chem. Rev.*, **96**, 1779 (1996).

11) Y. Tanigawa, *Yukagaku*, **34**, 973 (1985).

12) E. Kissa, Ed., "*Fluorinated Surfactants and Repellents, 2nd ed.*", Marcel Dekker, Inc., New York (2001).

13) a) T. M. Boudreau, C. J. Wilson, W. J. Cheong, P. K. Sibley, S. A. Mabury, D. C. G. Muir, K. R. Solomon, *Environ. Toxicol. Chem.*, **22**, 2739 (2003);

b) R. Renner, *Environ. Sci. Technol.*, **35**, 154A (2001).

14) a) B. D. Key, R. D. Howell, and C. S. Criddle, *Environ. Sci. Technol.*, **31**, 2445 (1997);

b) B. D. Key, R. D. Howell, and C. S. Criddle, *Environ. Sci. Technol.*, **32**, 2283 (1998);

c) A. B. Lindstrom, M. J. Strynar, and E. L. Libelo, *Environ. Sci. Technol.*, **45**, 7954 (1998).

15) a) M. Peschka, T. Frömel, N. Fichtner, W. Hierse, M. Kleineidam, E. Montenegro, and T. P. Knepper, *J. Chromatogr. A*, **1187**, 79 (2008);

b) M. Peschka, N. Fichtner, W. Hierse, P. Kirsh, E. Montenegro, M. Seidel, R. D. Wilken, and T. P. Knepper, *Chemosphere*, **72**, 1534 (2008).

16) a) S. Liu and S. P. Armes, *Curr. Opin. Colloid Interface Sci.*, **6**, 249 (2001);

b) A. Elaissari, Ed., "*Colloidal Polymers:Synthesis and Characterization*", Marcel Dekker, Inc., New York (2003).

17) K. Holmberg, B. Jönsson, B. Kronberg, and B. Lindman, "*Surfactants and Polymers in Aqueous Solution*", John Wiley & Sons, Ltd. (2002).

18) a) I. J. Park, S.-B. Lee, C. K. Choi, and K.-J. Kim, *J. Colloid Interface Sci.*, **181**, 284 (1996);

b) I. J. Park, S.-B. Lee, and C. K. Choi, *J. Appl. Polym. Sci.*, **54**, 1449 (1994);

c) R. R. Thomas, D. R. Anton, W. F. Graham, M. J. Darmon, B. B. Sauer, K. M. Stika, and G. Swartzfager, *Macromolecules*, **30**, 2883 (1997);

d) T. Imae, *Curr. Opin. Colloid Interface Sci.*, **8**, 307 (2003).

19) a) P. Anton, O. Koberle, and A. Laschewsky, *Makromol. Chem.*, **194**, 1 (1993);

b) D. Cochin, P. Hendlinger, and A. Laschewsky, *Colloid Polym. Sci.*, **273**, 1138 (1995).

20) H. Sawada, E. Sumino, M. Oue, M. Mitani, H. Nakajima, M. Nishida, and Y. Moriya, *J. Chem. Soc., Chem. Commun.*, 143 (1994).

21) H. Sawada, E. Sumino, M. Oue, M. Baba, T. Kira, S. Shigeta, M. Mitani, H. Nakajima, M. Nishida, and Y. Moriya, *J. Fluorine Chem.*, **21**, 74 (1995).

22) H. Sawada, Y. Minoshima, and H. Nakajima, *J. Fluorine Chem.*, **65**, 169 (1993).

23) H. Sawada, Y.-F. Gong, Y. Minoshima, T. Matsumoto, M. Nakayama, M. Kosugi, and T.

Migita, *J. Chem. Soc., Chem. Commun.*, 537 (1992).

24) H. Sawada, *J. Fluorine Chem.*, 101, 315 (2000).

25) a) M. Zanetti, S. Lomakin, and G. Camino, *Macromol. Mater. Eng.*, **279**, 1 (2000);

b) P. M. Ajayan, L. S. Schadler, and P. V. Braun, "*Nanocomposite Science and Technology*", Wiley-VCH, Weinheim (2003);

c) P. Gomez-Romro, and C. Sanchez, "*Functional Hybrid Materials*", Wiley-VCH, Weinheim (2004).

26) a) S. C. Yang, H. X. Ge, X. Q. Jiang, and C. Z. Yang, *Colloid Polym. Sci.*, **278**, 285 (2000);

b) T. Basinska, S. Slomkowski, A. Dworak, I. Panchev, and M. M. Chehimi, *Colloid Polym. Sci.*, **279**, 916 (2001);

c) N. Behan, and C. Birkinshaw, *Macromol. Rapid. Commun.*, **22**, 41 (2001);

d) C. Duan, Vo, D. Kuckling, H. - J. P. Adler, and M. Schonhoff, *Colloid Polym. Sci.*, **280**, 400 (2002);

e) T. Trimaille, C. Pichot, A. Elaissari, S. Briancon, and T. Delair, *Colloid Polym. Sci.*, **281**, 1184 (2003);

f) G. He and Q. Pan, *Macromol. Rapid. Commun.*, **25**, 1545 (2004);

g) K. Kauer, A. M. Imroz Ali, and M. Sedlak, *Colloid Polym. Sci.*, **283**, 351 (2005);

h) D. Shah, P. Maiti, D. D. Jiang, C. A. Batt, and E. P. Giannelis, *Adv. Mater.*, **17**, 525 (2005);

i) G. Liu, X. Li, S. Xiong, L. Li, P. K. Chu, K. W. K, Yeung, S. Wu, and Z. Xu, *Colloid Polym. Sci.*, **290**, 349 (2012).

27) a) F. Gröhn, G. Kim, B. Bauer, and E. J. Amis, *Macromolecules*, **34**, 2179 (2001);

b) A. K. Gupte and M. Gupta, *Biomater.*, **26**, 3995 (2005);

c) H. Cong, M. Radosz, B. F. Towler, and Y. Shen, *Sep. Purifi. Technol.*, **55**, 281 (2007).

28) a) C. H. M. Caris, L. P. M. Elven, A. M. Herk, and A. L. German, *Congr. FATIPEC, 19th*, 341 (1988);

b) T. Chen, P. J. Colver, and S. A. F. Bon, *Adv. Mater.* **19**, 2286 (2007).

29) a) W. J. E. Beek, M. M. Wienk, and R. A. J. Janssen, *Adv. Mater.*, **16**, 1009 (2004);

b) H.-M. Xiong, Z.-D. Wang, D.-P. Liu, J.-S. Chen, Y.-G. Wang, and Y.-Y. Xia, *Adv. Funct. Mater.*, **15**, 1751 (2005).

30) a) K. A. Mauritz, *Mater. Sci. Eng., C*, **6**, 121 (1998);

b) E. B.-Lami and J. Lang, *J. Colloid Interface Sci.*, **197**, 293 (1998);

c) P. Hajji, L. David, J. F. Gerard, J. P. Pascault, and G. Vigier, *J. Polym. Sci. Part B: Polym. Phys.*, **37**, 3172 (1999);

d) J. Jang and B. Lim, *Angew. Chem.*, **115**, 5758 (2003).

31) a) Q. Wang, H. Xia, and C. Zhang, *J. Appl. Polym. Sci.*, **80**, 1478 (2001);

b) M. Z. Rong, M. Q. Zhang, G. Shi, Q. L. Ji, B. Wetzel, and K. Friedrich, *Tribol. Intl.*, **36**, 697 (2003).

32) a) L. Cumbal, J. Greenleaf, D. Leun, and A. K. SenGupta, *React. Funct. Polym.*, **54**, 167 (2003);

b) R. Matsuno, K. Yamamoto, H. Otsuka, and A. Takahara, *Macromolecules*, **37**, 2203 (2004);

c) M. A. White, J. A. Johnson, J. T. Koberstein, and N. J. Turro, *J. Am. Chem. Soc.*, **128**, 11356 (2006);

d) E. Marutani, S. Yamamoto, T. Ninjbadgar, Y. Tsujii, T. Fukuda, and M. Takano, *Polymer*, **45**, 2231 (2004);

e) M. Liong, J. Lu, M. Kovochich, T. Xia, S. G. Ruehm, A. E. Nel, F. Tamanoi, and J. I. Zink, *ACS Nano*, **2**, 889 (2008).

33) a) L. Quaroni and G. Chumanov, *J. Am. Chem. Soc.*, **121**, 10642 (1999);

b) Z. Zhang, L. Zhang, S. Wang, W. Chen, and Y. Lei, *Polymer*, **42**, 8315 (2001);

c) L. Balan, R. Schneider, and D. J. Lougnot, *Prog. Org. Coat.*, **62**, 351 (2008).

34) a) T. K. Mandal, M. S. Fleming, and D. R. Walt, *Nano Lett.*, **2**, 3 (2002);

b) R. C. Hedden, B. J. Bauer, A. P. Smith, F. Gröhn, and E. Amis, *Polymer*, **43**, 5473

(2002).

35) a) S. Klingelhöfer, W. Heitz, A. Greiner, S. Oestreich, S. Förster, and M. Antonietti, *J. Am. Chem. Soc.*, **119**, 10116 (1997);

b) C. Caliendo, G. Contini, I. Fratoddi, S. Irrera, P. Pertici, G. Scavia, and M. V. Russo, *Nanotechnol.*, **18**, 125504 (2007).

36) a) C. J. Brinker and G. W. Scherer, "*Sol-Gel Science*", Academic Press, Boston, (1990);

b) J. Wen and G. L. Wilkes, *Chem. Mater.*, **8**, 1667 (1996);

c) P. Judeinstein and C. Snchez, *J. Mater. Chem.*, **6**, 511 (1996);

d) Z. Hua and K.-Y. Qiu, *Polymer*, **38**, 521 (1997);

e) M. A. S. Pedroso, M. L. Dias, R. A. S. San Gil, and C. G. Mothe, *Colloid Polym. Sci.*, **281**, 19 (2003);

f) A. Bandyopadhyay, M. D. Sarkar, and A. K. Bhowmick, *J. Polym. Sci. Part B: Polym. Phys.*, **43**, 2399 (2005);

g) S. Li, Z. Zhou, H. Abernathy, M. Liu, W. Li, J. Ukai, K. Hase, and M. Nakanishi, *J. Mater. Chem.*, **16**, 858 (2006).

37) a) O. Prucker and J. Ruhe, *Macromolecules*, **31**, 592 (1998);

b) B. De Boer, H. K. Simon, M. P. L. Werts, E. W. van Der Vegte, and G. Hadziioannou, *Macromolecules*, **33**, 349 (2000).

38) a) R. Jordan, A. Ulma, J. F. Kang, M. H. Rafailovich, and J. Sokolov, *J. Am. Chem. Soc.*, **121**, 1016 (1999);

b) B. Zhao and W. J. Brittain, *J. Am. Chem. Soc.*, **121**, 3557 (1999).

39) S.-W. Zhang, S.-X. Zhou, Y.-M. Weng, and L.-M. Wu, *Langmuir*, **21**, 2124 (2005).

40) a) D. H. Nguyen, and P. Vana, *Polym. Adv. Technol.*, **17**, 625 (2006);

b) C.-H. Liu, and C.-Y. Pan, *Polymer*, **48**, 3679 (2007);

c) Y. Li, and B. C. Benicewicz, *Macromolecules*, **41**, 7986 (2008);

d) R. Ranjan, and W. J. Brittain, *Macromol. Rapid. Commun.*, **29**, 1104 (2008).

41) a) M. Husseman, E. E. Maakmstrom, M. McNamara, M. Mate, D. Mecerreyes, D. G. Benoit, J. L. Hedrick, P. Mansky, E. Huang T. P. Russell, and C. J. Hawker, *Macromolecules*, **32**, 1424 (1999);

b) C. Bartholome, E. Beyou, E. Bourgeat-Lami, P. Chumont, and N. Zydowicz, *Macromolecules*, **36**, 7946 (2003).

42) a) K. Matyjaszewski and J. Xia, *Chem. Rev.*, **101**, 2921 (2001);

b) K. Ueno, A. Inaba, M. Kondoh, and M. Watanabe, *Langmuir*, **24**, 5253 (2008).

43) a) L. Matejka and J. Plestil, *Macromol. Symp.*, **122**, 191 (1997);

b) N. Juangvanich and K. A. Maurite, *J. Appl. Polym. Sci.*, **67**, 1799 (1998);

c) G. Schmid, Ed., "*Nanoparticles*", Wiley-VCH, Weinheim (2004);

d) Y.-L. Liu, and S.-H. Li, *Macromol. Rapid. Commun.*, **25**, 1392 (2004);

e) A. M. Granville and W. J. Brittain, *Macromol. Rapid. Commun.*, **25**, 1298 (2004).

44) L. Andruzzi, A. Hexemer, X. Li, C. K. Ober, E. J. Krmaer, G. Galli, E. Chiellini, and D. A. Fischer, *Langmuir*, **20**, 10498 (2004).

45) a) S. C. Teo and A. Elsenberg, *J. Appl. Polm. Sci.*, **21**, 875 (1977);

b) G. A. Olah, G. K. Prakash, and M. Arvanaghi, *J. Am. Chem. Soc.*, **102**, 6641 (1980);

c) P. L. Antonucci, A. S. Aricò, P. Cretì, E. Ramunni, and V. Antonucci, *Solid State Ionics*, **125**, 431 (1999);

d) K. D. Kreuer, *J. Membr. Sci.*, **185**, 29 (2001).

46) a) T. Mizota, S. Tsuneda, K. Saito, and T. Sugo, *Ind. Eng. Chem. Res.*, **33**, 2215 (1994);

b) S. Durmaz and O. Okay, *Polymer*, **41**, 3693 (2000);

c) K. Manabe and S. Kobayashi, *Adv. Synth. Catal.*, **344**, 270 (2002);

d) S. Iimura, K. Manabe, and S. Kobayashi, *J. Org. Chem.*, **68**, 8723 (2003);

e) A. R. Kiasat and M. F. Mehrjardi, *Catal. Commun.*, **9**, 1497 (2008).

47) a) B. Karimi and D. Zareyee, *Tetrahedron Lett.*, **46**, 4661 (2005);

b) D. Zareyee and B. Karimi, *Tetrahedron Lett.*, **48**, 1277 (2007);

c) J. Dhainaut, J.-P. Dacquin, A. F. Lee, and K. Wilson, *Green Chem.*, **12**, 296 (2010);

d) Y. Shao, J. Guan, S. Wu, H. Liu, B. Liu, and Q. Kan, *Micropor. Mesopor. Mater.*, **128**,

120 (2010).

48) a) J. A. Horsfall and K. V. Lovell, *Polym. Adv. Technol.*, **13**, 381 (2002);

b) C. Chanthad, K. Xu, H. Huang, and Q. Wang, *J. Polym. Sci. Part A: Polym. Chem.*, **48**, 4800 (2010).

49) a) H. Sawada, T. Matsumoto, and M. Nakayama, *Yuki Gosei Kagaku Kyokaishi*, **50**, 592 (1992);

b) H. Sawada, *J. Fluorine Chem.*, **105**, 219 (2000);

c) H. Sawada, and T. Kawase, *Kobunshi Ronbunshu*, **58**, 147 (2001);

d) H. Sawada, and T. Kawase, *Kobunshi Ronbunshu*, **58**, 255 (2001);

e) H. Sawada, *J. Fluorine Chem.*, **121**, 111 (2003);

f) H. Sawada, *Polym. J.*, **39**, 637 (2007);

g) H. Sawada, *Prog. Polym. Sci.*, **32**, 509 (2007);

f) H. Sawada, *Polym. Chem.*, **3**, 46 (2012).

50) a) H. Sawada, R. Furukuwa, K. Sasazawa, K. Toriba, K. Ueno, and K. Hamazaki, *J. Appl. Polym. Sci.*, **100**, 1328 (2006);

b) H. Sawada, R. Furukuwa, K. Sasazawa, M. Mugisawa, and K. Ohnishi, *Eur. Polym. J.*, **43**, 3258 (2007);

c) H. Sawada, A. Sasaki, K. Sasazawa, K. Toriba, H. Kakehi, M. Miura, and N. Isu,

*Polym. Adv. Technol.*, **19**, 419 (2008);

d) H. Sawada, T. Narumi, A. Kajiwara, K. Ueno, and K. Hamazaki, *Colloid Polym. Sci.*, **284**, 551 (2006).

e) H. Sawada, A. Sasaki, and K. Sasazawa, *Colloid Surf. A: Physicochem. Eng. Aspects*, **337**, 57 (2009).

51) H. Sawada, S. Katayama, Y. Ariyoshi, T. Kawase, Y. Hayakawa, T. Tomita, and M. Baba, *J. Mater. Chem.*, **8**, 1517 (1998).

CHAPTER 1

# Selective Preparation of Novel Fluoroalkyl End-capped Co-oligomeric Nanocomposites-encapsulated Magnetites and Magnetite-adsorbing Co-oligomeric Nanoparticles

## 1.1. Introduction

Much attention has been devoted recently to well-dispersed magnetic colloidal particles, owing to the broad range of potential applications in the fields of ferrofluids,[1, 2] high-density data storage,[3] disks and toner in printing,[4 ~ 6] magnetic resonance imaging,[7, 8] enzyme immobilization,[9] rapid biological separation,[10, 11] drug delivery,[12 ~14] biomedical materials,[15 ~ 17] immunoassays[18, 19] and biosensors.[20, 21] The development of colloidal-stable magnetic nanoparticles is essential from a practical point of view. The surface functionality of magnetic nanoparticles with functionalized polymers can form colloidal-stable magnetic nanoparticles. So far, numerous synthetic and natural polymers have been used to obtain stable colloidal dispersions of magnetic nanoparticles by coating and encapsulating the particles.[22 ~ 31] It is well known that fluorinated surfactants have excellent surface characteristics, including oleophobicity and hydrophobicity, neither of which can be achieved with corresponding nonfluorinated polymers.[32] Thus, it is of particular interest to develop new, tailored magnetic fluorinated polymer colloids that possess not only good dispersibility in various solvents but also the unique active surface characteristics imparted by fluorine. In fact, it has been already reported that fluoroalkyl end-capped oligomers containing not only carboxyl groups but also other functional groups such as phosphonic acid, sulfonic acid and sulfobetaine-type groups

can interact effectively with the residual hydroxyl groups on the magnetite surface to form new fluorinated magnetic nanocomposites with good dispersibility in a variety of solvents, including water. [33 ~ 36)] Such good dispersibility of tailored magnetic fluorinated polymer colloids is due to the presence of fluoroalkyl end-capped oligomers because fluoroalkyl end-capped oligomers can exhibit various unique properties such as high solubility, surface active properties, biological activities and nanometer scale self-assembled molecular aggregates, which cannot be achieved by the corresponding nonfluorinated, randomly fluoroalkylated and AB block-type fluoroalkylated polymers. [37 ~ 40)] With regard to these fluoroalkyl end-capped oligomers, it has been very recently found that crosslinked fluoroalkyl end-capped co-oligomers containing both oxime-blocked isocyanato and hydroxy adamantyl segments can form new crosslinked fluoroalkyl end-capped co-oligomeric nanoparticles containing adamantane segments through the deprotecting reaction of oxime-blocked isocyanato segments in co-oligomers. [41, 42)] It has been also found that fluoroalkyl end-capped 2-acrylamido-2-methylpropanesulfonic acid co-oligomers containing adamantane segments can form nanometer-scale particles, not only in water but also in various traditional organic solvents. [43, 44)] The architecture of such fluorinated fine nanoparticles is because of the moderate oleophilic–oleophobic balance in these co-oligomeric nanoparticles, corresponding to the oleophilic character of the bulky adamantyl segments and the oleophobic character of

end-capped fluoroalkyl groups. [41 ~ 44)] Therefore, it is expected that these fluorinated co-oligomeric nanoparticle cores should interact with magnetic nanoparticles as a guest molecule to form colloidal-stable fluorinated co-oligomeric nanocomposite-encapsulated magnetic particles. This chapter shows that magnetic nanoparticles can be encapsulated into crosslinked fluoroalkyl end-capped co-oligomeric nanoparticle cores containing adamantyl segments to form colloidally stable magnetic nanoparticles. Particular emphasis on the applications of these nanocomposites as surface modifications for traditional organic polymers is placed, providing both good oleophobicity due to the end-capped fluoroalkyl groups and also magnetic properties arising from the presence of magnetic nanoparticles. In fluorinated betaine-type co-oligomeric nanoparticles, it has been found that these fluorinated nanoparticles can effectively decrease the LCST (lower critical solution temperature) in *t*-butyl alcohol through the adsorption of magnetic nanoparticles outside the fluorinated particle cores. These results are described herein.

## 1.2. Experimental

### 1.2.1 Measurements

Nuclear magnetic resonance spectra were measured using a JEOL JNM-400 (400 MHz) FT NMR SYSTEM (Tokyo, Japan). Ultraviolet-visible spectra were measured using a Shimadzu UV-1600 UV-vis spectrophotometer (Kyoto, Japan). Dynamic light-scattering (DLS) measurements were taken using an Otsuka Electronics DLS-7000 HL system (Tokyo, Japan). Thermal analyses were recorded on a Bruker axs TG-DTA2000SA differential thermobalance (Kanagawa, Japan). Contact angles were measured using Kyowa Interface Science Drop Master 300 (Saitama, Japan). Transmission electron microscopy (TEM) was conducted using a JEOL JEM-1210 Electron microscope.

### 1.2.2. Materials

Isocyanatoethyl methacrylate 2-butanone oxime adduct (IEM-BO) was obtained from Showa Denko (Tokyo, Japan). 1-hydroxy-5-adamantylacrylate (Ad-HAc) and magnetic nanoparticles (**Magnt**; with an average particle size of 10 nm) were used as received from

Idemitsu Kosan (Tokyo, Japan) and Toda Kogyo Corporation (Hiroshima, Japan), respectively. 2-acrylamido-2-methylpropanesulfonic acid (AMPS) were purchased from Tokyo Kasei Kogyo.

### 1.2.3. Preparation of crosslinked fluoroalkyl end-capped co-oligomeric nanocomposite-encapsulated Magnt

A typical procedure for the preparation of crosslinked fluoroalkyl end-capped co-oligomeric nanocomposite-encapsulated **Magnt** by the use of a α, ω-bis(perfluoro-1-methyl-2-oxapentylated) isocyanatoethyl methacrylate 2-butanone oxime adduct–1-hydroxy-5-adamantylacrylate co-oligomers [$R_F$-(IEM-BO)$_x$-(Ad-HAc)$_y$-$R_F$; $R_F$ = $CF(CF_3)OC_3F_7$; $x$ : $y$ = 21 : 79; Mn = 2600] is as follows: magnetic nanoparticles (200 mg, with an average particle size of 10 nm) were added to an *N,N*-dimethylformamide (25 mL) solution of $R_F$-(IEM-BO)$_x$-(Ad-HAc)$_y$-$R_F$ co-oligomer (1.0 g), which was prepared by co-oligomerization of the corresponding monomers and fluoroalkanoyl peroxide according to the previously reported method.[41, 42)] The mixture was stirred at room temperature for 2 days under ultrasonic irradiation conditions and then stirred with a magnetic bar at 130 °C for 1 h. Methanol (20 mL) was added to the reaction mixture, and the mixture was stirred well for 30

min at room temperature. After the centrifugal separation (2000 r.p.m./30 min) at room temperature, the supernatant solution was evaporated under reduced pressure. The isolated crude product was reprecipitated from methanol–acetone to yield purified crosslinked fluorinated co-oligomeric nanocomposite-encapsulated **Magnt** (828 mg, Run 4 in Table 1-1). The nanocomposite particles exhibited the following Fourier transform infrared spectrum characteristics, with features corresponding to the presence of magnetic nanoparticles: infrared ($cm^{-1}$) 560. Other $R_F$-$(IEM)_x$-$(Ad\text{-}HAc)_y$-$R_F$ co-oligomeric nanocomposite-encapsulated **Magnt** were prepared under similar conditions (Runs 1~3 and 5~8 in Table 1-1).

### 1.2.4. Preparation of fluoroalkyl end-capped betaine-type co-oligomeric nanocomposite-encapsulated Magnt

A typical procedure for the preparation of fluoroalkyl end-capped betaine-type co-oligomeric nanocomposite-encapsulated **Magnt** by the use of α, ω-bis(perfluoro-1-methyl-2-oxapentylated) 2-acrylamido-2-methylpropane sulfonic acid–1-hydroxy-5-adamantylacrylate co-oligomer [$R_F$-$(AMPS)_x$-$(Ad\text{-}HAc)_y$-$R_F$; $R_F$ = $CF(CF_3)OC_3F_7$; $x$ : $y$ = 44 : 56 (the molecular weight of this co-oligomer cannot be determined by size exclusion chromatography because of the formation of nanoparticles)] is as follows:

magnetic nanoparticles (15 mg; with an average particle size of 10 nm) were added to a methanol (25 mL) solution of $R_F$-$(AMPS)_x$-$(Ad\text{-}HAc)_y$-$R_F$ co-oligomer (150 mg), which was prepared by the co-oligomerization of the corresponding monomers and fluoroalkanoyl peroxide according to the previously reported method.[43, 44] The mixture was stirred at room temperature for 6 h under ultrasonic irradiation conditions. After centrifugal separation (2000 r.p.m./30 min) at room temperature, the supernatant solution was evaporated under reduced pressure to yield purified fluorinated betaine-type co-oligomeric nanocomposite-encapsulated **Magnt** (112 mg, Run 10 in Table 1-3). These nanocomposite particles exhibited the following Fourier transform infrared spectrum characteristics, with features corresponding to the presence of magnetic nanoparticles: infrared ($cm^{-1}$) 560. Other $R_F$-$(AMPS)_x$-$(Ad\text{-}HAc)_y$-$R_F$ co-oligomeric nanocomposites-encapsulated **Magnt** were prepared under similar conditions (Runs 9 and 11~14 in Table 1-3).

### 1.2.5. Preparation of PMMA-modified film treated with crosslinked fluoroalkyl end-capped co-oligomeric nanocomposite-encapsulated Magnt

The poly(methyl methacrylate) (PMMA)-modified film (with a film thickness of 194 mm)

was prepared by casting mixed solutions of methanol and 1,2-dichloroethane (v/v = 5/20; 25 mL total volume) containing PMMA (990 mg) and crosslinked $R_F$-$(IEM)_x$-$(Ad\text{-}HAc)_y$-$R_F$ co-oligomeric nanocomposite-encapsulated **Magnt** (Run 4 in Table 1-1; 10 mg) on a glass plate. The solvent was evaporated at room temperature, and the resulting film was peeled off and dried at 50 °C for 24 h under vacuum to obtain the PMMA-modified film. Contact angles for dodecane on both the surface and the reverse sides of the modified film were measured at room temperature using a goniometer.

### 1.2.6. Measurements of the LCST of fluoroalkyl end-capped betaine-type co-oligomeric nanocomposite-encapsulated Magnt

The LCSTs of $R_F$-$(AMPS)_x$-$(Ad\text{-}HAc)_y$-$R_F$ co-oligomeric nanocomposite-encapsulated **Magnt** in *t*-butyl alcohol were measured using a turbidity method. A ultraviolet-visible spectrophotometer equipped with a temperature controller was used to trace the phase transition by monitoring the transmittance of light at a wavelength of 500 nm as a function of temperature. The concentration of the co-oligomeric nanocomposite solutions used was 4 $gdm^{-3}$, and the LCST was defined as the temperature at which the transmittance was 50 %.

## 1.3. Results and discussion

### 1.3.1. Preparation and characteristics of novel crosslinked fluoroalkyl end-capped co-oligomeric nanocomposite-encapsulated magnetic nanoparticles

The deprotecting reactions of fluoroalkyl end-capped isocyanatoethyl methacrylate 2-butanone oxime adduct–1-hydroxy-5-adamantylacrylate co-oligomers [$R_F$-(IEM-BO)$_x$-(Ad-HAc)$_y$-$R_F$] were carried out in *N,N*-dimethylformamide in the presence of magnetic nanoparticles (**Magnt**; with a mean diameter of 10nm) at 130 °C for 1 h, and the results are shown in Scheme 1-1 and Table 1-1.

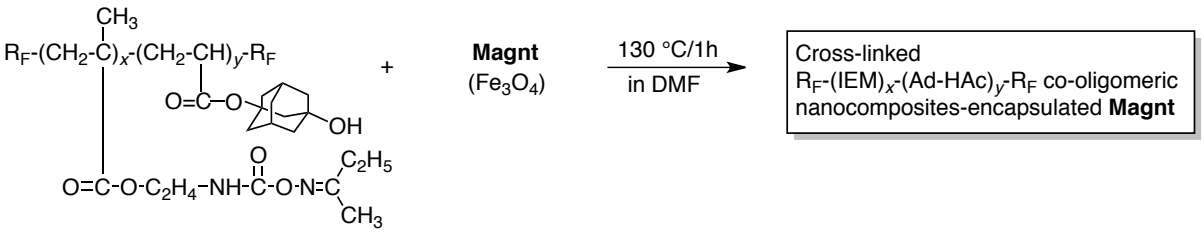


[$R_F$-(IEM-BO)$_x$-(Ad-HAc)$_y$-$R_F$]
*x* : *y* = 21: 79 (determined by $^1$H NMR); Mn = 2600
$R_F$ = $CF(CF_3)OC_3F_7$

Scheme 1-1

Table 1-1 Preparation of cross-linked $R_F$-(IEM)$_x$-(Ad-HAc)$_y$-$R_F$ co-olgomeric nanocomposites-encapsulated **Magnt**

| Run | $R_F$-(IEM-BO)$_x$-(Ad-HAc)$_y$-$R_F$ (g) | **Magnt** (size:10 nm) (mg) | Product yield [a)] (%) | Size of dispersed nanocompsites in methanol [b, c)] (nm ± STD) | Contens of **Magnt** in nanocomposites (%) |
|---|---|---|---|---|---|
| 1 | 1.0 | 20 | 57 | 154 ± 31 | 4 |
| 2 | | 50 | 61 | 175 ± 50 | 5 |
| 3 | | 100 | 64 | 168 ± 35 | 10 |
| 4 | | 200 | 69 | 192 ± 40 | 20 |
| 5 | | 400 | 62 | 168 ± 40 | 26 |
| 6 | | 600 | 71 | 186 ± 39 | 41 |
| 7 | | 800 | 43 | 279 ± 54 | 38 |
| 8 | | 1000 | 42 | 304 ± 45 | 31 |

[a]Yeilds were based on $R_F$-(IEM-BO)$_x$-(Ad-HAc)$_y$-$R_F$ and **Magnt**.
[b]Determined by dynamic light scattering measurements.
[c]Size of parent $R_F$-(IEM-BO)$_x$-(Ad-HAc)$_y$-$R_F$ co-oligomeric nanoparticles: 11 ± 1.1 nm.

As shown in Scheme 1-1 and Table 1-1, the deprotecting reactions were found to proceed under mild conditions to form a variety of crosslinked fluoroalkyl end-capped co-oligomeric nanocomposite-encapsulated **Magnt** in isolated yields of 42 ~ 69 %. The obtained crosslinked fluorinated co-oligomeric nanoparticle-encapsulated **Magnt** exhibited good dispersibility in methanol, tetrahydrofuran, dimethyl sulfoxide and *N,N*-dimethylformamide. The size of crosslinked fluorinated nanocomposite-encapsulated **Magnt** was measured in methanol solutions using DLS at a temperature of 30 °C. These results are also shown in Table 1-1.

The size (number-average diameter) of these fluorinated particles ranged from approximately 154 to 304 nm and were monodispersed. The size of these fluorinated nanocomposite-encapsulated **Magnt** was found to increase from approximately 11 nm to 154 ~ 304 nm after the encapsulation of **Magnt**. The size increase of the nanocomposites indicates that the encapsulations of **Magnt** proceeded smoothly toward the synthesis of very fine

crosslinked fluorinated co-oligomeric nanocomposite-encapsulated **Magnt**.

The contents of encapsulated **Magnt** in crosslinked fluorinated cooligomeric nanoparticles were estimated by thermogravimetric analyses (see Fig. 1-1).

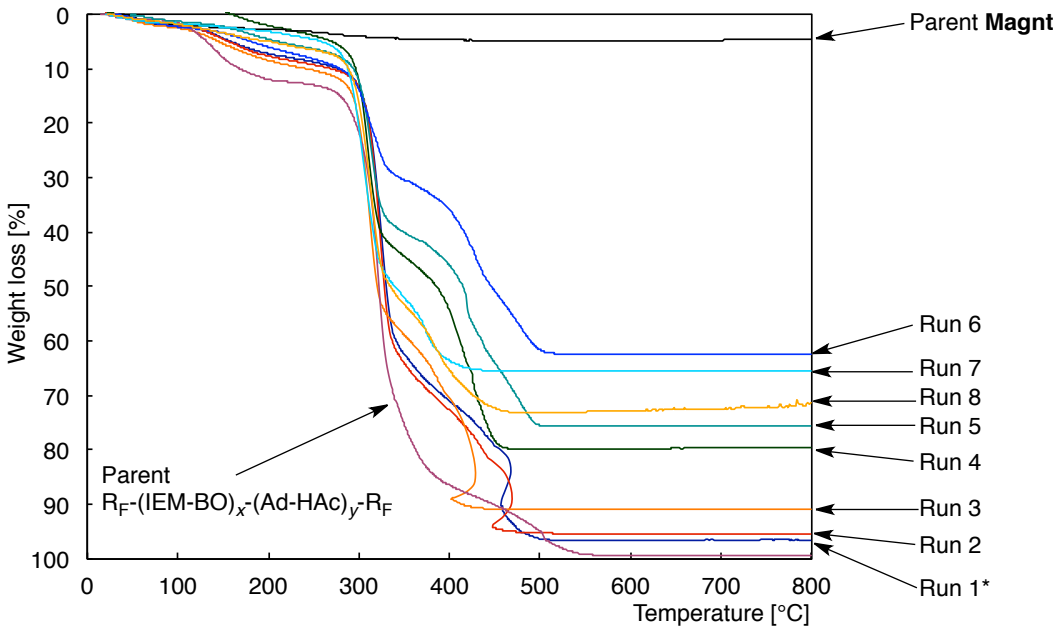


Fig. 1-1 Thermogravimetric analyses of $R_F$-(IEM)$_x$-(Ad-HAc)$_y$-$R_F$ co-oligomeric nanocomposite-encapsulated **Magnt.**
*Each run corresponds to the runs in Table 1-1.

In this process, the weight loss of nanocomposites was measured as the temperature was increased at a heating rate of 10 °Cmin$^{-1}$ to a maximum temperature of 800 °C under atmospheric conditions. The thermal stability of crosslinked fluorinated nanocomposite-encapsulated **Magnt** was inferior to that of the parent magnetic nanoparticles. In addition, the original $R_F$-(IEM-BO)$_x$-(Ad-HAc)$_y$-$R_F$ co-oligomer was found to completely

decompose around 550 °C. These results imply that the **Magnt** contents range from 4 to 41 % for the different samples, as listed in Table 1-1.

X-ray diffraction patterns of fluorinated crosslinked nanocomposite-encapsulated **Magnt** and parent **Magnt** were similar (see Fig. 1-2). However, the collected diffraction intensity was

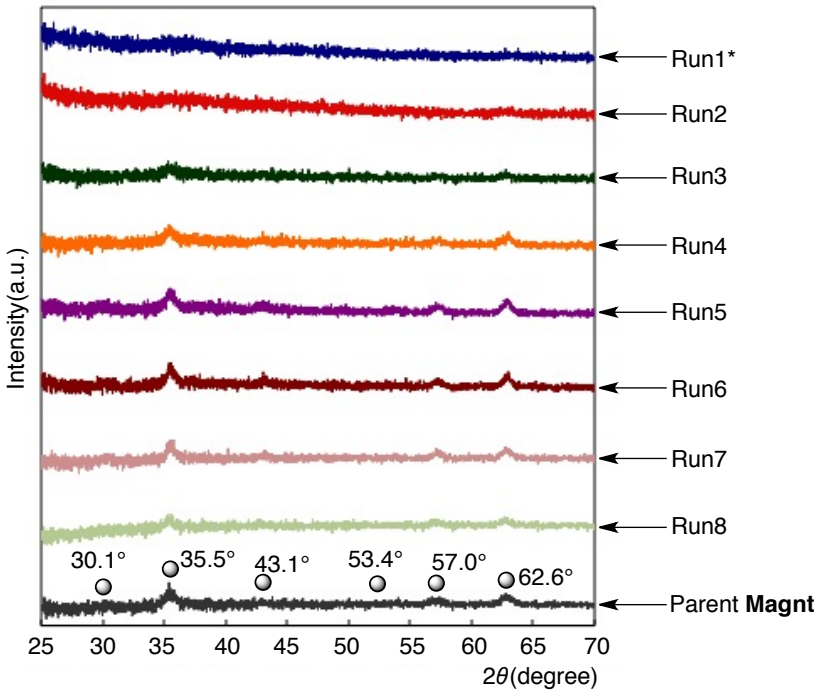


Fig. 1-2 X-ray diffraction patterns of parent magnetic nanoparticles and $R_F$-(IEM)$_x$-(Ad-HAc)$_y$-$R_F$ co-oligomeric nanocomposite-encapsulated **Magnt**.
*Each run corresponds to the runs in Table 1-1.

extremely weakened for the fluorinated nanoparticles possessing lower encapsulated ratios of **Magnt** (Runs 1 and 2 in Table 1-1). The Fourier transform infrared spectrum peak near 560 $cm^{-1}$ that was present for each fluorinated crosslinked nanocomposite implies the presence of encapsulated **Magnt** in the fluorinated crosslinked nanoparticle cores (Fig. 1-3).

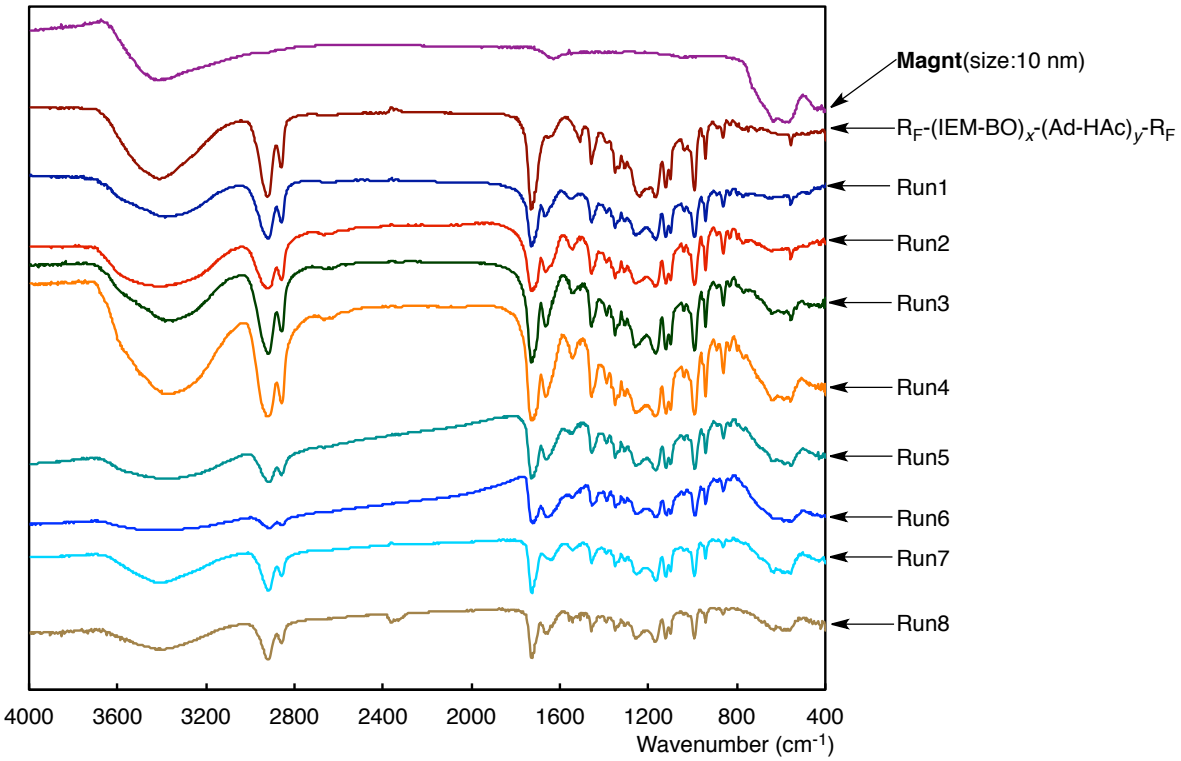


Fig.1-3 FT-IR spectra of $R_F$-(IEM)$_x$-(Ad-HAc)$_y$-$R_F$ cooligomeric nanocomposites-encapsulated **Magnt**, $R_F$-(IEM-BO)$_x$-(Ad-HAc)$_y$-$R_F$ and **Magnt**.
*Each run corresponds to the runs in Table 1-1.

To confirm the presence of encapsulated **Magnt** in the fluorinated nanoparticle cores, a methanol solution of crosslinked fluorinated co-ologomeric nanocomposite-encapsulated **Magnt** (listed as Run 2 in Table 1-1) was examined by using TEM. The TEM micrograph is shown in Fig. 1-4.

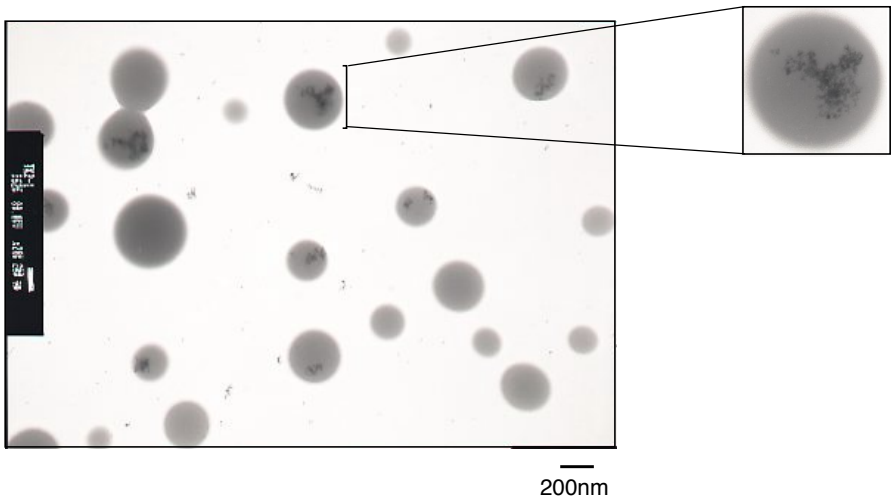


Fig. 1-4 TEM image of crosslinked fluorinated co-oligomeric nanocomposite-encapsulated **Magnt** (Run 2 in Table 1-1) in methanol.

The electron micrograph also shows the formation of crosslinked fluorinated nanocomposite-encapsulated magnetic fine particles, showing a mean nanoparticle diameter of 262 nm. This is similar to the number-average diameter of 175 ± 50 nm found in DLS measurements, shown in Table 1-1. Interestingly, TEM photographs show that the amounts of **Magnt** encapsulated into fluorinated composite cores can increase quite effectively with increasing **Magnt** content in the nanocomposites from 4 to 20 % (see Fig. 1-5).

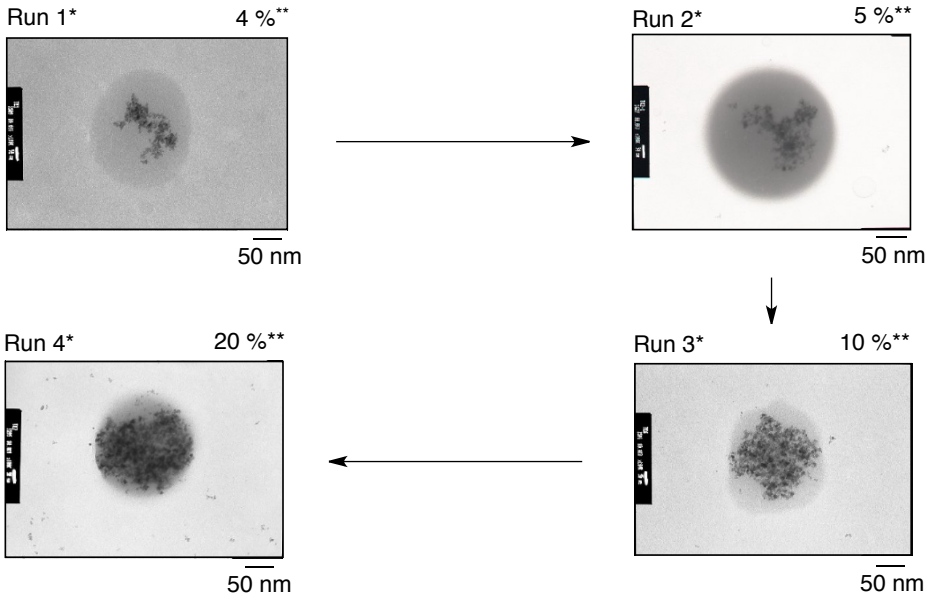


Fig. 1-5 TEM photographs of a variety of crosslinked fluorinated co-oligomeric nanocomposite-encapsulated **Magnt** in methanol.
*Each run corresponds to the runs in Table 1-1.
**Contents of **Magnt** in the nanocomposites were determined by thermogravimetric analyses.

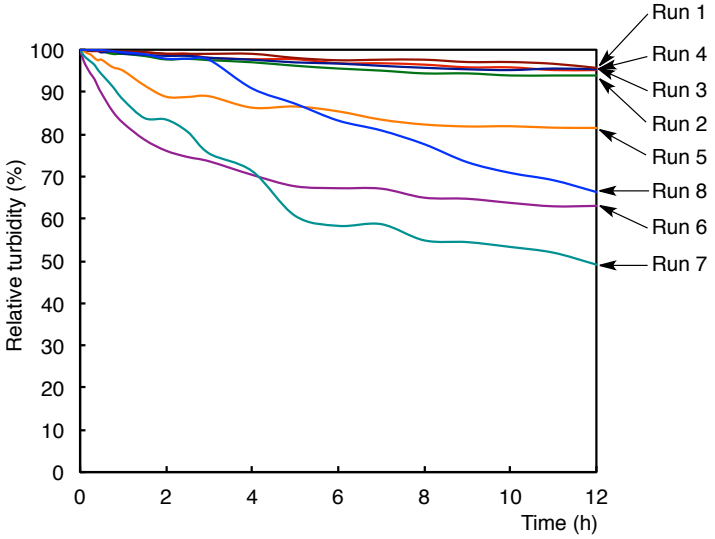


| Run* | Relative turbidity after 12 h (%) | Contents of **Magnt** in nanocomposites** (%) |
|---|---|---|
| 1 | 95 | 4 |
| 2 | 94 | 5 |
| 3 | 95 | 10 |
| 4 | 95 | 20 |
| 5 | 81 | 26 |
| 6 | 63 | 41 |
| 7 | 49 | 38 |
| 8 | 66 | 31 |

Fig. 1-6 UV-vis spectral changes of the absorbance at λ = 500 nm of methanol solutions containing $R_F$-(IEM)$_x$-(Ad-HAc)$_y$-$R_F$ cooligomeric nanocomposites-encapsulated **Magnt** as a function of time at 30 °C (174 mgdm$^{-3}$).
*Each run corresponds to the runs in Table 1-1.
**Contents of **Magnt** was determined by thermogravimetric analyses.
***Concentration of each magnetite nanoparticle in methanol.

Fig. 1-6 shows the UV-vis spectra changes of the absorbance at λ = 500 nm of methanol solutions containing fluorinated crosslinked nanocomposite-encapsulated **Magnt** as a function

of time. As shown in Fig. 1-6, it was clarified that the present fluorinated crosslinked nanocomposite are well-dispersed in methanol with a good stability.

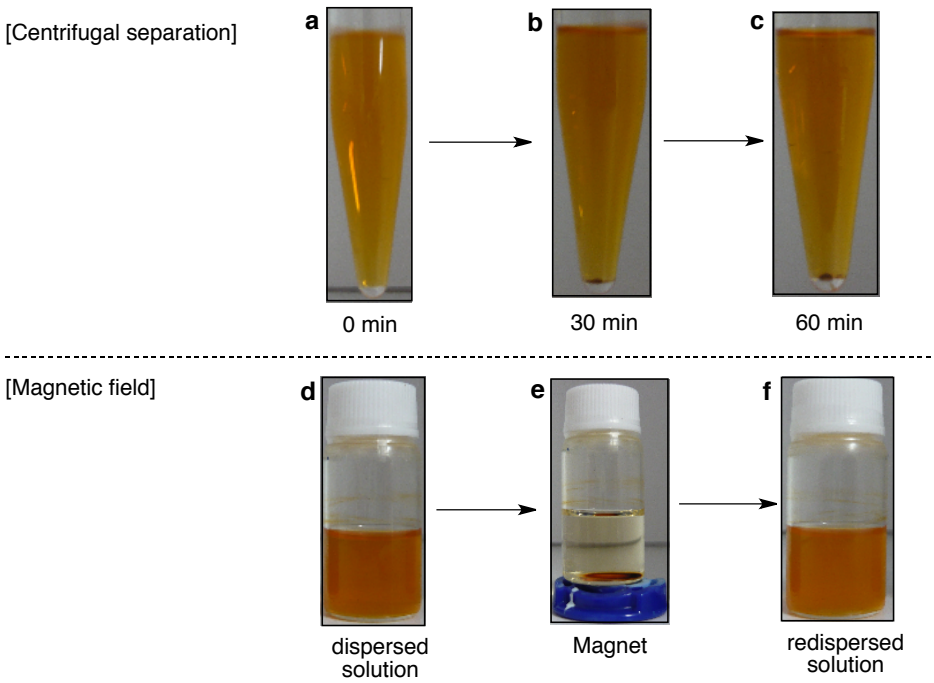


Fig. 1-7 Photographs of $R_F$-(IEM)$_x$-(Ad-HAc)$_y$-$R_F$ co-oligomeric nanocomposite-encapsulated **Magnt** (Run 4 in Table 1-1) in methanol (concentration of nanocompoistes in methanol: 1 gdm$^{-3}$).

As shown in Fig. 1-7, colloidal-stable magnetic particles were obtained in methanol solutions even under the following conditions: (a) centrifugal separation for 30 min (b) 60 min at 3000 r.p.m. and (c) at room temperature. To investigate the magnetic response of the colloidal-stable fluorinated nanocomposites in methanol solution against an external magnetic field, a permanent magnet was applied from the bottom of the sample tube containing this methanol solution (see Fig. 1-7 d ~ f). This nanocomposite exhibited good dispersibility in

methanol (Fig. 1-7 d); however, the composite instantaneously precipitated on application of the magnet (Fig. 1-7 e). A redispersed colloidal-stable nanocomposite solution after the magnet application (Fig. 1-7 f) that was similar to the original one (Fig. 1-7 d) was successfully prepared. This behavior indicates that the fluorinated magnetic nanocomposites still maintain their ferromagnetism.

### 1.3.2. Application of novel crosslinked fluoroalkyl end-capped co-oligomeric nanocomposite-encapsulated magnetic nanoparticles to the surface modification of traditional organic polymers

In this way, the present crosslinked fluorinated nanocomposites-encapsulated **Magnt** are very fine particles and have good dispersibility in a variety of organic media. Thus, it is of particular interest to apply these fluorinated nanocomposites as a surface modification for organic polymers such as PMMA. A PMMA-modified film has been prepared by casting homogeneous solutions of PMMA and fluorinated nanocomposites in the mixture of methanol and 1,2-dichloroethane (Runs 1 ~ 8, listed in Table 1-1). The contact angles of dodecane on the surface and reverse sides of the modified brown-colored PMMA films were measured, and the results are shown in Table 1-2. Film thickness ranged from 187 to 199 μm.

Table 1-2 Contact angles of dodecane on the modified PMMA filmes, treated with crosslinked fluorinated co-oligomeric nanocomposite-encapsulated **Magnt**

| Run[a] | Contents of **Magnt**[b] (%) | Contact angle (degree) Dodecane | | Film thickness ($\mu$m) |
|---|---|---|---|---|
| | | Surface side | Reverse side | |
| 1 | 4 | 10.9 | 0 | 187 |
| 2 | 5 | 21.6 | 0 | 192 |
| 3 | 10 | 19.1 | 0 | 199 |
| 4 | 20 | 12.5 | 0 | 194 |
| 5 | 26 | 20.6 | 0 | 196 |
| 6 | 41 | 14.3 | 0 | 190 |
| 7 | 38 | 12.8 | 0 | 195 |
| 8 | 31 | 14.2 | 0 | 193 |

[a]Each run corresponds to the runs in Table 1-1.
[b]Contents of **Magnt** in the nanocomposites were determined by thermogravimetric analyses.

As shown in Table 1-2, higher dodecane contact angles for dodecane on the surface side compared with the reverse side were obtained in each modified film, suggesting that fluorinated nanocomposites could be arranged on the polymer surface to exhibit strong oleophobicity because of the presence of end-capped fluoroalkyl segments on the surface. Interestingly, as shown in Fig. 1-8, the PMMA-modified film treated with fluorinated nanocomposites (Run 4 in Table 1-1) was found to interact with a permanent magnet, indicating that this modified polymer possesses not only oleophobic characteristics but also ferromagnetism.

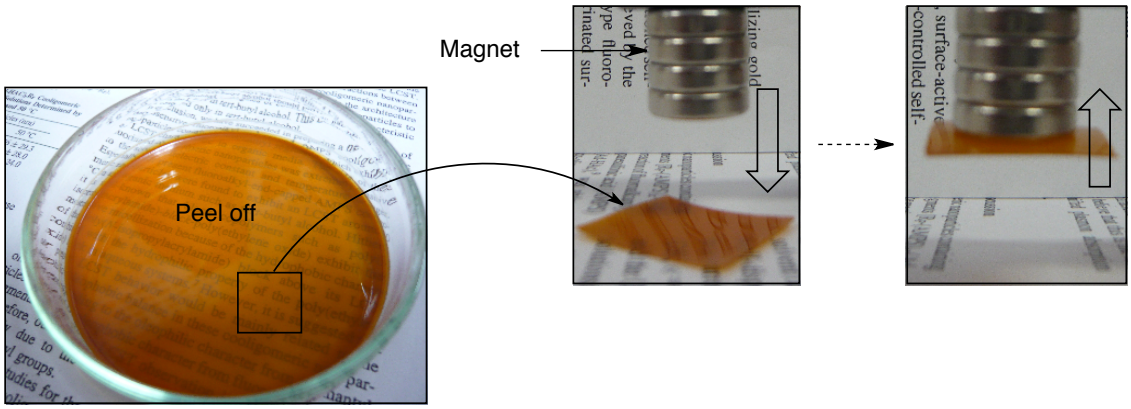


PMMA cast films* treated with $R_F$-(IEM)$_x$-(Ad-HAc)$_y$-$R_F$ co-oligomeric nanocomposite-encapsulated **Magnt** (Run 4 in Table 1-1)

Fig. 1-8 Photographs of modified PMMA filmes treated with crosslinked fluorinated nanocomposite-encapsulated magnetic nanoparticles.

*Concentration of $R_F$-(IEM)$_x$-(Ad-HAc)$_y$-$R_F$ co-oligomeric nanocomposite-encapsulated **Magnt** based on PMMA is 3 % (m/m).

### 1.3.3. Preparation and characteristics of novel crosslinked fluoroalkyl end-capped betaine-type co-oligomeric nanocomposite-encapsulated magnetic nanoparticles

Magnetic nanoparticles were attempted to encapsulate into fluoroalkyl end-capped co-oligomeric betaine-type nanoparticle cores. In fact, fluorinated betaine-type co-oligomeric nanocomposite-encapsulated **Magnt** was prepared in isolated yields of 34 ~ 68 % by the treatment of corresponding fluorinated betaine-type co-oligomeric nanoparticles with **Magnt** in methanol under ultrasonic irradiation conditions, as shown in Scheme 1-2 and Table 1-3.

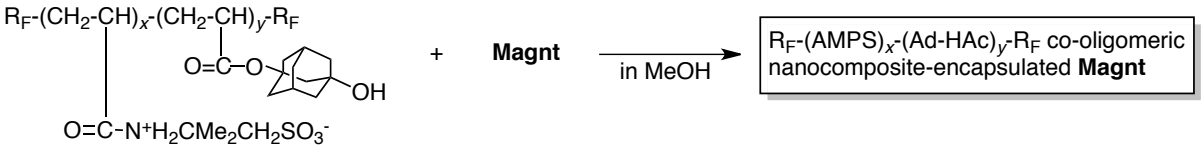


[$R_F$-(AMPS)$_x$-(Ad-HAc)$_y$-$R_F$]
$x$ : $y$ = 44: 56 (determined by $^1$H NMR)
$R_F$ = CF(CF$_3$)OC$_3$F$_7$

Scheme 1-2

Table 1-3 Preparation of cross-linked betaine-type co-olgomeric nanocomposites-encapsulated **Magnt**

| Run | $R_F$-(AMPS)$_x$-(Ad-HAc)$_y$-$R_F$ (mg) | **Magnt** (size:10 nm) (mg) | Product yields [a)] (%) | Size of dispersed nanocompsites [b, c)] (nm ± STD) | Size of redispersed nanocompsites [b, c)] (nm ± STD) | Contens of **Magnt** in nanocomposites (%) |
|---|---|---|---|---|---|---|
| 9 | 150 | 5 | 59 | 36 ± 2.3 | 124 ± 12 | 2 |
| 10 | | 15 | 68 | 58 ± 7.0 | 110 ± 11 | 13 |
| 11 | | 30 | 64 | 183 ± 41 | 80 ± 4.6 | 10 |
| 12 | | 60 | 49 | 25 ± 2.5 | 99 ± 13 | 19 |
| 13 | | 100 | 44 | 57 ± 9.6 | 136 ± 22 | 17 |
| 14 | | 150 | 34 | 49 ± 5.0 | 101 ± 22 | 16 |

[a]Yeilds were based on $R_F$-(AMPS)$_x$-(Ad-HAc)$_y$-$R_F$ and **Magnt**.
[b]Determined by dynamic light scattering measurements.
[c]Size of parent $R_F$-(AMPS)$_x$-(Ad-HAc)$_y$-$R_F$ co-oligomeric nanoparticles: 17 ± 2.5 nm.

The **Magnt** content in the nanocomposites in Table 1-3 was estimated to be between 2 and 19 % using thermogravimetric analyses. The **Magnt** content was found to increase when the feed amount of **Magnt** was increased from 5 to 150 mg. Above a feed amount of 60 mg, the **Magnt** content of the particles remained fairly constant, between 16 and 19 % (see Table 1-3). DLS measurements revealed that the size of nanocomposite particles increased from 17 nm (the number-average diameter size of parent fluorinated co-oligomeric nanoparticles) to between 25 and 183 nm in methanol after the composite reactions, indicating that **Magnt** was effectively encapsulated into the fluorinated co-oligomeric nanoparticle cores (see Table 1-3). Interestingly, these fluorinated nanocomposite-encapsulated **Magnt** exhibited good

dispersibility and redispersibility in methanol. The size (80–136 nm) of the redispersed fluorinated nanocomposite particles did not change, even after redispersion of the parent fluorinated nanocomposite-encapsulated **Magnt** powders (with diameters between 25 and 183 nm) in methanol. The size distributions of each nanocomposite were monodispersed (see Table 1-3).

To confirm the presence of encapsulated **Magnt** in fluorinated cooligomeric nanoparticle cores, a methanol solution of the fluorinated betaine-type co-oligomeric nanocomposite encapsulated **Magnt** was examined by using TEM (Run 9 in Table 1-3). The resulting micrographs are shown in Fig. 1-9. The electron micrograph shows the formation of fine particles of fluorinated nanocomposite-encapsulated **Magnt**, with mean diameters of 126 nm (Fig. 1-9). The particle diameters measured through TEM are quite similar to the values determined from DLS measurements (which gave number-average diameters of 124 ± 12 nm for redispersed nanocomposites, Run 9 in Table 1-3).

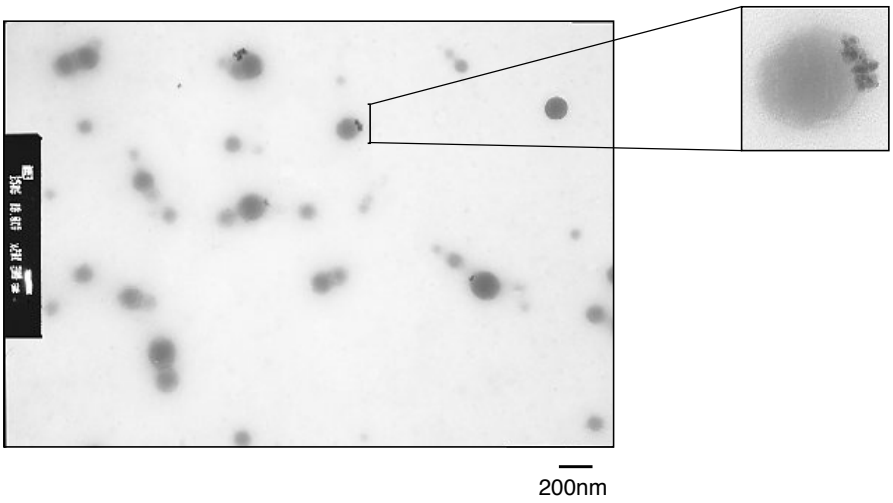


Fig. 1-9 TEM image of **Magnt** adsorbed on fluorinated betain-type co-oligomeric nanocomposites (Run 9 in Table 1-3).

Surprisingly, the encapsulation behavior of magnetic nanoparticles into fluorinated co-oligomeric nanoparticle cores, shown in Fig. 1-9, is quite different from that of fluorinated crosslinked nanocomposites-encapsulated **Magnt**, shown in Figs. 1-4 and 1-5. In fluorinated betaine-type co-oligomeric nanocomposites, magnetic nanoparticles are adsorbed outside the co-oligomeric particle cores through the effective covalently binding interaction between the sulfobetaine-type segments in co-oligomers and the residual hydroxyl groups in magnetic particles. In fact, it has already been reported that carboxy, [45] sulfo, [46] phosphate [47] and phosphoric [48, 49] groups can interact with magnetic nanoparticles through the covalent bonds. No covalent binding interactions in crosslinked fluorinated co-oligomeric nanoparticles (in Scheme 1-1) should allow the encapsulation of magnetic nanoparticles inside fluorinated co-oligomeric particle cores through the crosslinking reaction process. More interestingly,

TEM micrographs show that magnetic nanoparticles can be effectively adsorbed outside cooligomeric particle cores in each nanocomposite (Runs 9 ~ 13 in Table 1-3), as shown in Fig. 1-10.

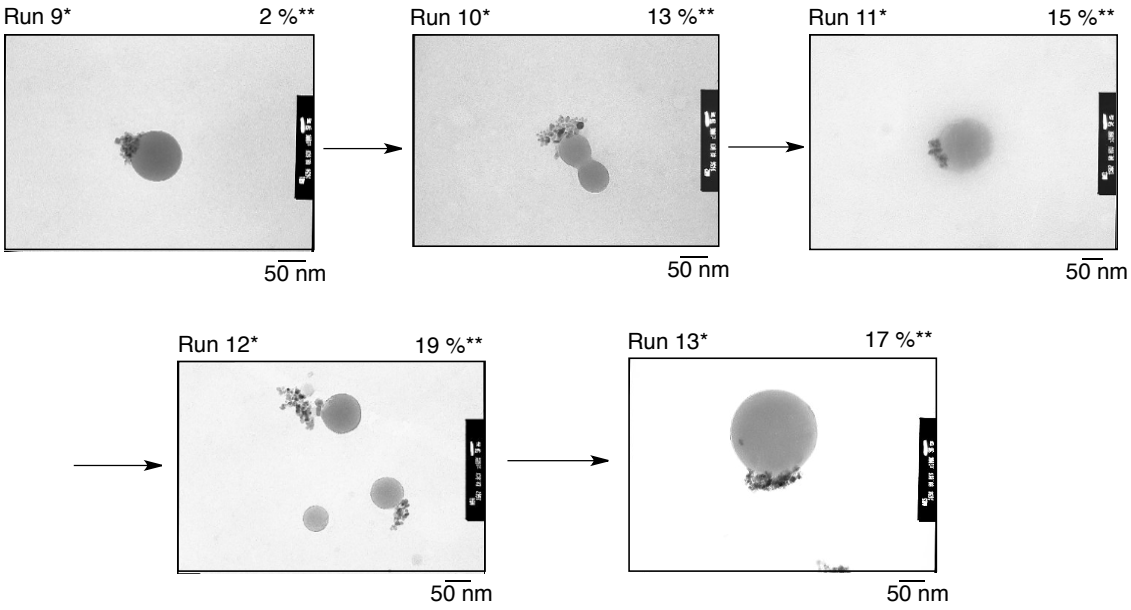


Fig. 1-10 TEM photographs of **Magnt** adsorbed on fluorinated betaine-type co-oligomeric nanocomposites in methanol.
*Each run corresponds to the runs in Table 1-3.
**Contents of **Magnt** in the nanocomposites were determined by thermogravimetric analyses.

### 1.3.4. The LCST characteristic of novel crosslinked fluoroalkyl endcapped betaine-type co-oligomeric nanocomposite-encapsulated magnetic nanoparticles in organic media

It is well known that block copolymers such as poly(*N*-isopropylacrylamide)-*block*-poly(ethylene oxide) can exhibit thermosensitive micellization arising from a combination of the hydrophobic character of the poly(*N*-isopropylacrylamide) block above its

LCST and the hydrophilic property of the poly(ethylene oxide) block in aqueous systems.[50, 51] In contrast, fluoroalkyl end-capped betaine-type co-oligomeric nanoparticles containing adamantane segments can exhibit the LCST behavior in organic media such as *t*-butyl alcohol because of the effective oleophilic-oleophobic balance between the oleophilic character from adamantyl segments and the oleophobic character from end-capped fluoroalkyl groups.[43, 44] This is the first example of the LCST behavior in organic media, although the LCST behavior of hydrocarbon polymers in ionic liquids has been previously reported by Watanabe et al.[52] Thus, it is of particular interest to study the LCST behavior of the present fluoroalkyl end-capped betaine-type co-oligomeric nanocomposite-encapsulated **Magnt** in organic media.

The size of fluorinated betaine-type co-oligomeric nanocomposite-encapsulated **Magnt** measured by the use of DLS in *t*-butyl alcohol at temperatures ranging from 40 to 80 °C (Table 1-4).

Table 1-4 Size of $R_F$-$(AMPS)_x$-$(Ad\text{-}HAc)_y$-$R_F$ cooligomeric nanocomposites-encapsulated **Magnt** in *t*-butyl alcohol solutions determined by dynamic light scattering measurements

| Run* | Contents of **Magnt**** (%) | Size of nanocomposite (nm ± STD) | |
|---|---|---|---|
| | | 40°C | 80°C |
| 9 | 2 | 18 ± 3.8 | 28 ± 4.8 |
| 10 | 13 | 17 ± 3.3 | 26 ± 5.7 |
| 11 | 19 | 17 ± 3.2 | 33 ± 5.6 |

*Each run corresponds to the runs in Table 1-3.
**Contents of **Magnt** in nanocomposites were determined by thermogravimetric analyses.

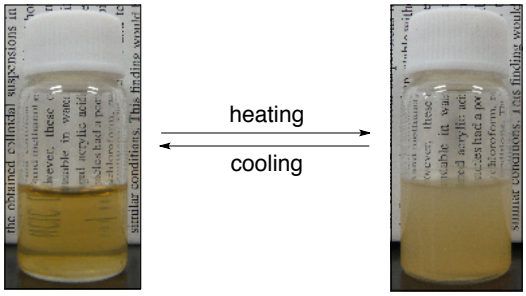


Fig. 1-11 Photographs of *t*-butyl alcohol solutions of $R_F$-$(AMPS)_x$-$(Ad\text{-}HAc)_y$-$R_F$ cooligomeric nanocomposites-encapsulated **Magnt** possessing the LCST characteristic (content of Magnt in the nanocomposites: 2 %*; concentration of the composites: 4 $gdm^{-3}$).

The size of each fluorinated nanocomposite-encapsulated **Magnt** was found to increase from 17 ~ 18 nm to 26 ~ 33 nm when the temperature was increased from 40 to 80 °C, indicating that each nanocomposite-encapsulated **Magnt** causes thermally induced phase transition in *t*-butyl alcohol. In fact, *t*-butyl alcohol solutions of fluorinated betaine-type co-oligomeric nanocomposite-encapsulated **Magnt** exhibited a cloud point when heated from 30 to approximately 80 °C (see Fig. 1-11). The LCST values of *t*-butyl alcohol solutions with concentrations of 4 $gdm^{-3}$ of the nanocomposites in Table 1-3 were measured, and results are shown in Fig. 1-12.

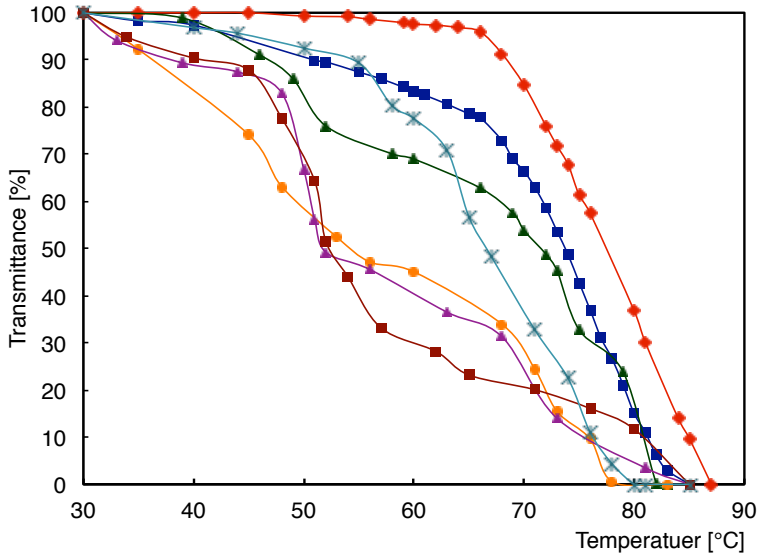


| Run [1] | Contents of **Magnt** [2] (%) | LCST [3] (°C) |
|---|---|---|
| — | 0 | 78 |
| 9 | 2 | 71 |
| 10 | 13 | 74 |
| 11 | 10 | 67 |
| 12 | 15 | 52 |
| 13 | 17 | 52 |
| 14 | 19 | 53 |

Fig. 1-12 Temperature dependence of transmittance at 500 nm for *t*-butyl alcohol solutions of 4 gdm$^{-3}$ $R_F$-$(AMPS)_x$-$(Ad\text{-}HAc)_y$-$R_F$ co-oligomeric nanocomposite-encapsulated **Magnt**.

[1]Each run corresponds to the runs in Table 1-3.

[2]Contents of **Magnt** in nanocomoposites was determined by thermogravimetric analyses.

[3]Defined by the temperature where the transmittance was 50%.

A phase separation in each nanocomposite was found to occur between 52 and 74 °C, at which point the solubility of the nanocomposites altered sharply. The relationship between the LCSTs and the **Magnt** contents in the nanocomposites is shown in Fig. 1-12. The encapsulation of **Magnt** into fluorinated betaine-type cooligomeric nanoparticles can effectively decrease the LCST from 78 to approximately 52 °C. The LCSTs were found to decrease with an increase in **Magnt** contents in the nanocomposite particles. Above a contents of 15 %, the LCST remained nearly constant. Such an effective decrease in the LCST by the encapsulation of **Magnt** is due to the magnetic interaction in each fluorinated nanocomposite particle. It is believed that this is the first example of the effective the LCST control governed

by the magnetic interaction derived from nanocomposite-encapsulated **Magnt**.

## 1.4. Conclusion

In summary, novel crosslinked fluorinated co-oligomeric nanocomposite-encapsulated **Magnt** could be prepared by the deprotecting reactions of the corresponding fluoroalkyl end-capped co-oligomers in the presence of **Magnt**. The fluorinated nanocomposite-encapsulated **Magnt** particles were applied as a surface modification to PMMA and exhibited not only good oleophobicity imparted by the end-capped fluoroalkyl groups but also magnetic properties related to the **Magnt** in the composites. Novel fluorinated betaine-type co-oligomeric nanocomposite-encapsulated **Magnt** was also prepared under very mild conditions. These fluorinated nanocomposite-encapsulated **Magnt** particles were found to exhibit the LCST behavior in *t*-butyl alcohol, and the magnetic interaction present effectively decreased the LCST compared with parent fluorinated betaine-type co-oligomeric nanoparticles without **Magnt**. Moreover, it was demonstrated that magnetic nanoparticles can be encapsulated inside the crosslinked fluorinated co-oligomeric nanoparticle cores. In contrast, magnetic nanoparticles were adsorbed outside the fluorinated betaine-type co-oligomeric nanoparticle cores. In this way, the fluorinated co-oligomers/**Magnt** nanocomposites that is presented in this study have high potential for use in new fluorinated polymeric functional materials, serving as surface modifications of wallpaper and textiles,

allowing for surface-active characteristics imparted by fluorine, as well as magnetic properties.

**References**


1) D. L. Huber, *Small*, **1**, 482 (2005).

2) J. Roger, J. N. Pons, R. Massart, A. Halbreich, and J. C. Bacri, *Eur. Phys. J. Apply. Phys.*, **5**, 321 (1999).

3) D. E. Speliotis, *J. Magn. Magn. Mater.*, **193**, 29 (1999).

4) J. M. D. Coey, *J. Magn. Magn. Mater.*, **196–197**, 1 (1999).

5) K. O'Grady and H. Laidler, *J. Magn. Magn. Mater.*, **200**, 616 (1999).

6) S. A. M. Tofail, I. Z. Rahman, and M. A. Rahman, *Appl. Organometal. Chem.*, **15**, 373 (2001).

7) J. M. Perez, F. J. Simeone, A. Tsourkas, L. Josephson, and R. Weissleder, *Nano Lett.*, **4**, 119 (2004).

8) U. O. Hafeli, *Int. J. Pharma.*, **277**, 19–24 (2004).

9) U. T. Bornscheuer, *Angew. Chem. Int. Ed. Eng.*, **42**, 3336 (2003).

10) J. Kim, J. D. Lee, H. B. Na, B. C. Kim, J. K. Youn, J. H. Kwak, K. Moon, E. Lee, J. Kim, J. Park, A. Dohnalkova, H. G. Park, M. B. Gu, H. N. Chang, J. W. Grate, and T. Hyeon, *Small*, **1**, 1203 (2005).

11) T. Yoshino, H. Hirabe, M. Takahashi, M. Kuhara, H. Takeyama, & T. Matsunaga, *Biotech. Bioeng.,* **101**, 470 (2008).

12) J. Dobson, *Drug Develop. Res.*, **67**, 55 (2006).

13) J. Kim, J. E. Lee, S. H. Lee, J. H. Yu, J. H. Lee, T. G. Park, and T. Hyeon, *Adv. Mater.*, **20**, 478 (2008).

14) S.-H. Hu, D.-M. Liu, W.-L. Tung, C.-F. Liao, and S.-Y. Chen, *Adv. Funct. Mater.*, **18**, 2946 (2008).

15) S. C. Wuang, K. G. Neoh, E.-T. Kang, D. W. Pack, and D. E. Leckband, *Adv. Funct. Mater.*, **16**, 1723 (2006).

16) V. Salgueirino-Maceira and M. A. Correa-Duarte, *Adv. Mater.*, **19**, 4131 (2007).

17) D. Shi, H. S. Cho, Y. Chen, H. Xu, H. Gu, J. Lian, W. Wang, G. Liu, C. Huth, L. Wang, R. C. Ewing, S. Budko, G. M. Pauletti, and Z. Dong, *Imaging and Hyperthermia.*, **21**, 2170 (2009).

18) P.-C. Lin, P.-H. Chou, S.-H. Chen, H.-K. Liao, K.-Y. Wang, Y.-J. Chen, and C.-C. Lin, *Small*, **2**, 485 (2006).

19) B. Srinivasan and X. Huang, *Chirality*, **20**, 265 (2008).

20) L. Li, X. He, L. Chen, and Y. Zhang, *Chem. Asian J.*, **4**, 286 (2009).

21) J. Gao, L. Li, P.-L. Ho, G. C. Mak, H. Gu, and B. Xu, *Adv. Mater.*, **18**, 3145 (2006).

22) B. H. Sohn and R. E. Cohen, *Chem. Mater.*, **9**, 264 (1997).

23) B. Lindlar, M. Boldt, S. Eiden-Assmann, and G. Maret, *Adv. Mater.*, **14**, 1656 (2002).

24) C. Flesch, Y. Unterfinger, E. Bourgeat-Lami, E. Duguet, C. Delaite, and P. Dumas, *Macromol. Rapid Commun.*, **26**, 1494 (2005).

25) W.-C. Wang, K.-G. Neoh, and E.-T. Kang, *Macromol. Rapid Commun.*, **27**, 1665 (2006).

26) I. Garcia, N. E. Zafeiropoulos, A. Janke, A. Tercjak, A. Eceiza, M. Stamm, and I. Mondragon, *J. Polym. Sci. Part A: Polym. Chem.*, **45**, 925 (2007).

27) G. Qiu, Q. Wang, and M. Nie, *Macromol. Mater. Eng.*, **291**, 68 (2006).

28) G. Song, J. Bo, and R. Guo, *Colloid Polym. Sci.*, **282**, 656 (2004).

29) I. Dumazet-Bonnamour and P. L. Perchec, *Colloid Surfaces A: Phys. Eng. Aspects*, **173**, 61 (2000).

30) M. Kryszewskia and J. K. Jeszkab, *Synthetic Metals*, **94**, 99 (1998).

31) M. T. Nguyen and A. F. Diaz, *Adv. Mater.*, **6**, 858 (1994).

32) T. Imae, *Curr. Opinion Colloid Interface Sci.*, **8**, 307 (2003).

33) H. Yoshioka, M. Suzuki, M. Mugisawa, N. Naitoh, and H. Sawada, *J. Colloid Interface Sci.*, **308**, 4 (2007).

34) H. Yoshioka, T. Narumi, and H. Sawada, *J. Oleo Sci.*, **56**, 377 (2007).

35) H. Yoshioka, K. Ohnishi, and H. Sawada, *J. Fluorine Chem.*, **128**, 1104 (2007).

36) H. Sawada, H. Yoshioka, T. Kawase, K. Ueno, and K. Hamazaki, *J. Fluorine Chem.*, **126**, 914 (2005).

37) H. Sawada, *Chem. Rev.*, **96**, 1779 (1996).

38) H. Sawada, *J. Fluorine Chem.*, **101**, 315 (2000).

39) H. Sawada, *Prog. Polym. Sci.*, **32**, 509 (2007).

40) H. Sawada, *Polym. J.*, **39**, 637 (2007).

41) M. Mugisawa, K. Ueno, K. Hamazaki, and H. Sawada, *Macromol. Rapid Commun.*, **28**, 733 (2007).

42) M., Mugisawa, R. Kasai, and H. Sawada, *Langmuir*, **25**, 415 (2009).

43) M. Mugisawa, K. Ohnishi, and H. Sawada, *Langmuir*, **23**, 5848 (2007).

44) M. Mugisawa and H. Sawada, *Langmuir*, **24**, 9215 (2008).

45) M.-H. Liao, K.-Y. Wu, and D.-H. Chen, *Chem. Lett.*, **32**, 488 (2003).

46) S.-Y. Mak and D.-H. Chen, *Macromol. Rapid Commun.*, **26**, 1567 (2005).

47) N. Joumaa, P. Toussay, M. Lansalot, and A. Elaissari, J. *Polym. Sci. Part A: Polym. Chem.*, **46**, 327 (2008).

48) R. Matsuno, K. Yamamoto, H. Otsuka, and A. Takahara, *Chem. Mater.*, **15**, 3 (2003).

49) R. Matsuno, K. Yamamoto, H. Otsuka, and A. Takahara, *Macromolecules*, **37**, 2203 (2004).

50) M. D. C. Topp, P. J. Dijkstra, H. Talsma, and J. Feijen, *Macromolecules*, **30**, 8518 (1997).

51) H.-H. Lin and Y.-L. Cheng, *Macromolecules*, **34**, 3710 (2001).

52) T. Ueki and M. Watanabe, *Langmuir*, **23**, 988–990 (2007).

CHAPTER 2

# Controlled Immobilization of Palladium Nanoparticles in Two Different Fluorinated Polymeric Aggregate Cores and Their Application in Catalysis

## 2.1. Introduction

Polymer nanocomposites have recently received considerable attention as multifunctional hybrid materials. [1 ~ 6] Especially, metal nanoparticles in polymer composites can exhibit different properties in comparison to their bulk materials. [7, 8] Metal nanoparticles of noble metals such as platinum and palladium are ideally suited as catalysts because of their high surface-to-volume ratio. [9, 10] In these noble metals, palladium is of tremendous commercial interest due to its catalytic properties, as well as its considerable affinity for hydrogen in gas-separation membranes and fuel cells. [11, 12] However, primary metal nanoparticles are difficult to handle or recycle and may coagulate. Thus, metal nanoparticles must be stabilized in solution in order to prevent flocculation of the nanoparticles. In this respect, formation of metal nanoparticles is usually carried out by reducing metal ions in the presence of stabilizers such as block copoymer micelles, dendrimers, microgels, and latex particles, which prevent the nanoparticles from aggregation and serve as carriers. [13 ~ 18] In fact, there have been a variety of studies on the spherical polyelectrolyte brushes, which are applicable to the immobilization and stabilization of metal nanoparticles. [19 ~ 22] From the developmental viewpoints of novel polymeric surfactants as carriers for catalytically active metal nanoparticles, it is of particular interest to apply fluorinated polymeric surfactants possessing a

high surface active characteristic imparted by fluorine as a carrier for metal nanoparticles; however, these studies have been hitherto very limited except for the recent report on the preparation of fluoroalkyl end-capped cooligomeric nanocomposites-encapsulated magnetic nanoparticles.[23] In a wide variety of fluorinated polymeric surfactants, fluoroalkyl end-capped polymers (oligomers) are of particular interest; because fluoroalkyl end-capped oligomers can exhibit a variety of unique properties such as high solubility, surface active properties, biological activities, and the formation of nanometer size-controlled self-assemblies through the aggregation of end-capped fluoroalkyl segments, which cannot be achieved by the corresponding non-fluorinated, randomly fluoroalkylated, and AB block-type fluoroalkylated ones.[24 ~ 27] In this chapter, two different fluorinated polymers: two fluoroalkyl end-capped sulfobetaine-types cooligomers containing adamantyl segments and outer blocks of poly(2,3,4,5,6-pentafluorostyrene)-containing ABA-triblock copolymers are applied to the preparation of colloidal stable palladium nanoparticles. The object of this study is also to investigate the different immobilization behaviors of growing palladium nanoparticles in two types of these fluorinated composite cores. In addition, these two different immobilized palladium nanoparticles have been apply to Suzuki-Miyaura cross-coupling reaction. These results will be described herein.

## 2.2. Experimental

### 2.2.1 Measurements

NMR spectra were measured using JEOL JNM-400 (400 MHz) FT NMR SYSTEM (Tokyo, Japan). Dynamic light-scattering (DLS) were measured by using Otsuka Electronics DLS-7000 HL (Tokyo, Japan). Molecular weight of $R_F$-(IEM-BO)$_x$-(Ad-HAc)$_y$-$R_F$ cooligomer was measured using a Shodex DS-4 (pump) and Shodex RI-71 (detector) Size Exclusion Chromatography (SEC; Tokyo, Japan) calibrated with polystyrene standard using tetrahydrofuran as the eluent. Molecular weight of PFS*m*-PEGPG-PFS*m* copolymers (see Scheme 3-3) was measured using a Bruker 250 MHz $^1$H NMR spectrometer. X-ray diffractions were measured by using MAC Science SRAM18XHF (Japan). Thermal analyses were recorded on Bruker axs TG-DTA2000SA differential thermobalance (Kanagawa, Japan). Transmission electron micrograph (TEM) was measured by using JEOL JEM-1210 Electron microscope (Tokyo, Japan). High-performance liquid chromatography (HPLC) analyses were conducted on a Shimadzu LC-20AD (Kyoto, Japan) using 95% aqueous methanol solution as the eluent.

### 2.2.2. Materials

2-Acrylamido-2-methylpropanesulfonic acid (AMPS) and palladium chloride were purchased from Tokyo Chemical Industry Co., Ltd. (Tokyo, Japan) and Kanto Chemical Co., Inc. (Tokyo, Japan), respectively. Isocyanatoethyl methacrylate 2-butanone oxime adduct (IEM-BO) was obtained from Showa Denko Co., Ltd. (Tokyo, Japan). 1-Hydroxy-5-adamantylacrylate (Ad-HAc) was used as received from Idemitsu Kosan Co., Ltd. (Tokyo, Japan). The bifunctional hydroxyl terminated random copolymer of 75 wt.% ethylene glycol (EG) and 25 wt.% propylene glycol (PG) (PEGPG) was used to design and synthesize two kinds of amphiphilic outer blocks of poly(2,3,4,5,6-pentafluorostyrene) (PFS)-containing ABA-triblock copolymers with different lengths. Detailed description of the synthesis of such ABAtriblock copolymers based on polyethers and PFS is given in the refereces: 28 ~ 30.

### 2.2.3. Preparation of fluoroalkyl end-capped betaine-type cooligomeric nanocomposites-encapsulated palladium nanoparticles

A typical procedure for the preparation of fluoroalkyl end-capped betaine-type

cooligomeric nanocomposites-encapsulated palladium nanoparticles by the use of α,ω-bis (perfluoro-1-methyl-2-oxapentylated) 2-acrylamido-2-methylpropanesulfonic acid–1-hydroxy-5-adamantylacrylate cooligomer [$R_F$-(AMPS)$_x$-(Ad-HAc)$_y$-$R_F$; $R_F$ = $CF(CF_3)OC_3F_7$; $x/y$ = 11/89; molecular weight of this cooligomer cannot be determined by SEC due to the formation of nanoparticles] is as follows: To a methanol (16 mL) solution of palladium chloride (680 mmol) and sodium chloride (700 mmol) was added $R_F$-(AMPS)$_x$-(Ad-HAc)$_y$-$R_F$ cooligomer (16 mg), which was prepared by the cooligomerization of fluoroalkanoyl peroxide with the corresponding monomers according to the previously reported method. [31] The mixture was stirred with a magnetic stirring bar at room temperature for 12 h. Sodium acetate (8,540 mmol) was added to the above described solution, and then this solution was stirred for 3 h at room temperature. After the centrifugal separation (2,000 rpm/30 min) of this mixture at room temperature, the supernatant solution was dialyzed in water at room temperature for 1 day. The solution was evaporated under reduced pressure to give the expected palladium nanocomposites. Fluorinated nanocomposite powders thus obtained were dried in vacuo at 50 °C for 2 days to yield purified fluorinated betaine-type cooligomeric nanocomposite-immobilized palladium nanoparticles [$R_F$-(AMPS)$_x$-(Ad-HAc)$_y$-$R_F$/Pd] (64 mg, Run 1 in Table 2-1). Other $R_F$-(AMPS)$_x$-(Ad-HAc)$_y$-$R_F$ cooligomeric nanocomposites-immobilized palladium

nanoparticles were prepared under similar conditions (Runs 2~8 in Table 2-1).

In addition, the cross-linked fluoroalkyl end-capped cooligomeric nanocomposites-encapsulated palladium nanoparticles were tried to prepare under similar conditions. The preparative method is as follows: To an *N*,*N*-dimethylformamide (DMF; 10 mL) solution of α,ω-bis(perfluoro-1-metyl-2-oxapentylated) isocyanatoethyl methacrylate 2-butanone oxime adduct–1-hydroxy-5-adamantylacrylate cooligomer [$R_F$-(IEM-BO)$_x$-(Ad-HAc)$_y$-$R_F$; $R_F$ = $CF(CF_3)OC_3F_7$; x/y = 21 : 79; Mn = 2,600] (2.0 g), which was prepared by the cooligomerization of the corresponding monomers with fluoroalkanoyl peroxide according to the previously reported method, [32, 33] were added palladium chloride (680 mmol) and sodium chloride (700 mmol). The mixture was stirred at room temperature for 2 days under ultrasonic irradiation conditions. Sodium acetate (8,540 mmol) was added to the above-described solution, and then this solution was stirred for 3 h at room temperature. The obtained solution was stirred with a magnetic bar at 130 °C for 1 h. Methanol (20 mL) was added to this reaction mixture, and this mixture was stirred well for 30 min at room temperature. After the centrifugal separation (2,000 rpm/30 min) of the mixture at room temperature, the supernatant solution was dialyzed in water at room temperature for 1 day; in contrast, the precipitate was dried in vacuo at 50 °C for 2 days to give palladium powders. The dialyzed solution was evaporated under reduced pressure. The isolated crude

product was reprecipitated from methanol–acetone; however, the expected cross-linked fluorinated cooligomeric nanocomposites-immobilized palladium nanoparticles [$R_F$-(IEM)$_x$-(Ad-HAc)$_y$-$R_F$/Pd] were not isolated at all (Run 9 in Table 2-2). Other fluorinated nanocomposites-immobilized palladium nanoparticles in Table 2-2 were also tried to prepare under similar conditions.

### 2.2.4. Preparation of PFS*m*-PEGPG-PFS*m* copolymeric nanocomposites-immobilized palladium nanoparticles

A typical procedure for the preparation of PFS*m*-PEGPG-PFS*m* nanocomposites-immobilized palladium nanoparticles by the use of [PFS*m*-PEGPG-PFS*m*; *m* = 24, 12] is as follows: A methanol (8 mL) solution of palladium chloride (340 mmol) and sodium chloride (350 mmol) was added with PFS*m*-PEGPG-PFS*m* (*m* = 24) copolymer (24 mg), which was prepared by atom transfer radical polymerization according to the previously reported methods. [28 ~ 30] The mixture was stirred with a magnetic stirring bar at room temperature for 12 h. Sodium acetate (4,270 mmol) was added to the above described solution, and then this solution was stirred for 3 h at room temperature. After the centrifugal separation (2,000 rpm/30 min) of this solution at room temperature, the supernatant solution was dialyzed

in water for 1 day at room temperature. The solution was evaporated under reduced pressure to give the expected palladium nanocomposites. Fluorinated nanocomposite powders thus obtained were dried in vacuo at 50 °C for 2 days to yield purified PFS*m*-PEGPG-PFS*m* [*m* = 24] copolymeric nanocomposites-immobilized palladium nanoparticles [PFS*m*-PEGPG-PFS*m* /Pd] (64 mg, Run 15 in Table 2-3). Other PFS*m*-PEGPG-PFS*m* copolymeric nanocomposites-immobilized palladium nanoparticles were also prepared under similar conditions (Run 16 in Table 2-3).

### 2.2.5. Suzuki-Miayura cross-coupling reaction

A DMF solution (5 mL) containing bromobenzene (1 mmol), phenylboronic acid (1.5 mmol), $R_F$-$(AMPS)_x$-$(Ad\text{-}HAc)_y$-$R_F$/Pd nanocomposites (17 mg, 0.1 mmol of Pd), and $K_2CO_3$ (2 mmol) were added to a 20 mL round-bottomed flask fitted with a reflux condenser. The mixture was stirred with a magnetic stirring bar at 100 °C for 8 h. After cooling to room temperature, $H_2O$ (5 mL) and $ClCH_2CH_2Cl$ (10 mL) were added to this mixture. The organic layer was washed with $H_2O$ and $ClCH_2CH_2Cl$. The product yield was calculated based on the consumed bromobenzene using HPLC analysis (87 %, Run 17 in Table 2-4). After centrifugal separation of this mixture, the recovered nanocomposites were then washed with $H_2O$ and

$ClCH_2CH_2Cl$, dried in vacuo at room temperature and reused for catalyst under similar conditions (Run 20 in Table 2-5). Suzuki–Miyaura cross-coupling reaction catalyzed by PFS*m*-PEGPG-PFS*m*/Pd nanocomposites was carried out under similar conditions (Runs 18 and 19 in Table 2-4) and these nanocomposites were reused for catalyst under similar conditions (Run 21 in Table 2-4).

## 2.3. Results and discussion

### 2.3.1. Preparation and property of novel fluoroalkyl end-capped betaine-type cooligomeric nanocomposites-encapsulated palladium nanoparticles

It have been recently reported that two fluoroalkyl end-capped sulfobetaine-type cooligomers containing adamantyl segments can form the nanometer size-controlled fine particles in aqueous and organic media. [31] In the case of fluoroalkyl end-capped sulfobetaine-type homooligomers possessing no adamantly segments, these fluorinated homooligomers can form the gels through the synergistic effect between the aggregation of end-capped fluoroalkyl groups and ionic interaction of sulfobetaine-type segments. [34] However, the introduction of bulky substituents such as adamantyl segments in the main chain of fluoroalkyl end-capped AMPS oligomers can afford not gels but the cooligomeric nanoparticles due to the presence of bulky adamantly segments. Thus, palladium nanoparticles were tried to immobilize into fluoroalkyl end-capped cooligomeric betaine-type nanoparticle cores. In fact, as shown in Scheme 1 and Table 1, fluorinated sulfobetaine-type cooligomeric nanocomposites-immobilized palladium nanoparticles were succeeded in preparing in 33 ~ 83 % isolated yields by the reduction of palladium chloride with sodium acetate in the presence of sodium chloride and the corresponding cooligomeric nanoparticles.

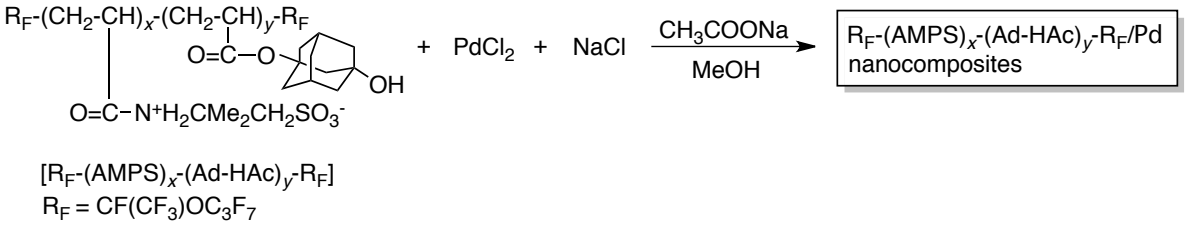


Scheme 2-1

Table 2-1 Preparation of $R_F$-$(AMPS)_x$-$(Ad$-$HAc)_y$-$R_F$ cooligomeric nanocomposite-immobilized palladium nanoparticles

| Run | $R_F$-$(AMPS)_x$-$(Ad$-$HAc)_y$-$R_F$ | | $PdCl_2$ | NaCl | $CH_3COONa$ | MeOH | Product yields[b] | Size of dispersed nanocomposites[c] | Size of redispersed nanocomposites[c] | Contents of palladium in nanocomposites[d] |
|---|---|---|---|---|---|---|---|---|---|---|
| | (mg) | [$x$/$y$][a] | ($\mu$mol) | ($\mu$mol) | ($\mu$mol) | (mL) | (%) | (nm) | (nm) | (%) |
| 1 | 16 | [11 : 89] | 680 | 700 | 8540 | 16 | 72 | 44 ± 5.1 | 60 ± 9.6 | 84 |
| 2 | 32 | | | | | | 64 | 49 ± 4.8 | 60 ± 10.7 | 81 |
| 3 | 48 | | | | | | 65 | 36 ± 2.3 | 70 ± 12.8 | 68 |
| 4 | 64 | | | | | | 60 | 65 ± 17.1 | 119 ±18.1 | 61 |
| 5 | 80 | | | | | | 44 | 86 ± 21.5 | 148 ± 33.3 | 33 |
| 6 | 96 | | | | | | 33 | 139 ± 21.8 | 140 ± 27.1 | 45 |
| 7 | 64 | [44 : 56] | 680 | 700 | 8540 | | 50 | 118 ± 28.3 | 56 ± 10.3 | 50 |
| 8 | 48 | | 68 | 70 | 854 | | 83 | 134 ± 30.0 | 179 ± 37.3 | 83 |

[a] Cooligomerization ratio ($x$/$y$) determined by $^1$H NMR.
[b] Yields were based on $R_F$-$(AMPS)_x$-$(Ad$-$HAc)_y$-$R_F$ and $PdCl_2$.
[c] Determined by dynamic light scattering measurements in methanol.
[d] Contents of palladium were determined by thermogravimetric analyses.

As shown in Table 2-1, the yields of fluoroalkyl end-capped sulfobetaine-type cooligomeric nanocomposites-immobilized palladium nanoparticles [$R_F$-$(AMPS)_x$-$(Ad$-$HAc)_y$-$R_F$/Pd nanocomposites] obtained are in general dependent upon the feed ratios of $R_F$-$(AMPS)_x$-$(Ad$-$HAc)_y$-$R_F$ cooligomer and palladium chloride employed, decreasing with greater feed ratios of $R_F$-$(AMPS)_x$-$(Ad$-$HAc)_y$-$R_F$ cooligomeric nanoparticles. This finding suggests that the formation of the expected fluorinated palladium nanocomposites is essential for the ionic interaction between palladium chloride and sulfobetaine-type segments in fluorinated cooligomer.

$R_F$-(AMPS)$_x$-(Ad-HAc)$_y$-$R_F$/Pd nanocomposites in Table 2-1 exhibited a good dispersibility and redispersibility not only in traditional organic solvents such as methanol, ethanol, dimethyl sulfoxide (DMSO), and *N*,*N*-dimethylformamide but also in water. Thus, the size of $R_F$-(AMPS)$_x$-(Ad-HAc)$_y$-$R_F$/Pd nanocomposites in methanol have been measured by the use of dynamic light-scattering measurements at 25 °C, and the size of these composites was found to be nanometer size-controlled (36 ~ 139 nm). The size of the nanocomposites was increased from 44 to 139 nm with the increase of the amounts of the used fluorinated cooligomeric nanoparticles from 16 to 96 mg as in Table 2-1. In contrast, the size of the composites was in general decreased from 139 or 86 to 60 nm with the increase of the contents of palladium nanoparticles in the composites from 45 % or 33 % to 84 % (see Table 2-1). These findings suggest that such increase of the size of $R_F$-(AMPS)$_x$-(Ad-HAc)$_y$-$R_F$/Pd nanocomposites would be due to the more effective interaction of original $R_F$-(AMPS)$_x$-(Ad-HAc)$_y$-$R_F$ cooligomeric nanoparticles in each other, compared to that of $R_F$-(AMPS)$_x$-(Ad-HAc)$_y$-$R_F$/Pd nanocomposites, of whose contents of palladium nanoparticles are relatively higher in the nanocomposites. Interestingly, isolated fluorinated nanocomposite powders in Table 2-1 were found to exhibit a superior redispersibility and stability in methanol, and the size of each particle showed a monodispersed characteristic.

In order to clarify the presence of palladium particles in the composites, thermal stability

of $R_F$-$(AMPS)_x$-$(Ad\text{-}HAc)_y$-$R_F$/Pd nanocomposites in Table 2-1 was studied by thermogravimetric analyses (TGA), in which the weight loss of these nanocomposites was measured by raising the temperature around 800 °C (the heating rate, 10 °C $min^{-1}$) in air atmosphere and the results are also shown in Table 2-1 and Figs. 2-1 and 2-2.

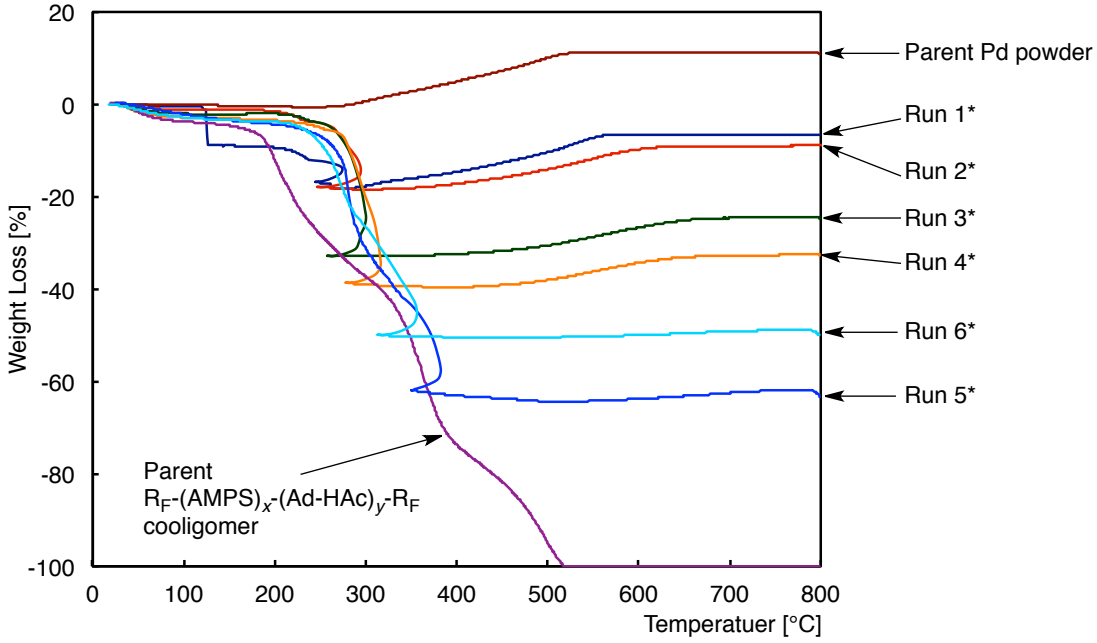


Fig. 2-1 Thermogravimetric analyses of palladium, $R_F$-$(AMPS)_x$-$(Ad\text{-}HAc)_y$-$R_F$/Pd nanocomposites (Runs 1* ~ 6*), parent $R_F$-$(AMPS)_x$-$(Ad\text{-}HAc)_y$-$R_F$ cooligomeric nanoparticles [$x$ : $y$ = 11: 89], and parent palladium powder.
*Each run corresponds to the runs in Table 2-1.

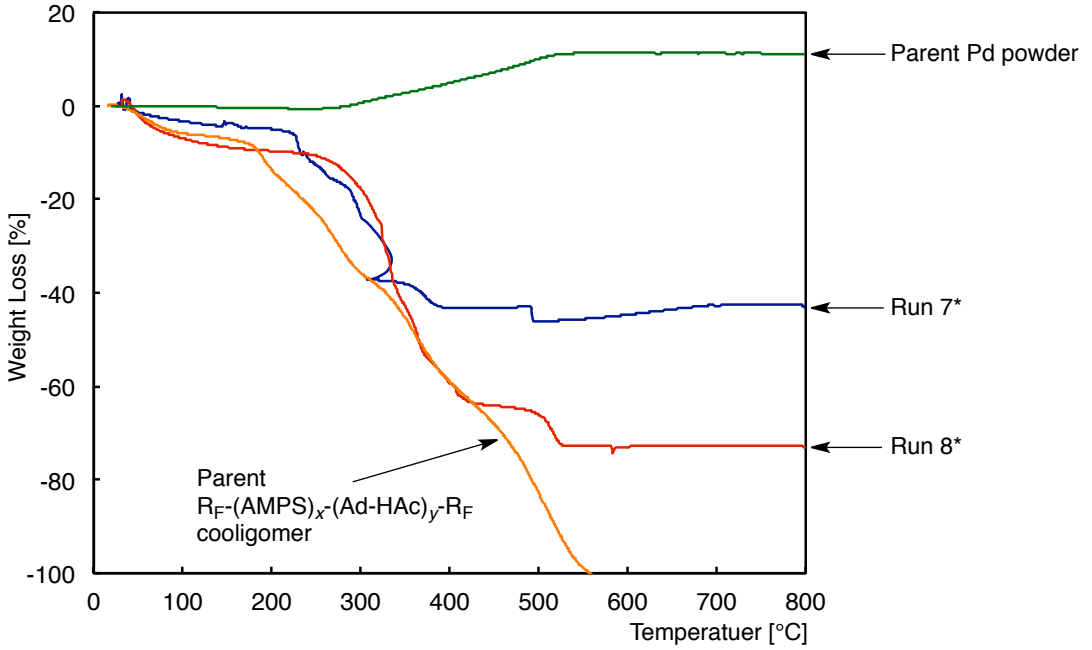


Fig. 2-2 Thermogravimetric analyses of palladium, $R_F$-(AMPS)$_x$-(Ad-HAc)$_y$-$R_F$/Pd nanocomposites (Runs 7* and 8*), parent $R_F$-(AMPS)$_x$-(Ad-HAc)$_y$-$R_F$ cooligomeric nanoparticles [$x$ : $y$ = 44: 56], and parent palladium powder.
*Each run corresponds to the runs in Table 2-1.

The contents of palladium particles in the nanocomposites in Table 1 were estimated to be 33 ~ 84 % by the use of thermogravimetric analyses (TGA data are shown in Figs. 2-1 and 2-2), and the contents of palladium particles in the composites were found to decrease from 84 % to 33 % with increasing the feed amounts of fluorinated cooligomer from 16 to 80 mg. This finding suggests that the used palladium chloride would react effectively with sodium acetate in the neighborhood of the sulfobetaine-type segments in fluorinated cooligomeric nanoparticles through the ionic interaction between palladium cations and anionic moieties in sulfobetaine segments to afford the expected palladium nanoparticles. A similar study on the formation of palladium nanoparticles by the reactions of palladium chloride with sodium

acetate has been already reported, and palladium nanoparticles were obtained in quantitative yields. [35] X-ray diffraction (XRD) patterns of the present fluorinated nanocomposites-immobilized palladium particles exhibit a similar characteristic to that of the parent palladium powders, indicating the formation of palladium particles in the nanocomposites (see Fig. 2-3).

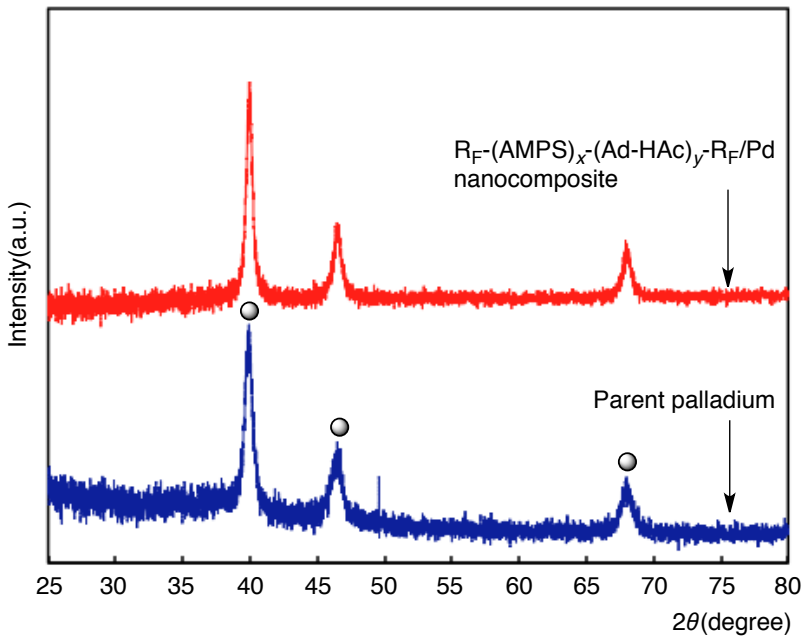


Fig. 2-3 X-ray diffraction patterns of parent palladium and $R_F$-(AMPS)$_x$-(Ad-HAc)$_y$-$R_F$ nanocomposite-immobilized palladium nanoparticles (Run 3 in Table 2-1).

In order to confirm in detail the presence of immobilized palladium particles in the fluorinated nanoparticle cores, transmission electron microscopy (TEM) photographs of methanol solutions of fluorinated coologomeric nanocomposites-immobilized palladium particles (Runs 1, 2, 3, 4, and 7 in Table 2-1) were recorded, and the results were shown in Fig. 2-4.

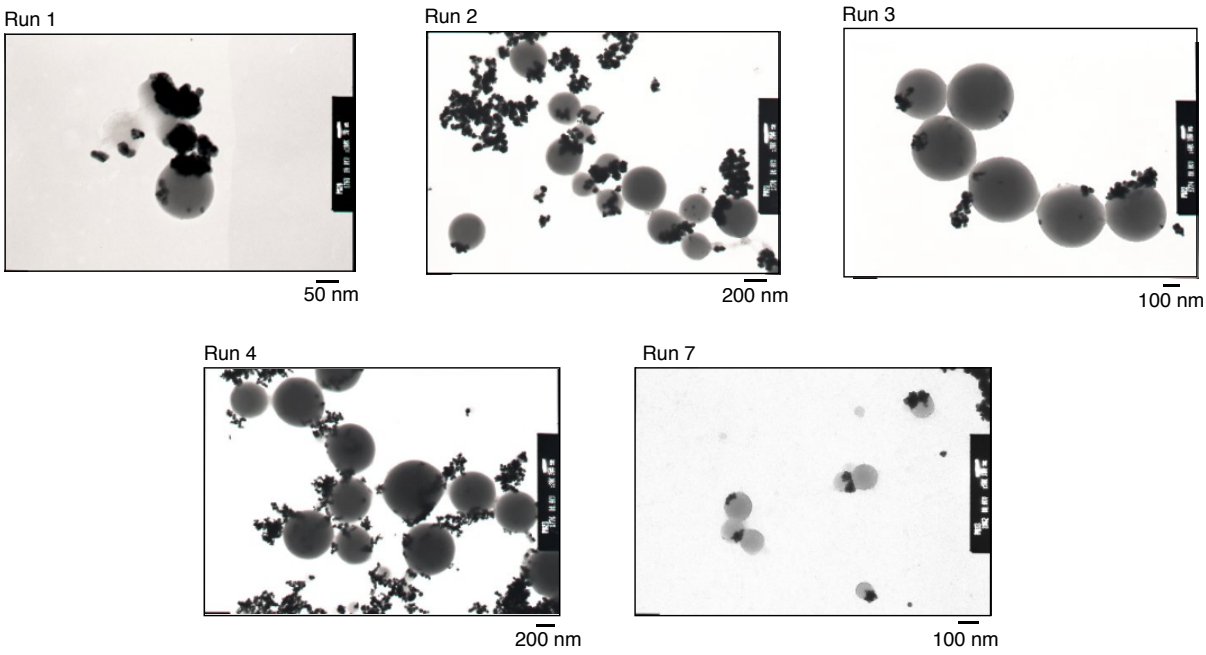


Fig. 2-4 TEM images of $R_F$-$(AMPS)_x$-$(Ad\text{-}HAc)_y$-$R_F$ cooligomeric nanocomposite-immobilized palladium nanoparticles (Runs 1, 2, 3, 4, and 7 in Table 2-1) in methanol.

Each electron micrograph shows the formation of fluorinated nanocomposites-immobilized palladium particles (mean diameters of these nanoparticles, 111, 265, 326, 584, and 106 nm). Interestingly, TEM images show that the amounts of palladium particles immobilized in the fluorinated composite cores can decrease effectively (from run 1 to runs 2, 3, 4, and 7) with increasing the feed amounts of fluorinated cooligomeric nanoparticles in the nanocomposites from 16 to 64 mg for the nanocomposite reactions in Scheme 2-1 and Table 2-1 (see Fig. 2-4).

More interestingly, palladium nanoparticles can be immobilized outside the cooligomeric particle cores through the effective coordinate binding interaction between the

sulfobetaine-type segments in cooligomers and palladium nanoparticles, because palladium nanoparticles should be effectively formed by the reduction of palladium cations with sodium acetate through the ionic interaction between palladium chloride and anionic moieties in sulfobetaine segments outside the fluorinated cooligomeric nanocomposite cores.

The deprotecting reactions of fluoroalkyl end-capped isocyanatoethyl methacrylate 2-butanone oxime adduct–1-hydroxy-5-adamantylacrylate cooligomers [$R_F$-(IEM-BO)$_x$-(Ad-HAc)$_y$-$R_F$] in the presence of magnetic nanoparticles were applied to the preparation of cross-linked fluoroalkyl end-capped cooligomeric nanocomposites-encapsulated magnetic nanoparticles. [23] Thus, fluoroalkyl end-capped cooligomeric nanocomposites-immobilized palladium nanoparticles were tried to prepare by the cross-linking reactions with $R_F$-(IEM-BO)$_x$-(Ad-HAc)$_y$-$R_F$ cooligomer, and the results were shown in Scheme 2-2 and Table 2-2.

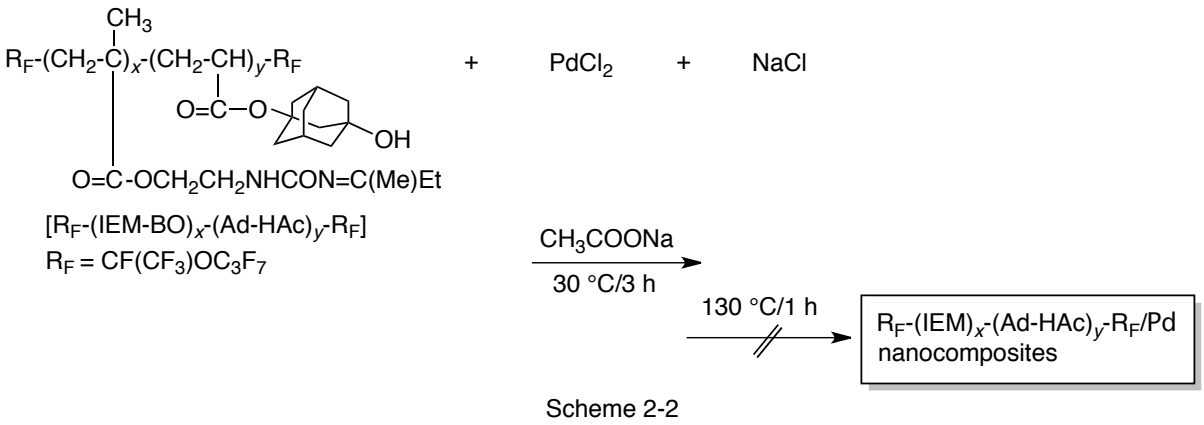


Scheme 2-2

Table 2-2 Preparation of $R_F$-(IEM)$_x$-(Ad-HAc)$_y$-$R_F$ cooligomeric nanocomposites-immobilized palladium nanoparticles

| Run | $R_F$-(IEM-BO)$_x$-(Ad-HAc)$_y$-$R_F$ [Mn = 2600; $x/y$ = 21 : 79 [a)] ] (mg) | $PdCl_2$ ($\mu$mol) | NaCl ($\mu$mol) | $CH_3COONa$ ($\mu$mol) | Product yields[b)] (%) |
|---|---|---|---|---|---|
| 9 | 2000 | 680 | 700 | 8540 | 0 |
| 10 | 1500 | | | | 0 |
| 11 | 1000 | | | | 0 |
| 12 | 500 | | | | 0 |
| 13 | 150 | | | | 0 |
| 14 | 100 | | | | 0 |

[a)]Mn was determined by SEC. Cooligomerization ratio ($x$ : $y$) determined by $^1$H NMR.
[b)]Yields were based on $R_F$-(IEM-BO)$_x$-(Ad-HAc)$_y$-$R_F$ and $PdCl_2$.

However, as shown in Scheme 2-2 and Table 2-2, the expected fluorinated cooligomeric nanocomposites-encapsulated palladium nanoparticles were unable to obtain at all, and only palladium powders were isolated in each case. XRD spectra of the isolated powders are well consistent with that of original palladium ones (see Fig. 2-5). Palladium chlorides would have no ionic interaction with $R_F$-(IEM-BO)$_x$-(Ad-HAc)$_y$-$R_F$ cooligomeric aggregates to afford $R_F$-(IEM)$_x$-(Ad-HAc)$_y$-$R_F$ cooligomer/palladium nanocomposites, because $R_F$-(IEM-BO)$_x$-(Ad-HAc)$_y$-$R_F$ cooligomer possesses no ionic moieties as in Scheme 2-2.

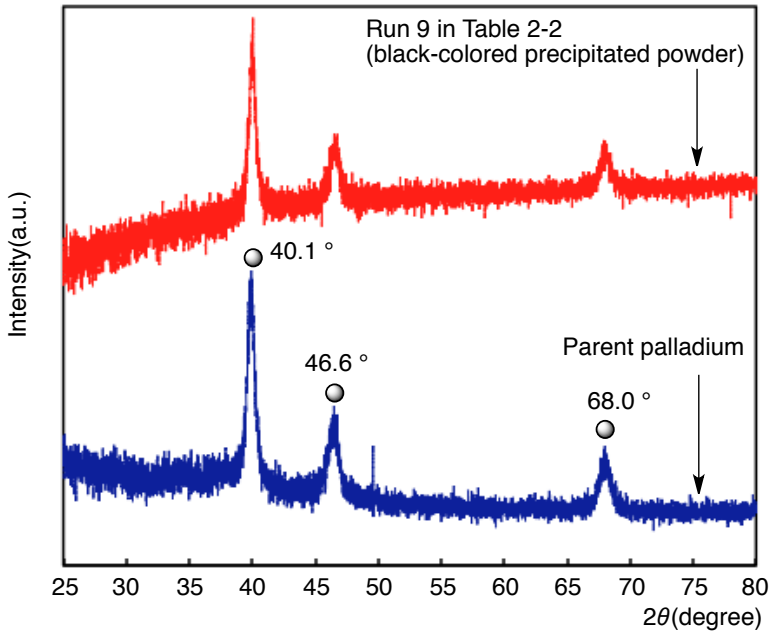


Fig. 2-5 X-ray diffraction patterns of the black-colored precipitated powders, which were obtained by the composite reaction in Run 9 in Table2-2.

### 2.3.2. Preparation and property of novel PFS*m*-PEGPG-PFS*m* copolymeric nanocomposites-immobilized palladium nanoparticles

From these findings, it is of particular interest to apply fluorinated polymers possessing some functional units such as poly(oxyethylene) and poly(2,3,4,5,6-pentafluorostyrene) units, which are likely to interact with palladium particles, to the immobilization of palladium nanoparticles into the corresponding fluorinated polymeric aggregated cores. Especially, it is suggested that the interaction of Pd nanoparticles with π-electrons of pentafluorostyrene units in polymers or ether oxygens in poly(oxyethylene) units in polymers is essential for the immobilization of palladium nanoparticles toward these fluorinated block copolymers.

Fluorinated copolymeric nanocomposites-immobilized palladium nanoparticles were tried to prepare by using outer blocks of poly(2,3,4,5,6-pentafluorostyrene)-containing ABA-triblock copolymers, which possess poly(oxyethylene–oxypropylene) segments in the main chain [PFS*m*-*b*-PEGPG-*b*-PFS*m*; *m* = 24, 12].[28 ~ 30] These results were shown in Scheme 2-3 and Table 2-3.

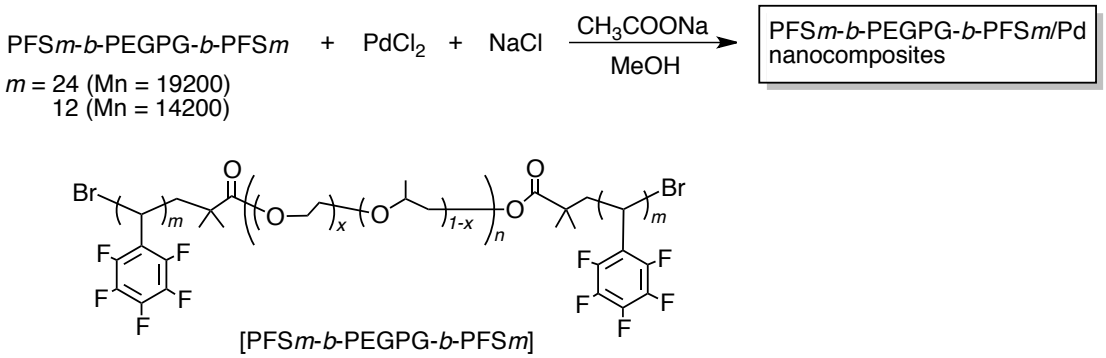


Scheme 2-3

Table 2-3 Preparation of PFE*m*-*b*-PEGPG-*b*-PFS*m* triblock copolymeric nanocomposite-immobilized palladium nanoparticles

| Run | Polymer | (mg) | $PdCl_2$ (μmol) | NaCl (μmol) | $CH_3COONa$ (μmol) | MeOH (mL) | Product yields[a] (%) | Size of redispersed nanocomposites[b] (nm) | Contents of palladium in nanocomposites[c] (%) |
|---|---|---|---|---|---|---|---|---|---|
| 15 | PFS24-*b*-PEGPG-*b*-PFS24 | 24 | 340 | 350 | 4270 | 16 | 53 | 78 ± 13.2 | 66 |
| 16 | PFS12-*b*-PEGPG-*b*-PFS12 | 24 | 340 | 350 | 4270 | 16 | 46 | 132 ± 17.4 | 81 |

[a]Yields were based on PFS24-*b*-PEGPG-*b*-PFS24 or PFS12-*b*-PEGPG-*b*-PFS12 and $PdCl_2$.
[b]Determined by dynamic light scattering measurements in methanol.
[c]Contents of palladium were determined by thermogravimetric analyses.

As shown in Scheme 2-3 and Table 2-3, PFS*m*-*b*-PEGPG-*b*-PFS*m* copolymeric nanocomposites-immobilized palladium nanoparticles have been succeeded in preparing in 53

(*m* = 24) and 46 % (*m* = 12) isolated yields, respectively. The contents of immobilized palladium particles in PFS*m*-*b*-PEGPG-*b*-PFS*m* copolymeric aggregate cores were estimated by the use of TGA analyses, and the contents of encapsulated palladium particles were estimated to be 66 (*m* = 24) and 81 % (*m* = 12), respectively, as shown in Table 2-3 (TGA data: see Figs. 2-6 and 2-7). X-ray diffraction patterns of PFS*m*-*b*-PEGPG-*b*-PFS*m*-immobilized palladium particles (*m* = 24 and 12) exhibited a similar characteristic to that of the parent palladium particles (see Fig. 2-8).

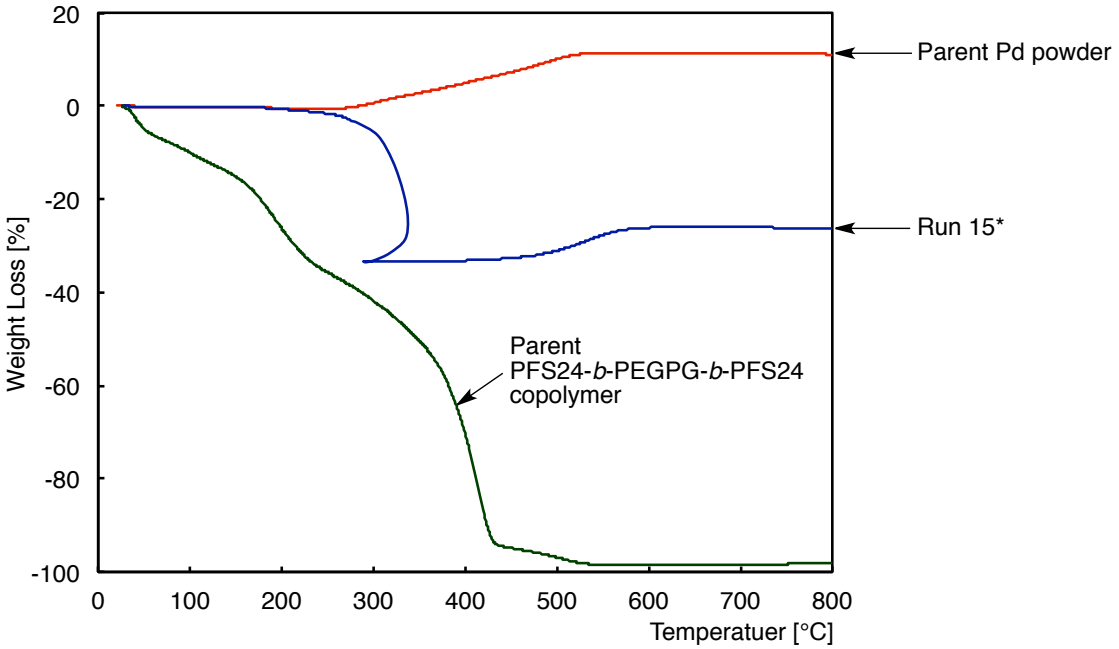


Fig. 2-6 Thermogravimetric analyses of parent palladium powder, PFS24-*b*-PEGPG-*b*-PFS24/Pd nanocomposites (Run 15*), and parent PFS24-*b*-PEGPG-*b*-PFS24 copolymer.
*Run 15 corresponds to that of Table 2-3.

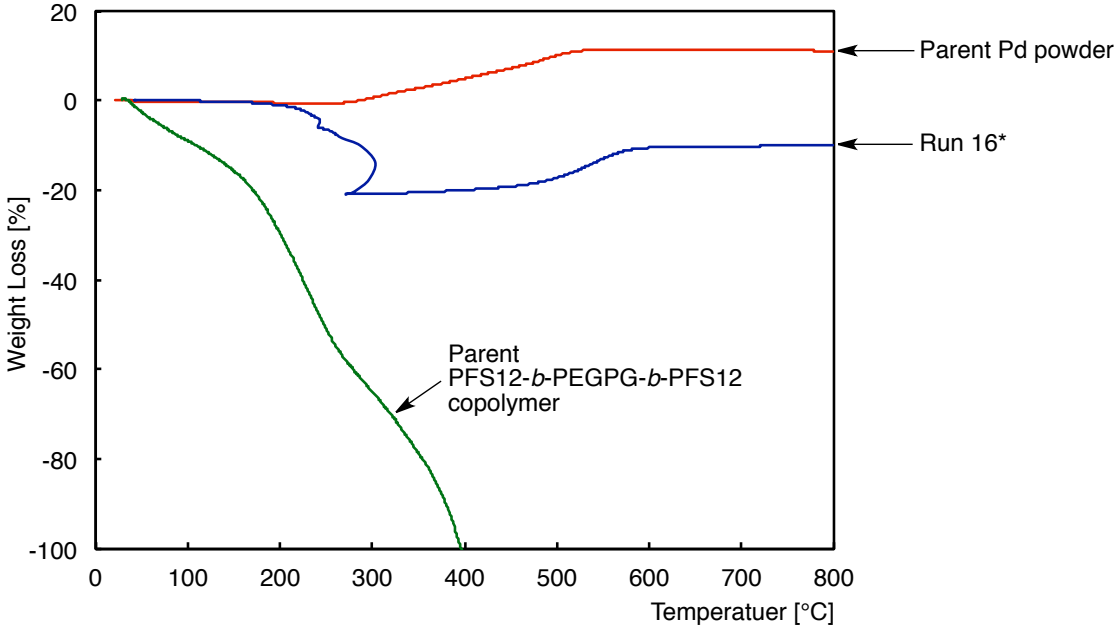


Fig. 2-7 Thermogravimetric analyses of parent palladium powder, PFS12-*b*-PEGPG-*b*-PFS12/Pd nanocomposites (Run 16*), and parent PFS12-*b*-PEGPG-*b*-PFS12 copolymer.
*Run 16 corresponds to that of Table 2-3.

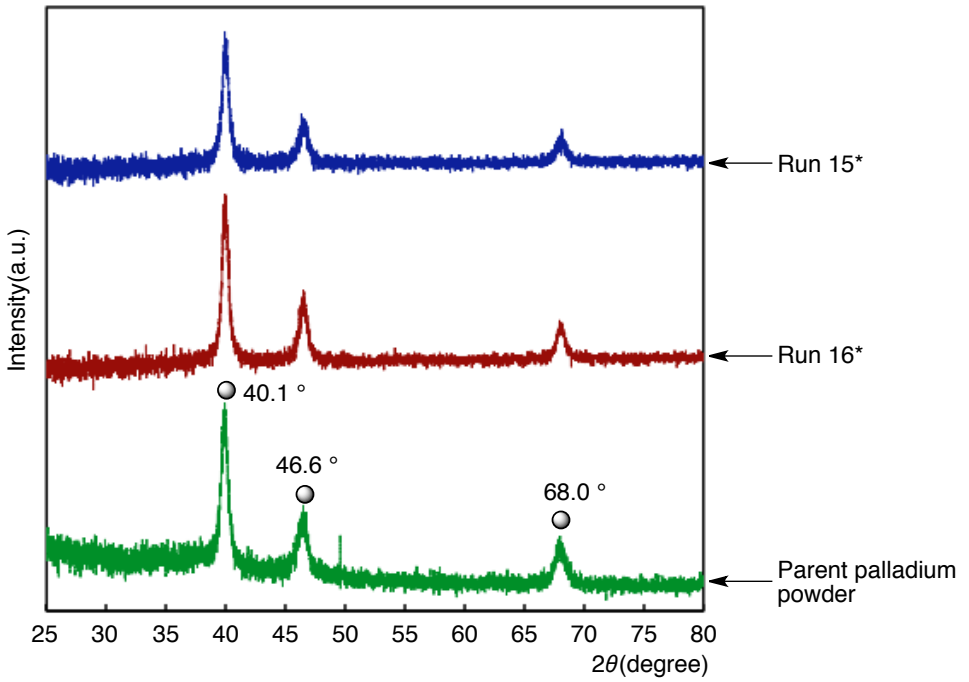


Fig. 2-8 X-ray diffraction patterns of parent palladium powders and PFS*m*-*b*-PEGPG-*b*-PFS*m*/Pd nanocomposites (Runs 15* and 16*)
*Each run corresponds to the runs in Table 2-3.

The present PFS*m*-*b*-PEGPG-*b*-PFS*m*-immobilized palladium particles were found to exhibit a good dispersibility and redispersibility not only in water but also in traditional organic solvents such as methanol, ethanol, acetone, tetrahydrofuran, toluene, benzene, hexane, 1,2-dichloroethane, DMSO, DMF, and fluorinated aliphatic solvents (AK-225; 1:1 mixed solvents of 1,1-dichloro-2,2,3,3,3-pentafluoropropane and 1,3-dichloro-1,2,2,3,3-pentafluoropropane). Thus, the size of PFSm-*b*-PEGPG-*b*-PFSm immobilized palladium particles in methanol solutions has been measured by DLS measurements at 25 °C. These results were also shown in Table 2-3.

The size (number-average diameter) of these fluorinated particles is 78 ~ 132 nm. The size of these fluorinated nanocomposites-immobilized palladium particles was found to decrease effectively from 135 ~ 397 nm to 78 ~ 132 nm after the immobilization of palladium particles into these nanocomposite cores. The decrease of the size of nanocomposites indicates that the immobilization of palladium particles could proceed through an effective interaction between fluorinated copolymeric aggregate cores and palladium particles to yield the expected fluorinated nanocomposites-immobilized palladium particles. Such decrease of the size of nanocomposites after immobilization would be due to the formation of flexible fluorinated block copolymeric composites cores, which are constructed through the fluorophilic–fluorophilic interaction between two end-capped poly(2,3,4,5,6-pentafluorostyrene) units in

block copolymers.

In order to verify the presence of immobilized palladium particles in the fluorinated nanocomposite cores, TEM photograph of methanol solution of fluorinated copolymeric nanocomposite-immobilized palladium particles was measured (Run 16 in Table 2-3), and the result was shown in Fig. 2-9.

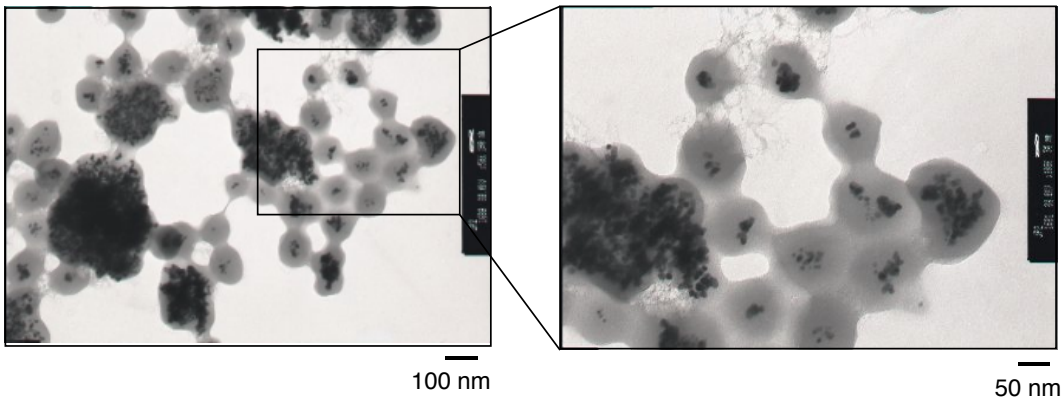


Fig. 2-9 TEM images of PFS12-*b*-PEGPG-*b*-PFS12 copolymeric nanocomposite-immobilized palladium nanoparticles (Run 16 in Table 2-3) in methanol.

The electron micrograph shows that palladium nanoparticles are effectively immobilized inside fluorinated copolymeric aggregate cores (mean diameters of these nanocomposites, 144 nm). This value is quite similar to that of DLS measurements (number-average diameter, 132 ± 17.4 nm) in Table 2-3.

In this way, $R_F$-(IEM-BO)$_x$-(Ad-HAc)$_y$-$R_F$ cooligomer in Scheme 2-2 was not applied to the immobilization of palladium nanoparticles into fluorinated cooligomeric aggregate cores;

however, PFS*m*-*b*-PEGPG-*b*-PFS*m* copolymers were able to interact with palladium chloride to afford PFS*m*-*b*-PEGPG-*b*-PFS*m*-immobilized palladium nanoparticles. These findings suggest that PFS*m*-*b*-PEGPG-*b*-PFS*m* copolymers possess not only poly(2,3,4,5,6-pentafluorostyrene) units but also poly(oxyethylene–oxypropylene) units in the main chain, of whose units can interact with palladium nanoparticles in the copolymeric aggregate cores to afford the expected PFS*m*-*b*-PEGPG-*b*-PFS*m* nanocomposites-immobilized palladium nanoparticles as shown in the TEM images in Fig. 2-9. On the other hand, $R_F$-(IEM-BO)$_x$-(Ad-HAc)$_y$-$R_F$ cooligomer possesses no such functional units in cooligomer to interact with palladium nanoparticles. Thus, this fluorinated cooligomer could not afford the corresponding fluorinated cooligomeric nanocomposites-immobilized palladium nanoparticles, and the original palladium powders would be formed under such conditions.

### 2.3.3. Application of the fluorinated nanocomposites-immobilized palladium nanoparticles to Suzuki-Miyaura cross-coupling reaction

It is well-known that palladium nanoparticles immobilized on spherical polyelctrolyte brushes are useful catalysts for Suzuki–Miyaura cross-coupling reactions.[36 ~ 38)] Especially, it has been demonstrated that palladium nanoparticles immobilized on spherical polyelectrolyte

brushes can be reused many times for Suzuki-Miyaura cross-coupling reactions. A quite different behavior for the formation of palladium nanoparticles was observed in two kinds of the present fluorinated polymers: $R_F$-$(AMPS)_x$-$(Ad\text{-}HAc)_y$-$R_F$ cooligomer and PFS*m*-*b*-PEGPG-*b*-PFS*m* copolymers. Palladium nanoparticles can be immobilized outside $R_F$-$(AMPS)_x$-$(Ad\text{-}HAc)_y$-$R_F$ cooligomeric aggregate cores; in contrast, palladium nanoparticles can be selectively immobilized inside PFS*m*-*b*-PEGPG-*b*-PFS*m* copolymeric aggregate cores. Thus, it is in particular interest to develop the present $R_F$-$(AMPS)_x$-$(Ad\text{-}HAc)_y$-$R_F$ nanocomposites-immobilized palladium nanoparticles and PFS*m*-*b*-PEGPG-*b*-PFS*m* nanocomposites-immobilized palladium nanoparticles into Suzuki-Miyaura cross-coupling reaction. Especially, it is very important to clarify the different catalytic activities in these two kinds of fluorinated polymeric nanocomposites. Suzuki–Miyaura cross-coupling reaction of bromobenzene and phenylboronic acid in the presence of these fluorinated nanocomposites was studied in order to verify the different reactivity. These results were shown in Scheme 2-4 and Table 2-4.

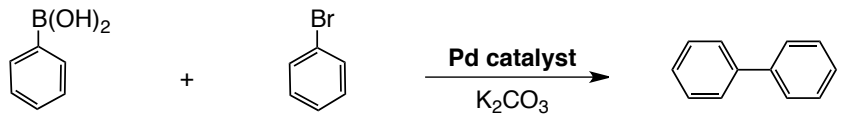


**Pd catalyst:** $R_F$-$(AMPS)_x$-$(Ad\text{-}HAc)_y$-$R_F$/palladium nanocomposites or PFS*m*-PEGPG-PFS*m*/palladium nanocomposites

Scheme 2-4

Table 2-4 Suzuki-Miyaura cross-coupling reaction of phenylboronic acid with bromobenzene catalyzed fluorinated polymers/Pd nanocomposites at 100 °C for 8 h in DMF

| Run | Phenylboronic Acid (mmol) | Bromobenzene (mmol) | Pd catalyst | Pd (mol%) in nanocomposites | DMF (mL) | $K_2CO_3$ (mmol) | Conversion[b] (%) | Yields[c] (%) | TON |
|---|---|---|---|---|---|---|---|---|---|
| 17 | 1.5 | 1.0 | $R_F$-(AMPS)$_x$-(Ad-HAc)$_y$-$R_F$/Pd | 10 (Run 4)[a] | 3 | 2.0 | 98 | 87 | 8.5 |
| 18 | 1.5 | 1.0 | PFS24-*b*-PEGPG-*b*-PFS24/Pd | 10 (Run 15)[a] | 3 | 2.0 | 99 | 53 | 5.3 |
| 19 | 1.5 | 1.0 | PFS12-*b*-PEGPG-*b*-PFS12/Pd | 10 (Run 16)[a] | 3 | 2.0 | 99 | 65 | 6.5 |

[a]Used nanocomposites Run nos. correspond to those of Table 2-1 and 2-3.
[b]Bromobenzene
[c]HPLC yields based on the consumed bromobenzene.

As shown in Scheme 2-4 and Table 2-4, phenylboronic acid reacted with bromobenzene in the presence of $R_F$-(AMPS)$_x$-(Ad-HAc)$_y$-$R_F$/Pd nanocomposites and PFS*m*-*b*-PEGPG-*b*-PFS*m*/Pd nanocomposites to afford biphenyl in 53 ~ 87 % yields. A higher yield of the product was obtained in $R_F$-(AMPS)$_x$-(Ad-HAc)$_y$-$R_F$/Pd nanocomposites, indicating that the immobilized palladium nanoparticles onto the $R_F$-(AMPS)$_x$-(Ad-HAc)$_y$-$R_F$/Pd nanocomposite cores should exhibit a higher catalytic activity toward the cross-coupling reaction in Scheme 2-4 than that of the immobilized palladium nanoparticles inside the PFS*m*-*b*-PEGPG-*b*-PFS*m*/Pd nanocomposite cores.

Table 2-5 Reusability of fluorinated polymers/palladium nanocomposites for Suzuki-Miyaura cross-coupling reaction

| Run | Use[a] | 1 | 2 | 3 | 4 | 5 |
|---|---|---|---|---|---|---|
| 20 | Nanocomposites (Run 17 in Table 2-4) Yield (%)[a] | 87 | 63 | 44 | 36 | 24 |
| 21 | Nanocomposites (Run 18 in Table 2-4) Yield (%)[a] | 53 | 47 | 46 | 48 | 43 |

[a]Recovered fluorinated nanocomposites were used successively (use 2, 3, 4, and 5).
[b]Reaction conditions are the same as those of Table 2-4.
[c]HPLC yields based on the consumed bromobenzene.

Of particular interest, these two types of fluorinated polymers/Pd nanocomposites in

Scheme 2-4 recovered quantitatively by simple centrifugal separation, and could be reused. The catalytic activity of the recovered PFS*m*-*b*-PEGPG-*b*-PFS*m*/Pd nanocomposite (Run 21 in Table 2-5) did decrease gradually after five uses, although the decrement is not so significant as with the other nanocomposites (see Run 20 in Table 2-5). However, $R_F$-$(AMPS)_x$-$(Ad\text{-}HAc)_y$-$R_F$/Pd nanocomposites were found to decrease their catalytic activity after five uses (see Run 20 in Table 2-5). These findings suggest that immobilized palladium nanoparticles on $R_F$-$(AMPS)_x$-$(Ad\text{-}HAc)_y$-$R_F$ cooligomeric nanocomposite cores are likely to have a releasing characteristic into reaction media during the reuse conditions, compared with immobilized palladium nanoparticles inside PFS*m*-*b*-PEGPG-*b*-PFS*m* copolymeric aggregate cores.

## 2.4. Conclusion

Fluoroalkyl end-capped betaine-type cooligomeric nanocomposites-immobilized palladium nanoparticles have been succeeded in preparing by the reactions of palladium chloride with sodium acetate in the presence of the corresponding fluorinated cooligomers. Outer blocks of poly(2,3,4,5,6-pentafluorostyrene)-containing copolymeric nanocomposites-immobilized palladium nanoparticles were also prepared under similar conditions. Controlled immobilization of palladium nanoparticles in these different fluorinated nanocomposite cores was observed, and palladium nanoparticles were immobilized onto fluorinated betaine-type cooligomeric nanocomposite cores; in contrast, palladium nanoparticles were effectively immobilized inside outer blocks of poly(2,3,4,5,6-pentafluorostyrene)-containing copolymeric nanocomposite cores. These fluorinated nanocomposites-immobilized palladium nanoparticles were applied to the catalysts for Suzuki-Miyaura cross-coupling reaction. Fluorinated betaine-type cooligomeric nanocomposites-immobilized palladium nanoparticles were able to afford the expected product in a higher yield; however, its catalytic activity was found to decrease after five uses. On the other hand, outer blocks of poly(2,3,4,5,6-pentafluorostyrene)-containing copolymeric nanocomposites were able to keep a higher catalytic activity even after five uses.

**References**


1) M. R. Bockstaller, R. A. Mickiwicz, E. L. Thomas, *Adv. Mater.*, **17**,1331 (2005).

2) M. Kawazoe and H. Ishida, *Macromolecules*, **41**, 2931 (2008).

3) L. L. Beecroft and C. K. Ober, *Chem. Mater.*, **9**,1302 (1997).

4) N. Semagina, A. Renken, and L. Kiwi-Minsker, *J. Phys. Chem. C*, **111**, 13933 (2007).

5) L. N. Lewis, *Chem. Rev.*, **93**, 2693 (1993).

6) A. P. Alivisatos, *Science*, **271**, 933 (1996).

7) C. Burda, X. Chen, R. Narayanan, and M. A. EI-Sayed, *Chem. Rev.*, **105**, 1025 (2005).

8) R. Ferrando, J. Jellinek, and L. Johnston, *Chem. Rev.*, **108**, 845 (2008).

9) S. Praharaj, S. Nath, S. Ghosh, S. Kundu, and T. Pal, *Langmuir*, **20**, 9889 (2004).

10) R. W. J. Scott, O. M. Wilson, and R. M. Crooks, *J. Phys. Chem. B*, **109**, 692 (2005).

11) N. W. Ockwig and T. M. Nenoff, *Chem. Rev.*, **107**, 4078 (2007).

12) S. N. Paglieri and J. D. Way, *Sep. Purif. Rev.*, **31**, 1 (2002).

13) J. K. Esumi, R. Isono, and T. Yoshimura, *Langmuir*, **20**, 237 (2004).

14) M. Zhao and R. M. Crooks, *Angew. Chem. Int. Ed.*, **38**, 364 (1999).

15) S. Zhang, E. Xu, and E. Kumacheva, *J. Am. Chem. Soc.*, **126**, 7908 (2004).

16) J. E. Wong, A. K. Gaharwar, D. Muller-Schlte, D. Bahaudur, and W. Richtering, *J. Colloid*

*Interface Sci.*, **324**, 47 (2008).

17) J. Zhang, E. Xu, and E. Kumacheva, *Adv. Mater.*, **17**, 2336 (2005).

18) Q. Sun and Y. Deng, *Langmuir*, **21**, 5812 (2005).

19) Y. Mei, G. Sharma, Y. Lu, M. Drechsler, T. Irrgang, R. Kempe, and M. Ballauff, *Langmuir*, **21**, 12229 (2005).

20) G. Sharma and M. Ballauff, *Macromol. Rapid Commun.*, **25**, 547 (2004).

21) M. Schrinner, F. Polzer, Y. Mei, Y. Lu, B. Haupt, M. Ballauff, A. Goldel, M. Drechsler, J. Preussner, and U. Glatzel, *Macromol. Chem. Phys.*, **208**, 1542 (2007).

22) Y. B. Malysheva, A. V. Guschchin, Y. Mei, Y. Lu, M. Ballauff, S. Proch, and R. Kempe, *Eur. J. Inorg. Chem.*, **379**, 383 (2008).

23) H. Sawada, T. Kijima, and M. Mugisawa, *Polym. J.*, **42**, 494 (2010).

24) H. Sawada, *Chem. Rev.*, **96**, 1779 (1996).

25) H. Sawada, *J. Fluorine Chem.*, **105**, 219 (2000).

26) H. Sawada, *Prog. Polym. Sci.*, **32**, 509 (2007).

27) H. Sawada, *Polym. J.*, **39**, 637 (2007).

28) K. Jankova, X. Chen, J. Kops, and W. Batsberg, *Macromolecules*, **31**, 538 (1998).

29) K. Jankova, P. Jannasch, and S. Hvilsted, *J. Mater. Chem.*, **14**, 2902 (2004).

30) K. Jankova and S. Hvilsted, *J. Fluorine Chem.*, **126**, 241 (2005).

31) M. Mugisawa, K. Ohnishi, and H. Sawada, *Langmuir*, **23**, 5848 (2007).

32) M. Mugisawa, K. Ueno, K. Hamazaki, and H. Sawada, *Macromol. Rapid Commun.*, **28**, 733 (2007).

33) M. Mugisawa, R. Kasai, and H. Sawada, *Langmuir*, **25**, 415 (2009).

34) H. Sawada, S. Katayama, Y. Ariyoshi, T. Kawase, Y. Hayakawa, T. Tomita, and M. Baba, *J. Mater. Chem.*, **8**, 1517 (1998).

35) M. Tristany, J. Courmarcel, P. Dieudonne, M. Moreno-Manas, R. Pleixats, A. Rimola, M. Sodupe, and S. Villarroya, *Chem. Mater.*, **18**, 716 (2006).

36) M. Yu, Y. Lu, M. Schrinner, F. Polzer, and M. Ballauff, *Macromol. Symp.*, **254**, 42 (2007).

37) Y. Lu, A. Wittemann, and M. Ballauff, *Macromol. Rapid Commun.*, **30**, 806 (2009).

38) S. Proch, Y. Mei, J. M. Rivera Villanueva, Y. Lu, A. Karpov, and M. Ballauff, *Adv. Synth. Catal.*, **350**, 493 (2008).

CHAPTER 3

# Coloring-Decoloring Behavior of Fluoroalkyl End-Capped 2-Acrylamido-2-methylpropanesulfonic Acid Oligomer/Acetone Composite in Methanol

## 3.1. Introduction

There has been great interest in block copolymers containing long perfluoroalkyl groups, which can self-assemble into polymeric aggregates resembling micelles in aqueous and organic media. [1 ~ 12)] ABA triblock fluoroalkyl end-capped oligomers [$R_F$-$(M)_n$-$R_F$; $R_F$ = fluoroalkyl groups; M = radical polymerizable monomer] are particularly attractive functional polymers, because they are very soluble, surface and biologically active, and they can form nanoscale controlled molecular aggregates. The corresponding non-fluorinated, randomly or block fluoroalkylated polymers, and low molecular weight fluorinated surfactants do not exhibit these properties. [13 ~ 18)] For example, fluoroalkyl end-capped 2-acrylamido-2-methylpropane-sulfonic acid (AMPS) co-oligomers containing adamantyl segments can form size-controlled nanoparticles in a wide variety of solvents, including water. The fluorinated co-oligomeric nanoparticles exhibit the low critical solution temperature (LCST) of around 52 °C, because of the oleophobic-oleophobic (fluorophilic-fluorophilic) interaction between end-capped fluoroalkyl segments in organic media, such as t-butyl alcohol. [19)] These fluorinated co-oligomeric nanoparticles have been used to encapsulate a variety of metal nanoparticles to afford stable colloidal fluorinated nanocomposites. [20 ~ 22)] Therefore, it is particularly desirable to develop fluoroalkyl end-capped AMPS co-oligomeric nanoparticles

for encapsulating organic guest molecules. In general, fluoroalkyl end-capped AMPS-1-hydroxy-5-adamantyl acrylate (Ad-HAc) coligomers [$R_F$-$(AMPS)_x$-$(Ad\text{-}HAc)_y$-$R_F$] obtained by using fluoroalkanoyl peroxide [$R_F$-C(=O)OO(O=)C-$R_F$; $R_F$ = fluoroalkyl group] can be purified by reprecipitation with ethanol/acetone. [23] The fluorinated $R_F$-$(AMPS)_x$-$(Ad\text{-}HAc)_y$-$R_F$ co-oligomers with lower co-oligomerization ratios of $x$ = 11 ~ 44 % were isolated as white powders. [23] However, the fluorinated co-oligomers with higher co-oligomerization ratios of $x$ = 58 ~ 81 % were isolated as reddish-brown powders through the same reprecipitation technique. This chapter demonstrates that the coloring behavior is caused by the formation of the corresponding oligomer/acetone composites, especially the formation of acetone aldol polycondensation products in the fluorinated oligomeric cores.

## 3.2. Experimental

### 3.2.1 Measurements

Fourier-transform infrared (FT-IR) spectra were measured with a FT-IR spectrophotometer (FTIR-8400, Shimadzu, Japan). $^{1}H$ NMR spectra were recorded using a 500 MHz FT NMR spectrometer (JNM-ECA 500, JEOL, Japan). Ultraviolet-visible (UV–vis) spectra were carried out using a UV-Vis spectrophotometer (UV-1800, Shimadzu, Japan). UV irradiation was performed by using a UV lamp (SLUV-6, AS ONE, Japan). The pH measurement was performed by using a pH meter (PH-02, AS ONE, Japan).

### 3.2.2. Materials

AMPS, acetone, sulfuric acid ($H_2SO_4$), and nitric acid ($HNO_3$) were purchased from Wako Pure Chemical Industries; 1-hydroxy-5-adamantyl acrylate (Ad-HAc) was used as received from Idemitsu Kosan Co., Ltd; 2-(methacryloyloxy)ethanesulfonic acid (MES) was purchased from Polysciences Inc., and phosphoric acid ($H_3PO_4$) was purchased from Kishida Chemical Co., Ltd. The $R_F$-$(AMPS)_n$-$R_F$ homo-oligomer and fluoroalkyl end-capped MES

homo-oligomer [$R_F$-($CH_2CMeCO_2CH_2CH_2SO_3H$)$_n$-$R_F$; $R_F$ = $CF(CF_3)OC_3F_7$: $R_F$-(MES)$_n$-$R_F$] were prepared by reacting fluoroalkanoyl peroxide with the corresponding monomers according to the previously reported method. [24, 25)]

In the case of $R_F$-(AMPS)$_n$-$R_F$ homo-oligomer, this homooligomer was obtained as a white powder by reprecipitation with water-tetrahydrofuran, and was dried under vacuum at 50 °C for 2 days. [24)]

### 3.2.3. Synthesis of fluoroalkyl end-capped 2-acrylamido-2-methylpropanesulfonic acid co-oligomer containing adamantyl segments

Perfluoro-2-methyl-3-oxahexanoyl peroxide (3.06 mmol: 2.0 g) in AK-225$^{TR}$ ($Cl_2CHCF_2CF_3$/$CClF_2CF_2CHClF$, 1 : 1; 25 g) was added to an aqueous solution (50 %, w/w) of AMPS (2.78 mmol: 5.8 g), Ad-HAc (13.9 mmol: 3.1 g), and AK-225 (200 g). The heterogeneous mixture was stirred at 45 °C for 5 h under nitrogen. The solvent was removed and the product was reprecipitated from ethanol–acetone to give an α,ω-bis(perfluoro-1-methyl-2-oxapentylated) AMPS–Ad-HAc co-oligomer [$R_F$-(AMPS)$_x$-(Ad-HAc)$_y$-$R_F$; $R_F$ = $CF(CF_3)OC_3F_7$; $x$ : $y$ = 11 : 89]. The product was dried under vaccum at 50 °C for 2 days to give a white powder [2.7 g (yield: 50 %)]. The yield was

based on the decarboxylated $R_F$-$R_F$ units in peroxide, Ad-HAc and AMPS.

IR (ν/cm$^{-1}$) 3382 (OH, NH), 2920 (CH), 1731 (CO), 1654 (CONH), 1307 ($CF_3$), 1242 ($CF_2$); $^1$H NMR ($CD_3OD$) δ 1.10–1.85 (CH, $CH_2$, $CH_3$), 1.85–2.15 ($CH_2$), 2.15–2.45 (CH). The co-oligomerization ratio was determined by $^1$H NMR as $x$ : $y$ = 11 : 89.

The other fluorinated co-oligomers were synthesized and characterized using the same method. The molecular weights of the co-oligomers could not be determined by gel permeation chromatography because of the formation of nanoparticles.

**$R_F$-(AMPS)$_x$-(Ad-HAc)$_y$-$R_F$, $R_F$ = $CF(CF_3)OC_3F_7$**: IR (ν/cm$^{-1}$) 3355 (OH, NH), 2923 (CH), 1731 (CO), 1654 (CONH), 1303 ($CF_3$), 1234 ($CF_2$); $^1$H NMR ($CD_3OD$) δ 1.00–1.80 (CH, $CH_2$, $CH_3$), 1.80–2.20 ($CH_2$), 2.20-2.40 (CH) [$x$ : $y$ = 26 : 74].

**$R_F$-(AMPS)$_x$-(Ad-HAc)$_y$-$R_F$, $R_F$ = $CF(CF_3)OC_3F_7$**: IR (ν/cm$^{-1}$) 3361 (OH, NH), 2923 (CH), 1732 (CO), 1653 (CONH), 1305 ($CF_3$), 1245 ($CF_2$); 1H NMR ($CD_3OD$) δ 0.80–1.80 (CH, $CH_2$, $CH_3$), 1.80–2.15 ($CH_2$), 2.15–2.30 (CH) [$x$ : $y$ = 44 : 56].

**$R_F$-(AMPS)$_x$-(Ad-HAc)$_y$-$R_F$, $R_F$ = $CF(CF_3)OC_3F_7$**: IR (ν/cm$^{-1}$) 3363 (OH, NH), 2921 (CH), 1732 (CO), 1653 (CONH), 1306 ($CF_3$), 1244 ($CF_2$); 1H NMR ($CD_3OD$) δ 1.14–1.86 (CH, $CH_2$, $CH_3$), 1.86–2.20 ($CH_2$), 2.20–2.42 (CH) [$x$ : $y$ = 58 : 42].

**$R_F$-(AMPS)$_x$-(Ad-HAc)$_y$-$R_F$, $R_F$ = $CF(CF_3)OC_3F_7$**: IR (ν/cm$^{-1}$) 3370 (OH, NH), 2920 (CH), 1730 (CO), 1654 (CONH), 1308 ($CF_3$), 1250 ($CF_2$); 1H NMR ($CD_3OD$) δ 1.15–1.83 (CH, $CH_2$, $CH_3$), 1.83–2.16 ($CH_2$), 2.16–2.40 (CH) [$x$ : $y$ = 79 : 21].

**$R_F$-(AMPS)$_x$-(Ad-HAc)$_y$-$R_F$, $R_F$ = $CF(CF_3)OC_3F_7$**: IR (ν/cm$^{-1}$) 3360 (OH, NH), 2923 (CH), 1732 (CO), 1650 (CONH), 1302 ($CF_3$), 1243 ($CF_2$); 1H NMR ($CD_3OD$) δ 1.10–1.84 (CH, $CH_2$, $CH_3$), 1.84–2.16 ($CH_2$), 2.16–2.40 (CH) [$x$ : $y$ = 81 : 19].

### 3.2.4. Coloring-decoloring behavior of $R_F$-(AMPS)$_x$-(Ad-HAc)$_y$-$R_F$ co-oligomers in methanol

The reddish-brown $R_F$-(AMPS)$_x$-(Ad-HAc)$_y$-$R_F$ [$x$ : $y$ = 79 : 21] co-oligomer (300 mg) was dissolved in methanol (10 mL) and stirred at room temperature for 30 min to give a clear reddishbrown solution. The solution was kept at room temperature for 1 day. The solvent was evaporated under reduced pressure, and the crude product was dried at 50 °C for 12 h under vacuum to afford a pale yellow $R_F$-(AMPS)$_x$-(Ad-HAc)$_y$-$R_F$ powder. Acetone (5 mL) was added to the $R_F$-(AMPS)$_x$-(Ad-HAc)$_y$-$R_F$ powder (100 mg), and the mixture was heated at 70 °C for 3 h. The product was dried in vacuo at 50 °C for 12 h to afford a reddish-brown $R_F$-(AMPS)$_x$-(Ad-HAc)$_y$-$R_F$ powder (98 mg).

The fluoroalkyl end-capped AMPS homo-oligomer [$R_F$-(AMPS)$_n$-$R_F$; $R_F$ = $CF(CF_3)OC_3F_7$]/acetone composites, nonfluorinated AMPS homo-oligomer [-(AMPS)$_n$-]/acetone composite, $H_2SO_4$/acetone composite, fluoroalkyl end-capped MES homo-oligomer [$R_F$-(MES)$_n$-$R_F$]/acetone composite, $HNO_3$/acetone composite, and $H_3PO_4$/acetone composite were prepared under similar conditions.

### 3.2.5. Changes in the UV-vis spectra of the $R_F$-(AMPS)$_n$-$R_F$/acetone composite in methanol

A solution of the $R_F$-(AMPS)$_n$-$R_F$/acetone composite (16 mg) in MeOH (4 mL) was stirred in the dark at 25 °C for 10 min. The UV-vis spectra of the solutions were measured at various times in the dark, in natural light, and under UV ($\lambda_{max}$ = 365 nm) irradiation at 25 °C.

### 3.3. Results and discussion

#### 3.3.1. Coloring-decoloring behavior of fluoroalkyl end-capped 2-acrylamido-2-methylpropanesulfonic acid co-oligomer containing adamantyl segments

Fluoroalkyl end-capped AMPS - Ad-HAc co-oligomers [$R_F$-(AMPS)$_x$-(Ad-HAc)$_y$-$R_F$; $R_F$ = $CF(CF_3)OC_3F_7$] with a variety of co-oligomerization ratios ($x$ : $y$) were prepared from fluoroalkanoyl peroxide, AMPS, and Ad-HAc, according to the previously reported method (Scheme 3-1, Table 3-1, Fig. 3-1). [23)]

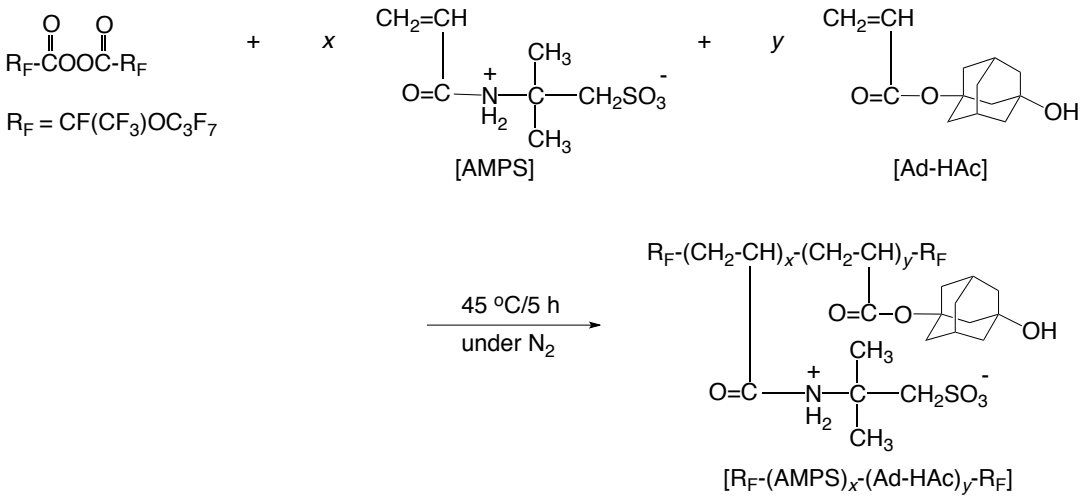


Scheme 3-1

Table 3-1 Preparation of fluoroalkyl end-capped 2-acrylamido-2-methylpropanesulfonic acid co-oligomers containing adamantane units

| Run | $R_F$ in Peroxide (mmol) | AMPS (mmol) | Ad-HAc (mmol) | Product yields[a] (%) | Cooligomerization ratio ($x$ : $y$)[b] |
|---|---|---|---|---|---|
| | $R_F = CF(CF_3)OC_3F_7$ | | | | |
| 1 | 3.06 | 2.78 | 13.9 | 50 | 11 : 89 |
| 2 | 2.94 | 5.56 | 13.9 | 50 | 26 : 74 |
| 3 | 2.81 | 10.8 | 13.5 | 57 | 44 : 56 |
| 4 | 5.95 | 23.8 | 29.8 | 42 | 58 : 42 |
| 5 | 5.95 | 29.8 | 11.9 | 38 | 79 : 21 |
| 6 | 5.95 | 35.7 | 6.00 | 56 | 81 : 19 |

[a]Yields were based on the decarboxylated $R_F$-$R_F$ units in peroxide, Ad-HAc and comonomer.
[b]Cooligomerization ratio ($x$ : $y$) was determined by $^1$H NMR.

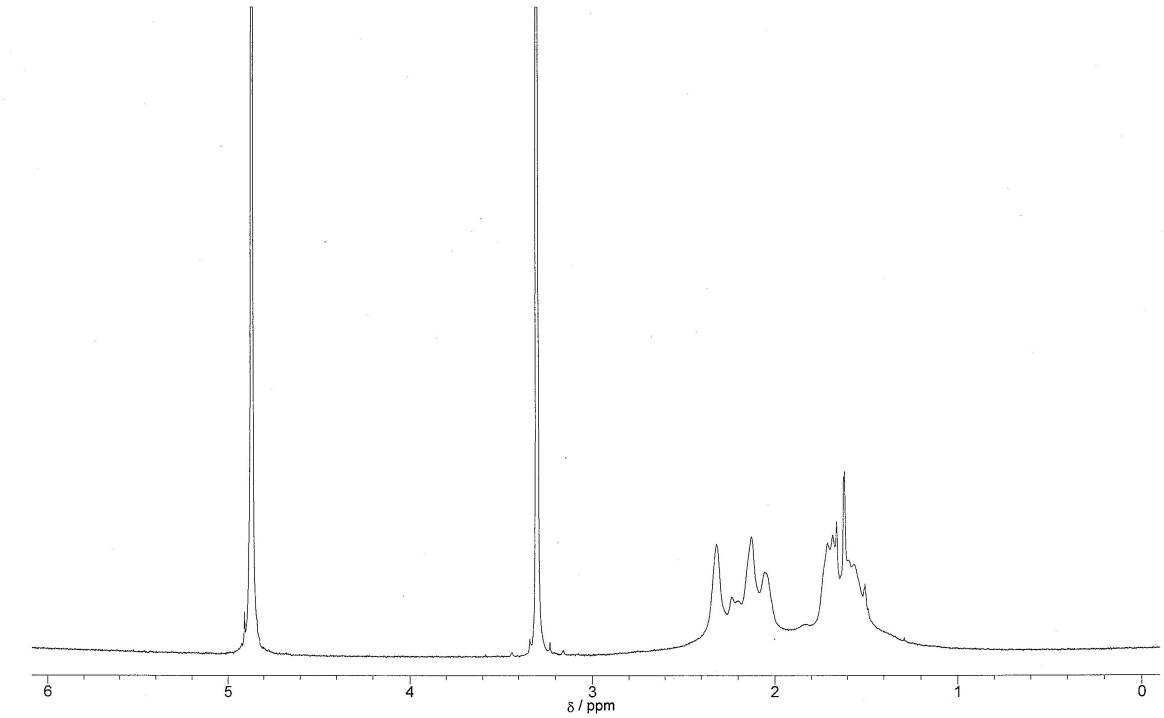


Fig. 3-1 $^1$H NMR spectrum of $R_F$-$(AMPS)_x$-$(Ad\text{-}HAc)_y$-$R_F$ cooligomer (Run 1 in Table 3-1) in $CD_3OD$.

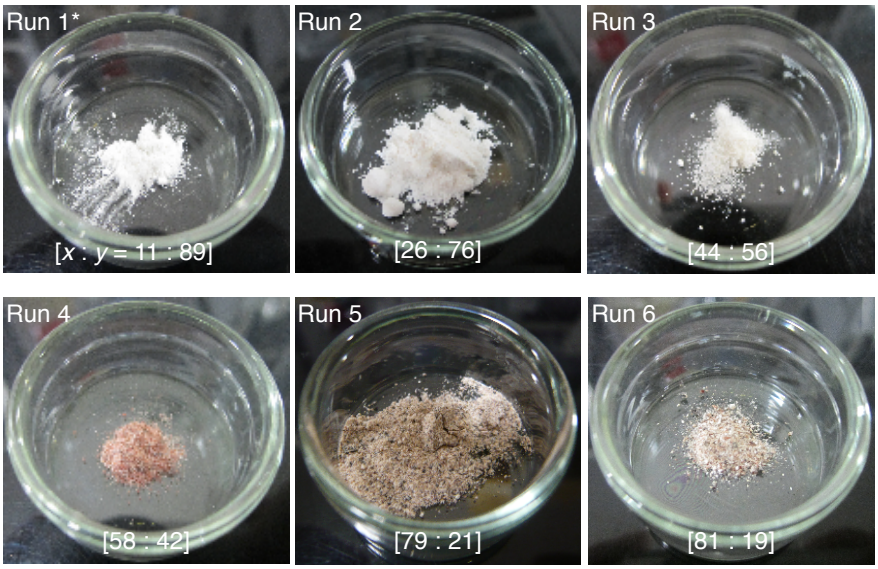


Fig. 3-2 Photographs of $R_F$-(AMPS)$_x$-(Ad-HAc)$_y$-$R_F$ cooligomeric powders, isolated by reprecipitation.
*The run numbers correspond to those in Table 3-1.

Each $R_F$-(AMPS)$_x$-(Ad-HAc)$_y$-$R_F$ co-oligomer in Scheme 3-1 and Table 3-1 was purified by reprecipitation with ethanol/acetone. The $R_F$-(AMPS)$_x$-(Ad-HAc)$_y$-$R_F$ co-oligomers with lower co-oligomerization ratios ($x$ = 11 ~ 44 %, Runs 1 ~ 3 in Table 3-1) were isolated as white powders after they were purified and dried (Fig. 3-2). However, the fluorinated co-oligomers with higher co-oligomerization ratios ($x$ = 58 ~ 81 %, Runs 4 ~ 6 in Table 3-1) were isolated as reddish-brown powders. The UV-vis spectra of $R_F$-(AMPS)$_x$-(Ad-HAc)$_y$-$R_F$ co-oligomers (Runs 1 ~ 6 in Fig. 3-2) in methanol are shown in Fig. 3-3.

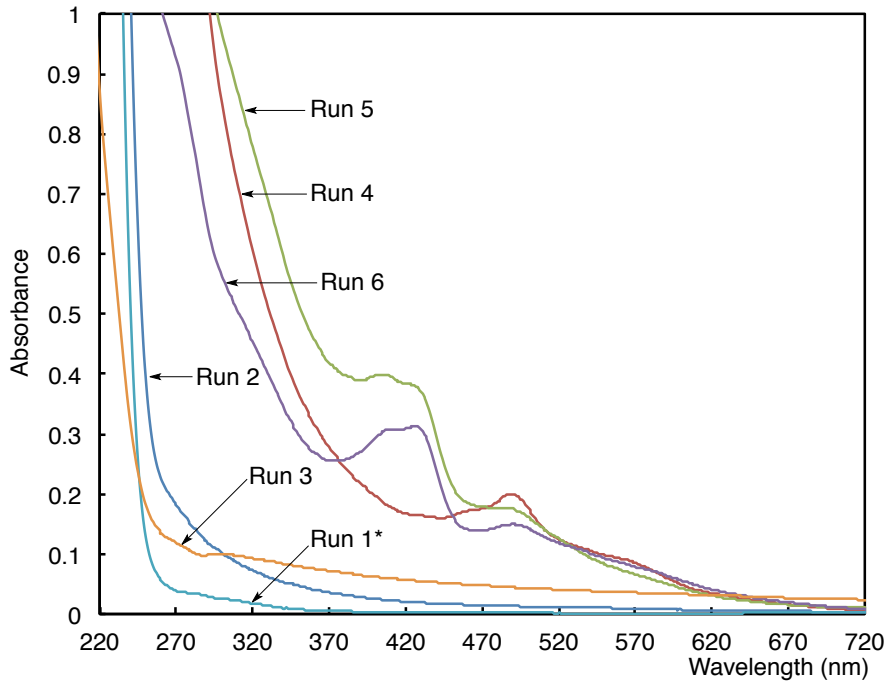


Fig. 3-3 UV-vis spectra of methanol solutions of $R_F$-$(AMPS)_x$-$(Ad\text{-}HAc)_y$-$R_F$ co-oligomer. The concentration of the co-oligomers was 1.0 $gdm^{-3}$.
*Each run correspond to the runs in Table 3-1.

The $R_F$-$(AMPS)_x$-$(Ad\text{-}HAc)_y$-$R_F$ co-oligomers with lower co-oligomerization ratios for the AMPS units ($x$ = 11 ~ 44 %, Runs 1 ~ 3 in Fig. 3-2) did not show any absorption peaks at 370 to 600 nm. However, clear absorption peaks at 430 to 490 nm (Runs 4 ~ 6 in Fig. 3-3) were observed for $R_F$-$(AMPS)_x$-$(Ad\text{-}HAc)_y$-$R_F$ co-oligomers with higher AMPS co-oligomerization ratios ($x$ = 58 ~ 81 %, Runs 4 ~ 6 in Fig. 3-2).

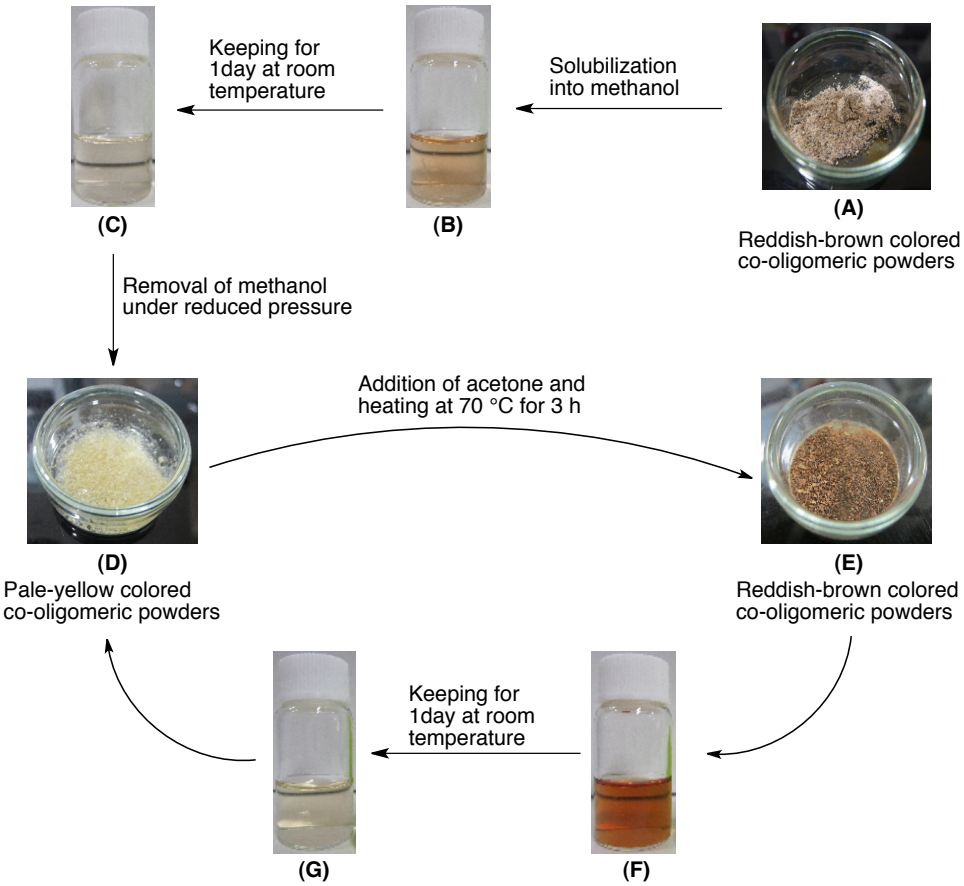


Fig. 3-4 Photographs of $R_F$-(AMPS)$_x$-(Ad-HAc)$_y$-$R_F$ co-oligomeric powders (x : y = 79 : 21, Run 5 in Table 3-1) and methanol solutions.

The reddish-brown $R_F$-(AMPS)$_x$-(Ad-HAc)$_y$-$R_F$ co-oligomeric powders ($x$ : $y$ = 79 : 21, Run 5 in Table 3-2) in Fig. 3-4(A) were very soluble in methanol to give a reddish-brown solution [Fig. 3-4(B)]. However, after the solution was kept at room temperature for 1 day, the reddish-brown solution turned colorless [Fig. 3-4(C)]. The solvent was removed under reduced pressure and the oligomeric powder was pale yellow [Fig. 3-4(D)]. When acetone was added to the pale yellow fluorinated oligomeric powders, and the mixture was heated at 70 °C for 3 h, it turned reddish-brown [Fig. 3-4(E)]. When the colored fluorinated oligomeric powders were

dissolved in methanol, the solution changed from reddish-brown [Fig. 3-4(F)] to colorless [Fig. 3-4(G)] after 1 day at room temperature. The coloring-decoloring behavior was repeatable. Fig. 3-5 shows the UV-vis spectra corresponding to the coloring-decoloring behavior in Fig. 3-4.

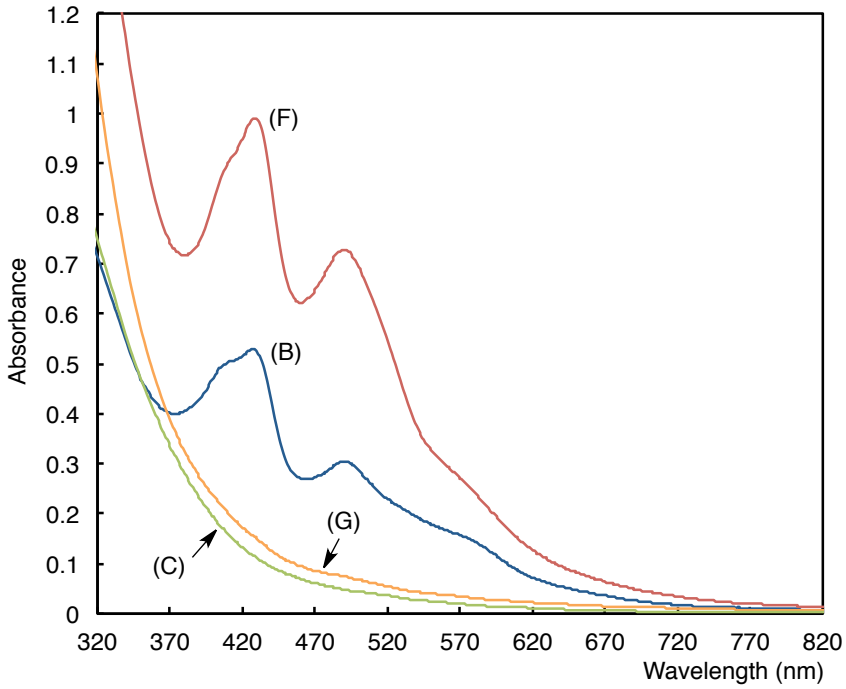


Fig. 3-5 UV-vis spectra of methanol solutions of $R_F$-(AMPS)$_x$-(Ad-HAc)$_y$-$R_F$ co-oligomer (Run 5, Table 3-1). The spectra B, C, G, and F correspond to the solutions in Fig. 3-4(B, C ,G ,F). The concentration of the co-oligomers was 5.0 gdm$^{-3}$.

The absorption peaks related to the color in Fig. 3-4(B, F) were present at 437 and 490 nm, respectively [Fig. 3-5(B, F)]. However, the peaks disappeared when the solution became colorless [Fig. 3-5(C, G)]. This suggests that the color arises from the aborption peaks at 427 ~ 490 nm. The color of the $R_F$-(AMPS)$_x$-(Ad-HAc)$_y$-$R_F$ co-oligomers with higher AMPS cooligomerization ratios ($x$ = 58 ~ 81 %, Runs 4 ~ 6 in Fig. 3-2) may be caused by the

interaction of the AMPS units with acetone. Thus, the interaction of the $R_F$-$(AMPS)_n$-$R_F$ homo-oligomer with no adamantyl segments with acetone was examined under the same conditions.

### 3.3.2. Preparation and property of fluoroalkyl end-capped 2-acrylamido-2-methylpropanesulfonic acid homo-oligomer/acetone composite

$R_F$-$(AMPS)_n$-$R_F$/acetone composites were prepared by treating mixtures of fluorinated homo-oligomer and acetone at 80 °C for 3 h (Table 3-2). The fluorinated acetone composites corresponding to Runs 11 ~ 15 were isolated as reddish-brown powders, and the other composites were isolated as pale yellow powders. The UV-vis spectra of each $R_F$-$(AMPS)_n$-$R_F$/acetone composite was measured (Table 3-2, Fig. 3-6).

Table 3-2 Preparation of $R_F$-$(AMPS)_n$-$R_F$ /acetone composites

| Run | $R_F$-$(AMPS)_n$-$R_F$ (mg) | Acetone (mL) | MeOH (mL) | Temperature (°C) | Time (h) | Product yields (mg) |
|---|---|---|---|---|---|---|
| 7 | 100 | 0.05 | 1 | 80 | 3 | 91 |
| 8 | | 0.1 | | | | 91 |
| 9 | | 0.5 | | | | 90 |
| 10 | | 1 | | | | 93 |
| 11 | | 5 | | | | 86 |
| 12 | | 10 | | | | 97 |
| 13 | | 20 | | | | 90 |
| 14 | | 30 | | | | 91 |
| 15 | | 50 | | | | 93 |

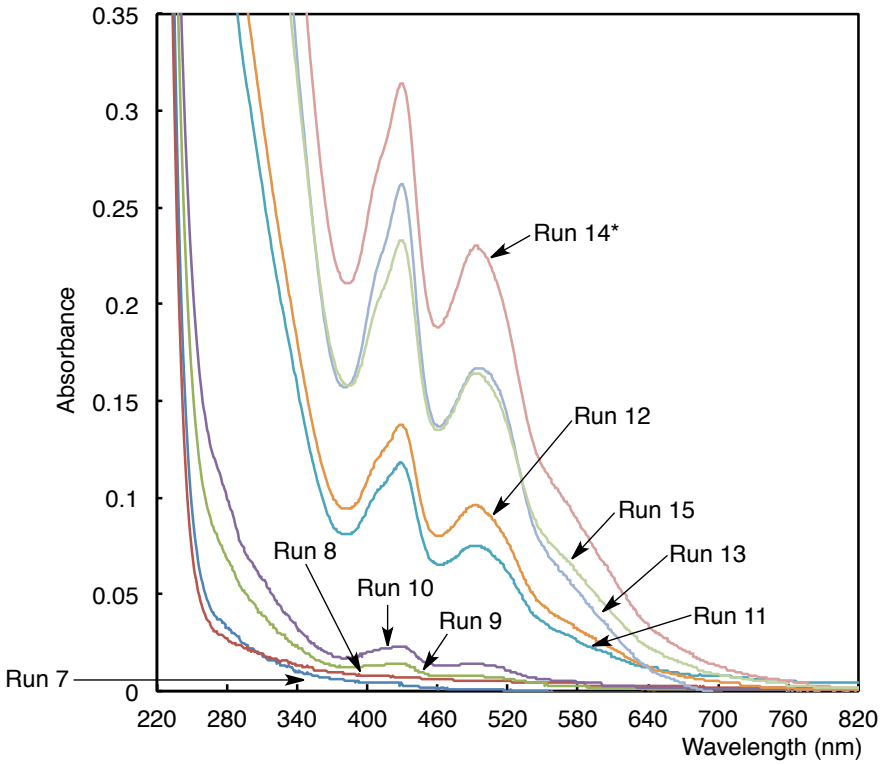


Fig. 3-6 UV-vis spectra of methanol solutions of $R_F$-(AMPS)$_n$-$R_F$/acetone composites. The run number correspond to those in Table 3-2. The concentration of composites was 1.0 gdm$^{-3}$.

Fig. 3-6 shows that the colored fluorinated composites had absorption peaks around 428 and 490 nm (Runs 11 ~ 15); however, these absorption peaks decreased dramatically in the pale yellow composites (Runs 7 ~ 10). The absorbances at 428 and 490 nm in the colored composites increased with the amount of acetone used (0.05 ~ 30 mL), and the highest aborbance was observed for 30 mL of acetone. Previously, $R_F$-(AMPS)$_n$-$R_F$ homo-oligomer was reported to form gels in methanol through the synergy between the aggregation of the end-capped fluoroalkyl groups and the ionic interaction of the sulfobetaine segments. [17, 18, 24] Thus, the acetone should be encapsulated in the $R_F$-(AMPS)$_n$-$R_F$ homo-oligomeric gel network cores as a guest molecule, and produces the coloring-decoloring behavior.

The coloring-decoloring behavior was investigated by studying the interaction of acetone with the $R_F$-$(AMPS)_n$-$R_F$ homo-oligomer, the corresponding non-fluorinated AMPS homooligomer [-$(AMPS)_n$-], and with other fluoroalkyl end-capped homo-oligomers, such as the fluoroalkyl end-capped MES homo-oligomer [$R_F$-$(MES)_n$-$R_F$]. The interaction of acetone with traditional sulfuric, nitric, and phosphoric acid aldol condensation catalysts was also examined under similar conditions (Table 3-3, Fig. 3-7).

Table 3-3 Reaction of acetone with the -$(AMPS)_n$- homo-oligomer, $R_F$-$(MES)_n$-$R_F$ homo-oligomer, sulfuric acid, nitric acid and phosphoric acid

| Run | Oligomer or Acid | Acetone (mL) | MeOH (mL) | Temperature (°C) | Time (h) | Isolated yields (mg) |
|---|---|---|---|---|---|---|
| 16 | -$(AMPS)_n$- 100 mg | 5 | 1 | 80 | 3 | 97 |
| 17 | $R_F$-$(MES)_n$-$R_F$ 100 mg | 5 | 1 | 80 | 3 | 83 |
| 18 | $H_2SO_4$ (97 %)[a] 48.5 mg [0.48 mmol] | 5 | 1 | 80 | 3 | 82 |
| 19 | $HNO_3$ (60 %)[a] 50.4 mg [0.48 mmol] | 5 | 1 | 80 | 3 | Not isolated |
| 20 | $H_3PO_4$ (85 %)[a] 55.3 mg [0.48 mmol] | 5 | 1 | 80 | 3 | Not isolated |
| 11[b] | $R_F$-$(AMPS)_n$-$R_F$ 100 mg | 5 | 1 | 80 | 3 | 98 |

[a]Concentration of used acids.
[b]See Run 11 in Table 3-2.

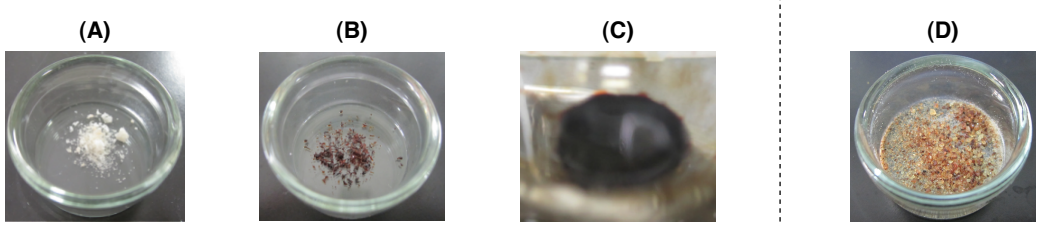


-$(AMPS)_n$-/acetone composites (Run 16)* [White colored powders]

$R_F$-$(MES)_n$-$R_F$/acetone composites (Run 17)* [Dark-brown colored powders]

$H_2SO_4$/acetone composites (Run 18)* [Viscous liquid]

$R_F$-$(AMPS)_n$-$R_F$/acetone composites (Run 11)* [Redissh-brown colored powders]

Fig. 3-7 Photographs of (A)-$(AMPS)_n$-, (B)$R_F$-$(MES)_n$-$R_F$, (C)sulfuric acid, and (D)$R_F$-$(AMPS)_n$-$R_F$/acetone composites.
*The run numbers correspond to those in Table 3-2.

The non-fluorinated -(AMPS)$_n$- homo-oligomer did not undergo a color change [Fig. 3-7(A)], indicating that the -(AMPS)$_n$- homooligomer did not form a gel network that encapsulated acetone as a guest molecule in the network cores. In contrast, the $R_F$-(MES)$_n$-$R_F$ homo-oligomer turned dark brown [Fig. 3-7(B)], similar to the $R_F$-(AMPS)$_n$-$R_F$ homo-oligomer [Fig. 3-7(D)]. This suggests that the $R_F$-(MES)$_n$-$R_F$ homoligomer formed self-assembled molecular aggregates, and the aggregations of the end-capped fluoroalkyl groups in methanol interacted with acetone as a guest molecule [17, 18, 25] to give the dark-brown $R_F$-(MES)$_n$-$R_F$/acetone composite powder under the conditions for Run 17 in Table 3-3. The UV-vis spectra of the $R_F$-(MES)$_n$-$R_F$/acetone composite in methanol (Fig. 3-8) contained absorption peaks similar to those of the $R_F$-(AMPS)$_n$-$R_F$/acetone composite (Fig. 3-9). However, the $R_F$-(MES)$_n$-$R_F$/acetone composite also showed an absorption peak at 604 nm as well as peaks at 428 and 490 nm (Fig. 3-8).

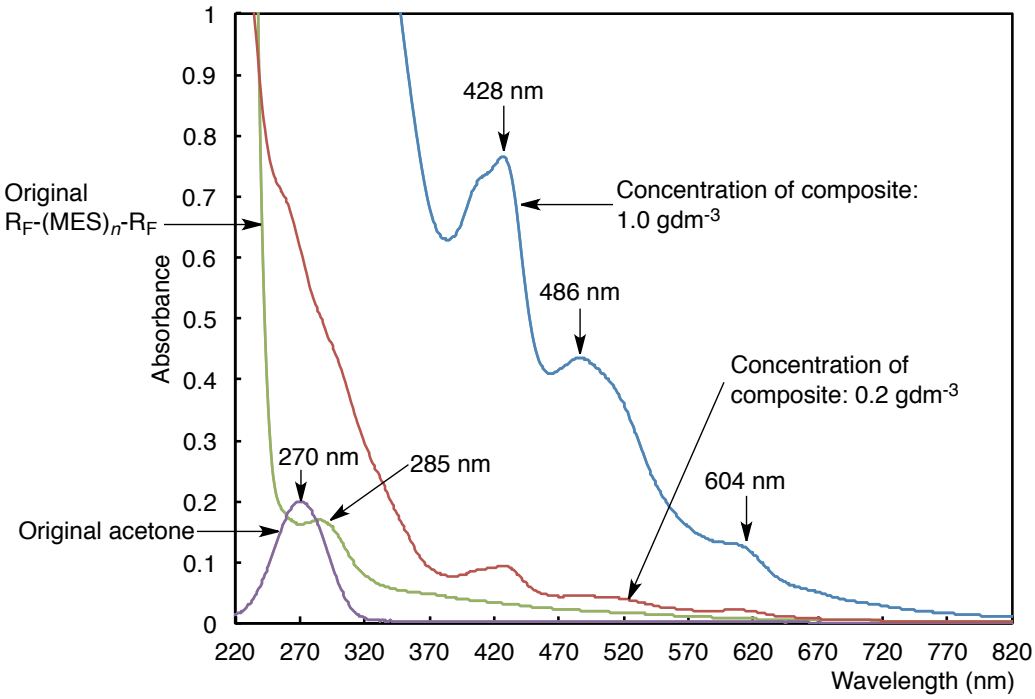


Fig. 3-8 UV-vis spectra of methanol solutions of the $R_F$-(MES)$_n$-$R_F$/acetone composites (Run 17 in Table 3-3; 1.0 and 0.2 gdm$^{-3}$), the $R_F$-(MES)$_n$-$R_F$ homo-oligomer (5.0 gdm$^{-3}$), and acetone (1.4 x 10$^{-5}$ mM).

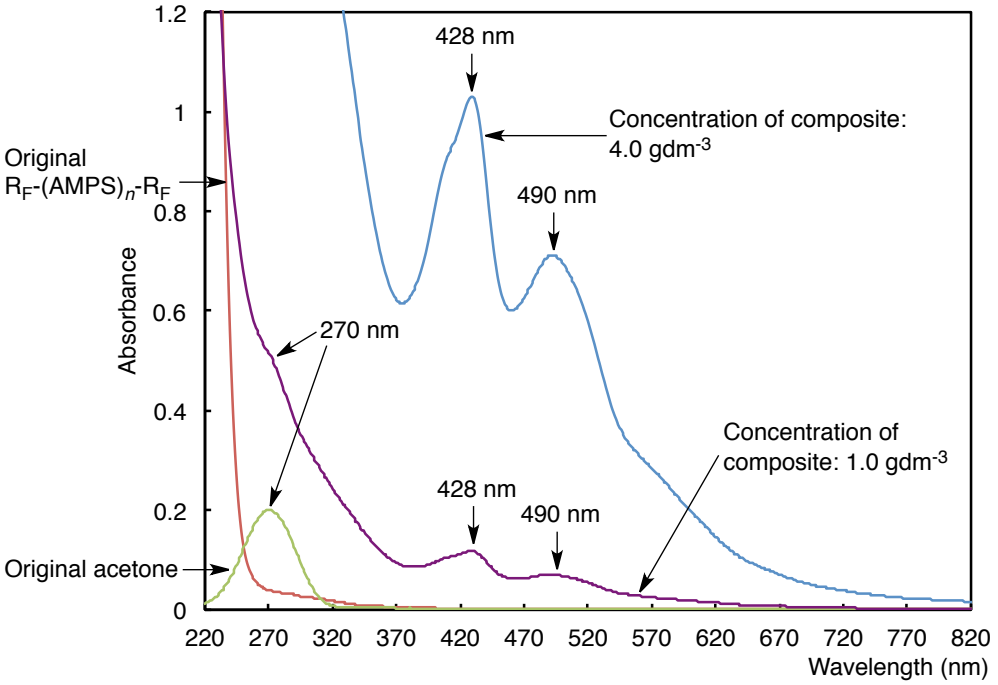


Fig. 3-9 UV-vis spectra of methanol solutions of the $R_F$-(AMPS)$_n$-$R_F$/acetone composites (Run 11 in Table 3-2; 4.0 and 1.0 gdm$^{-3}$), the $R_F$-(AMPS)$_n$-$R_F$ homo-oligomer (5.0 gdm$^{-3}$), and acetone (1.4 x 10$^{-5}$ mM).

Nitric acid and phosphoric acid did not react with acetone to produce a color change (Table 3-3); however, sulfuric acid did react with acetone to afford a dark brown viscous liquid [Fig. 3-7(C)]. The UV-vis spectra of the dark brown product in methanol showed an absorption peak at 428 nm, which was different from those of the $R_F$-$(AMPS)_n$-$R_F$/acetone and $R_F$-$(MES)_n$-$R_F$/acetone composites. This suggests that the color depends on the acidity of these catalysts. Thus, the pH values of the catalyts, the $R_F$-$(AMPS)_n$-$R_F$ homo-oligomer, the $R_F$-$(MES)_n$-$R_F$ homo-oligomer, and the -$(AMPS)_n$- homo-oligomer were measured at 25 °C as followings:

| $H_2SO_4$ | $HNO_3$ | $R_F$-$(MES)_n$-$R_F$ | $H_3PO_4$ | $R_F$-$(AMPS)_n$-$R_F$ | -$(AMPS)_n$- |
|---|---|---|---|---|---|
| 2.28[a)] | 2.48[a)] | 2.76[b)] | 2.81[a)] | 2.86[b)] | 3.21[b)] |

[a)]Concentration of acid catalyst: 4.8 mmoldm$^{-3}$.
[b)]Concentration of oligomer based on monomer unit: 4.8 mmoldm$^{-3}$.

The acidity of $HNO_3$, $H_3PO_4$, and -$(AMPS)_n$- was lower that that of $H_2SO_4$, which suggests that they cannot interact with acetone and produce the color. The acidity of the $R_F$-$(MES)_n$-$R_F$ and $R_F$-$(AMPS)_n$-$R_F$ homo-oligomers was also lower than that of $H_2SO_4$, although these fluorinated oligomers were colored. This suggests that acetone is likely to interact with the sulfo groups (-$SO_3H$) in the fluorinated oligomeric aggregate cores and sulfobetaine segments (-$NH(C{=}O)CMe_2CH_2SO_3H$) in the gel network cores, to produce the color.

The polyaldol condensations of phenylacetaldehyde, acetaldehyde, and acetone have been investigated.[26 ~ 35)] The polyaldol condensation of phenylacetaldehyde catalyzed by sulfuric

acid in dioxane leads to the formation of polyphenylacetylene.[26] The aldol condensation of acetaldehyde catalyzed by silica supported ziriconium oxide selectively produces crotonaldehyde.[28] Transition metal alkyls are useful catalysts for the preparation of poly(acetaldehyde) through the acetaldehyde polyaldol condensation.[27] The acetone polyaldol condensation catalyzed by acidic molecular sieves at 21 ~ 115 °C gives the diacetone alcohol (acetone dimer), mesityl oxide (acetone dimer), phorone (acetone trimer), and isophorone (acetone trimer), which have absorption peaks around 200 ~ 385 nm.[29] It has been reported that acetone reacts with sulfuric acid to give mesityl oxide ($\lambda_{max}$ = 284 nm) and phorone ($\lambda_{max}$ = 339 nm).[33] In contrast, the reaction of acetone with sulfuric acid at 25 °C for 120 h or 150 °C for 18 h formed acetone polyaldol condensation products, such as mesityl oxide, phorone, acetone tetramers, acetone pentamers, and acetone hexamers.[35] The acetone tetramers, pentamers, and hexamers have absorption peaks ($\lambda_{max}$) at 335, 360 ~ 380, and 441 nm, respectively (Scheme 3-2).[35]

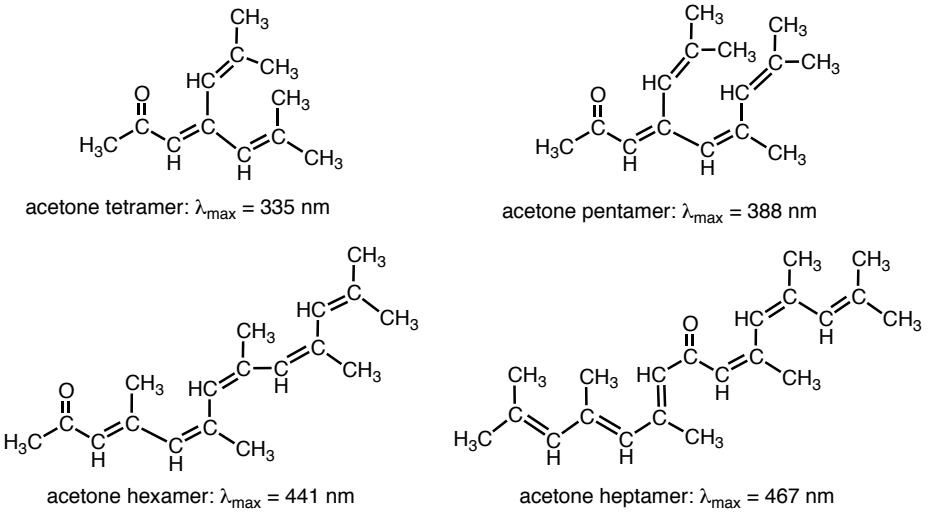


Scheme 3-2 Proposed structures of the acetone tetramer, pentamer, hexamer, and heptamer polyaldol condensation products. [35)]

Sodium hydroxide is required to neutralize the free sulfuric acid during the isolation of the acetone polyaldol condensation products. [35)] The absorption peak at $\lambda_{max}$ = 428 nm in the dark brown product derived from the acetone/sulfuric acid composite in Fig. 3-10 may arise from the formation of acetone hexamers.

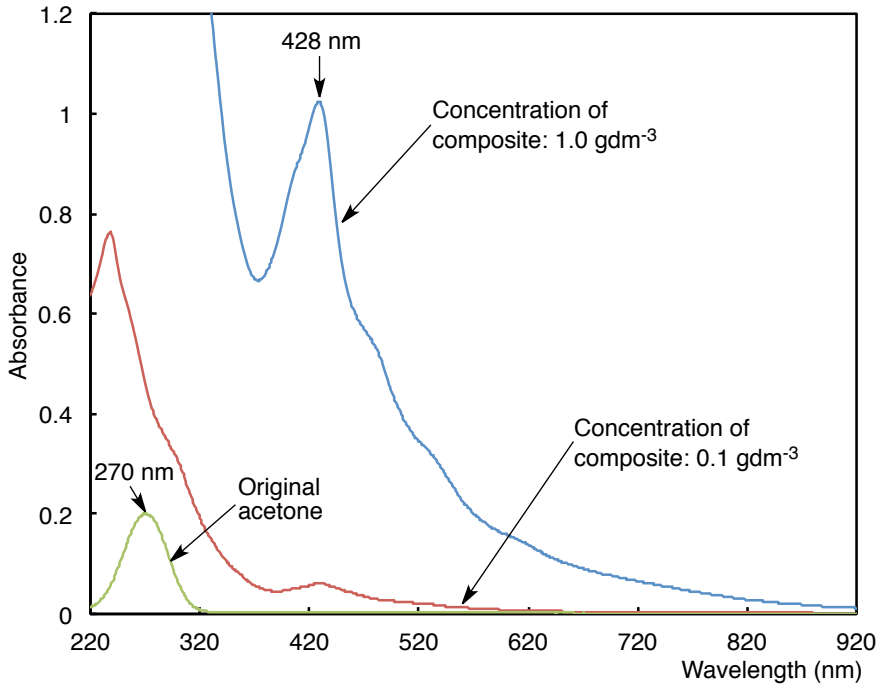


Fig. 3-10 UV-vis spectra of methanol solutions of the $H_2SO_4$/acetone composites (Run 18 in Table 3-3; 1.0 and 0.1 $gdm^{-3}$), and acetone (1.4 x $10^{-5}$ mM).

Fig. 3-9 shows the $R_F$-$(AMPS)_n$-$R_F$/acetone composite absorption peaks around 428 nm and 490 nm, indicating that the acetone polyaldol condensations proceeded more effectively in the $R_F$-$(AMPS)_n$-$R_F$ homo-oligomeric gel network cores, compared with the usual acetone polyaldol condensations by sulfuric acid, and also produce acetone heptamers ($\lambda_{max}$ = 490 nm). Cataldo reported that the absorption peak of acetone heptmers is around 467 nm (Scheme 3-2). [35]

The $R_F$-$(MES)_n$-$R_F$ homo-oligomer is more acidic than the $R_F$-$(AMPS)_n$-$R_F$ homo-oligomer. Thus, in the $R_F$-$(MES)_n$-$R_F$ homooligomer, the acetone should interact more effectively with the sulfo groups in the fluorinated oligomeric aggregate cores, compared with

the $R_F$-$(AMPS)_n$-$R_F$ homo-oligomeric gel network cores. This interaction should produce an additional red-shifted absorption peak at 486 nm, from the formation of further polycondensation products (Fig. 3-9).

### 3.3.3. Decoloring behavior of fluoroalkyl end-capped 2-acrylamido-2-methylpropane-sulfonic acid homo-oligomer/acetone composite in methanol

Dissolving the reddish-brown $R_F$-$(AMPS)_x$-$(Ad\text{-}HAc)_y$-$R_F$/acetone composite powders in methanol produced a colorless solution. Figs. 3-11 ~ 3-13 show the changes in the UV-vis spectrum of the $R_F$-$(AMPS)_n$-$R_F$ /acetone composite (Run 11, Table 3-2) in methanol solution at room temperature, when the solution was kept in the dark, in natural light, and under UV irradiation ($\lambda_{max}$ = 365 nm).

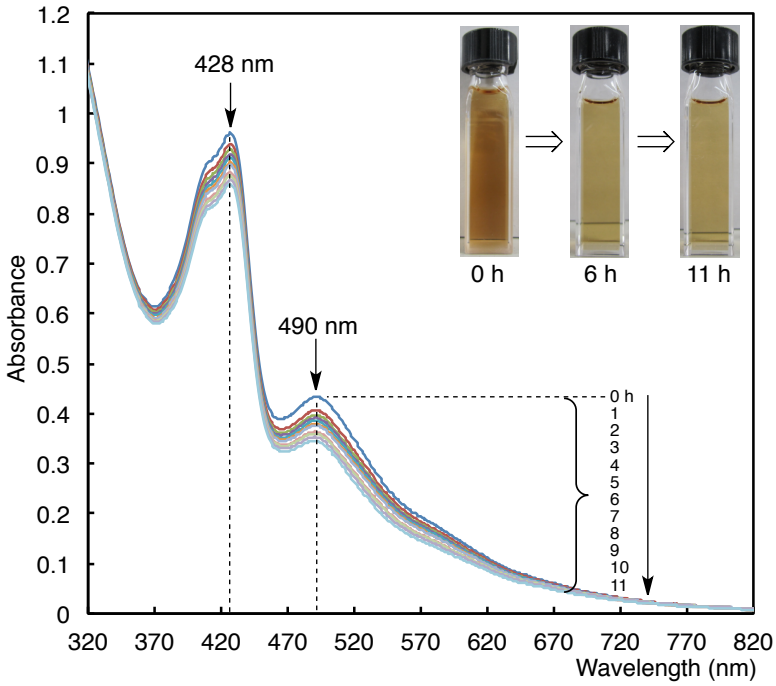


Fig. 3-11 Change in UV-vis spectra of methanol solutions of $R_F$-$(AMPS)_n$-$R_F$/acetone composite (Run 11 in Table 3-2; 4.0 $gdm^{-3}$) in the dark at 25 °C.

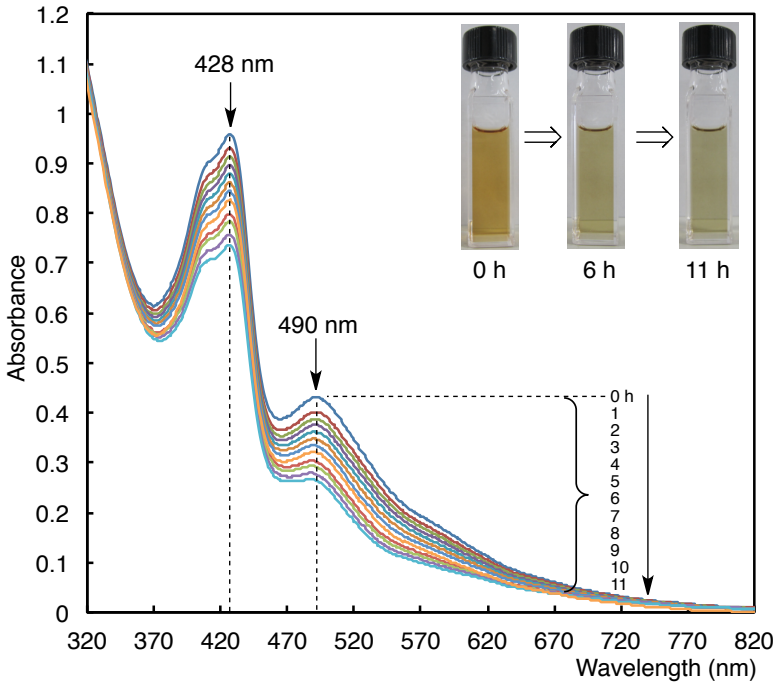


Fig. 3-12 Change in UV-vis spectra of methanol solutions of $R_F$-$(AMPS)_n$-$R_F$/acetone composite (Run 11 in Table 3-2; 4.0 $gdm^{-3}$) in natural light at 25 °C.

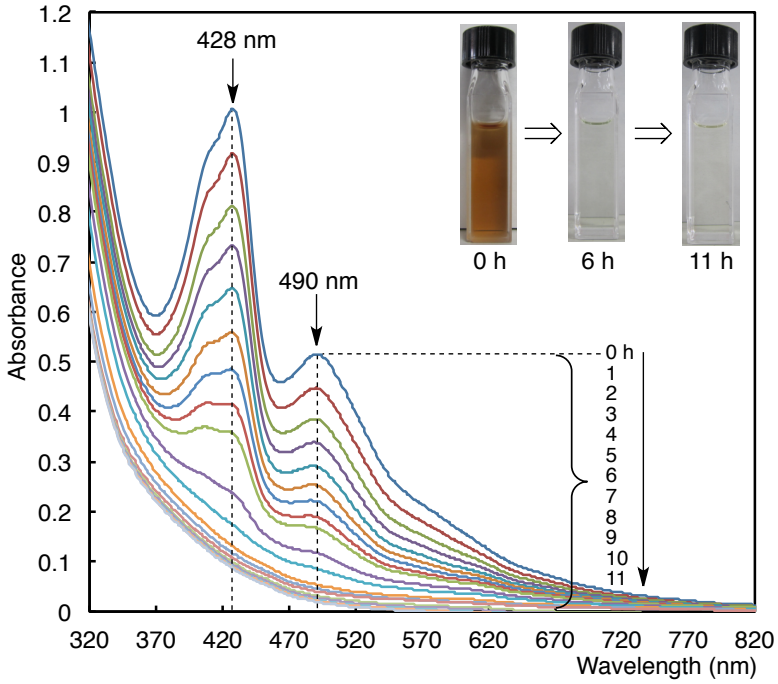


Fig. 3-13 Change in UV-vis spectra of methanol solutions of $R_F$-$(AMPS)_n$-$R_F$/acetone composite (Run 11 in Table 3-2; 4.0 $gdm^{-3}$) under UV irradiation at 25 °C.

The colored $R_F$-$(AMPS)_n$-$R_F$/acetone composite powders were very stable and did not change color at room temperature in natural light after 2 years. However, the absorption peaks at 428 and 490 nm in the $R_F$-$(AMPS)_n$-$R_F$/acetone composite methanol solutions decreased over time in the dark at 25 °C (Fig. 3-11). A faster decrease in the absorption peaks was observed in the light, and the fastest decrease was observed under UV irradiation (Figs. 3-12 and 3-13). The first-order rate constants ($k$) for the decrease in the absorbances at 428 and 490 nm at 25 °C were determined using these absorption peaks as following:

| | *k* (at 428 nm) ($h^{-1}$) | *k* (at 490 nm) ($h^{-1}$) |
|---|---|---|
| Dark | $1.09 \times 10^{-2}$ | $2.21 \times 10^{-2}$ |
| Natural light | $2.30 \times 10^{-2}$ | $4.35 \times 10^{-2}$ |
| UV irradiation[a)] | $7.66 \times 10^{-1}$ | $8.29 \times 10^{-1}$ |

[a)]Rate constants based on a function of time from 0 to 3 h.

The decrease followed a first-order equation, and the rate constants increased from $1.09 \times 10^{-2}$ (428 nm) and $2.21 \times 10^{-2}$ (490 nm) in the dark to $7.66 \times 10^{-1}$ (428 nm) and $8.29 \times 10^{-1}$ (490 nm) under UV irradiation. The fastest decolorization was about 70-fold faster for the absorption peak at 428 nm and about 38-fold faster at 490 nm for the measurements under UV irradiation compared with the dark. This suggests that the acetone retro-aldol polycondensation proceeded faster under UV irradiation (Scheme 3-3).

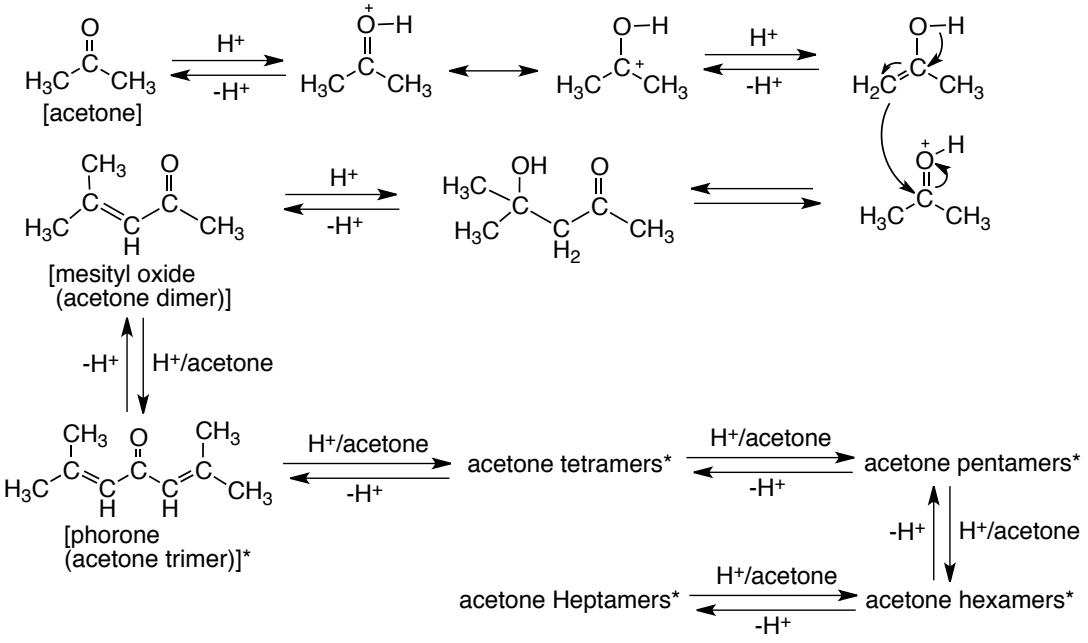


*For the formation of these oligomers: see Ref. 16

Scheme 3-3 Proposed mechanism for the acid-catalysed acetone aldol and retoro-aldol polycondensation.

In this retro-aldol polycondensation, acetone is formed as the final product. The acetone absorption peak at 270 nm increased (Fig. 3-9) with the increase in rate constant ($k$ = 1.09 × $10^{-1}$ $h^{-1}$) for the $R_F$-$(AMPS)_n$-$R_F$/acetone composite methanol solution (1.0 $gdm^{-3}$, Run 11, Table 3-2) under UV irradiation at 25 °C.

The $R_F$-$(AMPS)_n$-$R_F$ and $R_F$-$(MES)_n$-$R_F$ homo-oligomers probably contain trace amounts of water, because they possess sulfobetaine segments and sulfo groups in their fluorinated oligomers, respectively. This means that the acid-catalyzed retro-aldol polycondensation, where the carbonium ion undergoes nucleophilic attack by water, should proceed smoothly in the fluorinated oligomeric aggregates cores (Scheme 3-4).

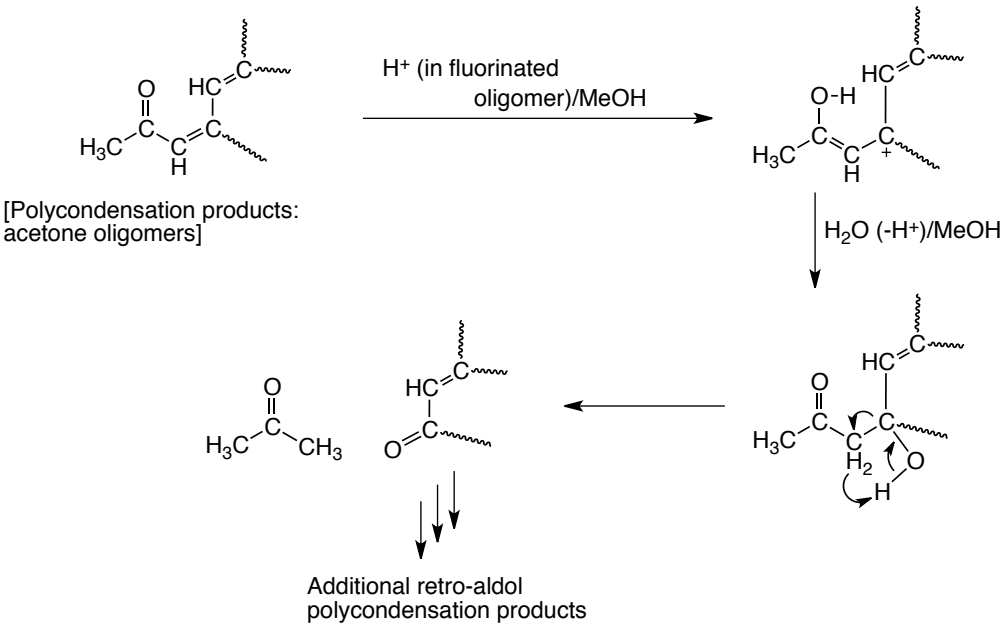


Sheme 3-4 Proposed mechanism for the retro-aldol polycondensation of acetone under acidic conditions.

Acid catalyzed polyaldol condensations have been thoroughly investigated. [26 ~ 29, 31, 35] However, the polycondensation products are usually isolated after the free acid catalysts are neutralized. Thus, the retro-aldol condensation has not been extensively studied except for the amino acids such as glycine-catalyzed retroaldol condensation of α,β-unsaturated aldehydes. [36, 37] Thus, this is the first example of the retro-aldol polycondensation of acetone under very mild conditions.

### 3.4. Conclusion

A reddish-brown fluoroalkyl end-capped AMPS homooligomer [$R_F$-(AMPS)$_n$-$R_F$]/acetone composite was prepared by heating a mixture of the corresponding white oligomer with acetone at 80 °C for 3 h. The color was not observed in the corresponding non-fluorinated AMPS oligomer/acetone composite, which was prepared under similar conditions. The color may arise from acetone encapsulated in the fluorinated oligomeric gel network cores forming acetone polyaldol condensation products. The colored $R_F$-(AMPS)$_n$-$R_F$/acetone composite was very stable, and did not change color after 2 years in natural light at room temperature. The colored composite was very soluble in methanol and decolored over 1 day at room temperature because of the retropolyaldol condensation. The rate of the retro-polyaldol condensation increased between 38- and 70-fold under UV irradiation, compared with the reaction in the dark. The coloring–decoloring was repeatable; therefore the fluorinated oligomer/acetone composites are promising candidates for new fluorinated coloring materials.

**References**


1) B. Ameduri, B. Boutevin, Well-Architectured Fluoropolymers: Synthesis, Properties and Applications; Amsterdam: Elsevier, 231 (2004).

2) J.-F. Berret, D. Calvet, A. Collet, and M. Viguier, *Curr. Opin. Colloid Interface Sci.*, **8**, 296 (2003).

3) T. Imae, *Curr. Opin. Colloid Interface Sci.*, **8**, 307 (2003).

4) T. Imae, H. Tabuchi, K. Funayama, A. Sato, T. Nakamura, and N. Amaya, *Colloids Surf. A*, **167**, 73 (2000).

5) P. Lebreton, B. Ameduri, B. Boutevin, and J. M. Corpart, *Macromol. Chem. Phys.*, **203**, 522 (2002).

6) M. J. Monteiro, M. M. Adamy, B. J. Leeuwen, A. M. Van Herk, and M. Destarac, *Macromolecules*, **38**, 1538 (2005).

7) A. E. Feiring, E. R. Wonchoba, F. Davdson, V. Percec, and B. Barboiu, *J. Polym. Sci. Part A: Polym. Chem.*, **38**, 3313 (2000).

8) M. Destarac, K. Matyjaszewski, E. Silverman, B. Ameduri, and B. Boutevin, *Macromolecules*, **33**, 4613 (2000).

9) Z. Shi and S. Holdcroft, *Macromolecules*, **38**, 4193 (2005).

10) K. Jankova and S. Hvilsted, *J. Fluorine Chem.*, **126**, 241 (2005).

11) G. Laruelle, E. Nicol, B. Ameduri, J. F. Tassin, and N. Ajellal, *J. Polym. Chem. Sci. Part A: Polym. Chem.*, **49**, 3960 (2011).

12) Y. Patil and B. Ameduri, *Polym. Chem.*, **4**, 2783 (2013).

13) H. Sawada, *Chem. Rev.*, **96**, 1779 (1996).

14) H. Sawada and T. Kawase, *Kobunshi Ronbunshu*, **58**, 147 (2001).

15) H. Sawada and T. Kawase, *Kobunshi Ronbunshu*, **58**, 255 (2001).

16) H. Sawada, *J. Fluorine Chem.*, **105**, 219 (2000).

17) H. Sawada, *Prog. Polym. Sci.*, **32**, 509 (2007).

18) H. Sawada, *Polym. Chem.*, **3**, 46 (2012).

19) M. Mugisawa, K. Ohnishi, and H. Sawada, *Langmuir*, **23**, 5848 (2007).

20) M. Mugisawa and H. Sawada, *Langmuir*, **24**, 9215 (2008).

21) H. Sawada, T. Kijima, and M. Mugisawa, *Polym. J.*, **42**, 494 (2010).

22) T. Kijima, I. Javakhishvili, K. Jankova, S. Hvilsted, S. Kodama, M. Sugiya, and H. Sawada, *Colloid Polym. Sci.*, **290**, 589 (2012).

23) M. Mugisawa, K. Ueno, K. Hamazaki, and H. Sawada, *Macromol. Rapid Commun.*, **28**, 733 (2007).

24) H. Sawada, S. Katayama, A. Ariyoshi, T. Kawase, Y. Hayakawa, T. Tomita, and M. Baba,

*J. Mater. Chem.*, **8**, 1517 (1998).

25) H. Sawada, A. Ohashi, M. Baba, T. Kawase, and Y. Hayakawa, *J. Fluorine Chem.*, **79**, 149 (1996).

26) F. Cataldo, *Polym. Int.*, **39**, 91 (1996).

27) T. Yamamoto, S. Konagaya, and A. Yamamoto, *J. Polym. Sci.: Polym. Lett. Ed.*, **16**, 7 (1978).

28) V. V. Ordomsky, V. L. Sushkevich, I. I. Ivanova, *J. Mol. Catal. A*, **333**, 85 (2010).

29) C. Flego and C. Perego, *Appl. Catal. A*, **192**, 317 (2000).

30) R. J. Gillespie and J. S. Hartman, *Can. J. Chem.*, **46**, 3799 (1968).

31) H. Miyama and M. Kamachi, *J. Polym. Sci. Part B: Polym. Lett.*, **3**, 241 (1965).

32) F. Cataldo, *Angew. Makromol. Chem.*, **236**, 21 (1996).

33) S. Nagakura, A. Minegishi, and K. Stanfield, *J. Am. Chem. Soc.*, **79**, 1033 (1957).

34) C. G. Swain and A. S. Rosenberg, *J. Am. Chem. Soc.*, **83**, 2154 (1961).

35) F. Cataldo, *Angew. Makromol. Chem.*, **236**, 1 (1996).

36) W. A. W. Wolken, R. T. Have, and M. J. van der Werf, *J. Agric. Food Chem.*, **48**, 5401 (2000).

37) W. A. M. Wolken, J. Tramper, and M. J. van der Werf, *Flavour Fragr. J.*, **19**, 115 (2004).

CHAPTER 4

# Homoaldol Condensation of Aromatic Ketones in Fluoroalkyl End-Capped 2-Acrylamido-2-methylpropanesulfonic Acid Oligomeric Gel Network Cores

## 4.1. Introduction

Organofluorine compounds possessing longer fluoroalkyl groups are attractive materials due to a variety of unique properties such as surface active properties, and excellent thermal and chemical stability that set them apart from the corresponding non-fluorinated materials. [1 ~ 23)] Especially, fluoroalkyl end-capped oligomers are attractive functional materials because they exhibit a variety of unique properties such as high solubility, surface active properties, biological activities, and nanometer size-controlled self-assembled molecular aggregates which cannot be achived by the corresponding non-fluorinated and randomly fluoroalkylated ones. [24 ~ 29)] In these fluoroalkyl end-capped oligomers, fluoroalkyl end-capped 2-acrylamido-2-metylpropanesulfonic acid oligomer [$R_F$-(AMPS)$_n$-$R_F$] can form the gel under non-crosslinking conditions through the synergistic interaction between the aggregation of terminal fluoroalkyl segments and the ionic interaction of sulfobetain-type segments in oligomer. [30, 31)] Fluoroalkyl end-capped 2-acrylamido-2-metylpropanesulfonic acid cooligomers containing adamantyl segments were also prepared by reaction of fluoroalkanoyl peroxide with 2-acrylamido-2-metylpropanesulfonic acid (AMPS) and 3-hydoroxy-1-adamantyl acrylate (Ad-HAc). [32, 33)] These obtained fluorinated AMPS–Ad-HAc cooligomers can form the nanometer size-controlled fine particles not only in water but also in

a large variety of traditionally organic solvents. [32, 33] Fluoroalkyl end-capped 2-acrylamido-2-methylpropanesulfonic acid cooligomeric nanoparticles containing adamantyl segments were able to interact with a variety of metal particles such as magnetic nanoparticles, [34] gold nanoparticles [35] and palladium nanoparticles [36] to give the colloidal stable fluorinated sulfobetaine-type cooligomeric nanocomposites-encapsulated such metal nanoparticles. Therefore, it is particularly desirable to develop fluoroalkyl end-capped AMPS oligomeric nanoparticles for encapsulating not only metal nanoparticles but also organic guest molecules. In fact, the encapsulation of acetone in fluoroalkyl end-capped AMPS oligomeric aggregate cores was observed to give the reddish-brown fluorinated AMPS oligomer $[R_F\text{-}(AMPS)_n\text{-}R_F]$/acetone composite. [37] It has been demonstrated that the color can arise from acetone encapsulated in the fluorinated AMPS oligomeric gel network cores forming acetone polyaldol condensation products. [37] In addition, the retro-polyaldol condensation of acetone was also found to decolor the solution after 1 day at room temperature. [37] This chapter demonstrates that $R_F\text{-}(AMPS)_n\text{-}R_F$ oligomer can interact with not only acetone but also aromatic ketones such as 4'-methoxyacetophnone to give the homoaldol condensation product under mild conditions, although the corresponding non-fluorinated AMPS oligomer and sulfuric acid cannot afford the corresponding products at all under similar conditions.

## 4.2. Experimental

### 4.2.1 Measurements

$^{1}$H NMR spectra were recorded using a JEOL JNM-ECA 500 (500 MHz) FT NMR SYSTEM (Tokyo, Japan). Ultraviolet–visible (UV–vis.) spectra were carried out using a Shimadzu UV-1800 UV–vis. spectrophotometer (Kyoto, Japan). UV irradiation was performed by using a UV lamp (SLUV-6, AS ONE, Japan). The pH measurement was performed by using a pH meter (PH-02, AS ONE, Japan). GC-MS spectra were obtained with a Hewlett PACARD 5890 GC/5972 MSD or a JEOL JMS AX-505H spectrometer equipped with a JEOL JMA 5000 mass data system using an electron-impact ionization technique at 70 eV.

### 4.2.2. Materials

4'-Methoxyacetophenone (MAP), acetophenone (AP), 4-acetylbiphenyl (ABP), 2-acetyl-6-methoxynaphthalene (AMN) were purchased from Tokyo Chemical Indusrty Co., Ltd. (Tokyo, Japan). AMPS monomer was received from Wako Pure Chemical Industries, Ltd.

(Osaka, Japan). The $R_F$-$(AMPS)_n$-$R_F$ oligomer was prepared by reacting fluoroalkanoyl peroxide with the corresponding monomer according to the previously reported method.[30, 31] The $R_F$-$(AMPS)_n$-$R_F$ oligomer was obtained as a white powder by reprecipitation with water-tetrahydrofuran, and was dried under vacuum at 50 °C for 2 days.[30, 31] The molecular weight of this oligomer cannot be determined due to the gelling characteristic.[30, 31]

### 4.2.3. Preparation of $R_F$-$(AMPS)_n$-$R_F$/MAP composite

4'-Methoxyacetophenone (MAP: 11 mmol) was directly added to the methanol solution (22 mL) of fluoroalkyl end-capped 2-acrylamido-2-metylpropanesulfonic acid oligomer [$R_F$-$(AMPS)_n$-$R_F$; $R_F$ = $CF(CF_3)OC_3F_7$; (2.21 g)], and the mixture was heated at 80 °C for 3 h under the air. The obtained product was dried in vacuo at room temperature for 12 h to give $R_F$-$(AMPS)_n$-$R_F$/MAP composite powders (3.49 g).

Non-fluorinated 2-acrylamido-2-metylpropanesulfonic acid oligomer [-$(AMPS)_n$-]/MAP composite and $H_2SO_4$/MAP composite were also prepared under similar conditions.

### 4.2.4. Extraction of homoaldol conadensation product of MAP from $R_F$-$(AMPS)_n$-$R_F$/MAP composite

A solution of $R_F$-(AMPS)$_n$-$R_F$/MAP composite (3.49 g) in MeOH (240 mL) was added to 1,2-dichloroethane (480 mL) and water (600 mL), and then stirring with a magnetic stirring bar. After the mixture was stirred at room temperature for 10 min, the organic layer was concentrated in vacuum to give the expected product in 0.54 g isolated yield.

## 4.3. Results and discussion

### 4.3.1. Preparation of $R_F$-(AMPS)$_n$-$R_F$/MAP composites and characterization of homoaldol product of MAP

Fluoroalkyl end-capped AMPS oligomer [$R_F$-(AMPS)$_n$-$R_F$; $R_F$ = $CF(CF_3)OC_3F_7$] interacted with 4'-methoxyacetophenone (MAP) at 80 °C for 3 h to give the $R_F$-(AMPS)$_n$-$R_F$/MAP composite as shown in Scheme 4-1. Similarly, a variety of $R_F$-(AMPS)$_n$-$R_F$/aromatic ketones composites were prepared by treating mixtures of fluorinated oligomer and aromatic ketones such as acetophenone (AP), 4-acetylbiphenyl (ABP), 2-acetyl-6-methoxynaphthalene (AMN) under similar conditions. These results were also show in Scheme 4-1.

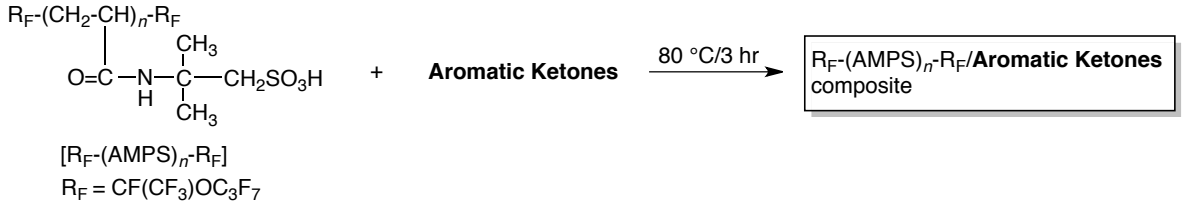


$[R_F\text{-}(AMPS)_n\text{-}R_F]$

$R_F = CF(CF_3)OC_3F_7$

| $R_F$-$(AMPS)_n$-$R_F$ [g] | Aromatic Ketones [mmol (g)] | | Isolated yield of the composite [g] |
|---|---|---|---|
| 2.21 | 4'-methoxyacetophenone (MAP) [11.0 (1.69)] | 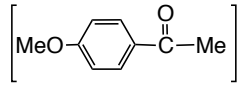 | 3.49 |
| 0.10 | acetophenone (AP) [0.50 (0.06)] | 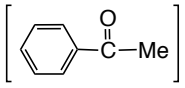 | 0.12 |
| 0.10 | 4-acetylbiphenyl (ABP) [0.50 (0.10)] | 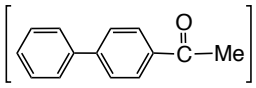 | 0.19 |
| 0.10 | 2-acetyl-6-methoxynaphtalene (AMN) [0.50 (0.10)] | 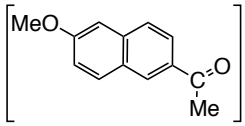 | 0.19 |

Scheme 4-1 Preparation of $R_F$-$(AMPS)_n$-$R_F$/aromatic ketones composite

The obtained $R_F$-$(AMPS)_n$-$R_F$/MAP composite was solubilized into methanol, extracted with the mixture of 1,2-dichloroethane and water [8/10 (vol./vol.)]. The organic solution was concentrated in vacuum to give the expected product in 35 % isolated yield (based on the used MAP) (see Scheme 4-2).

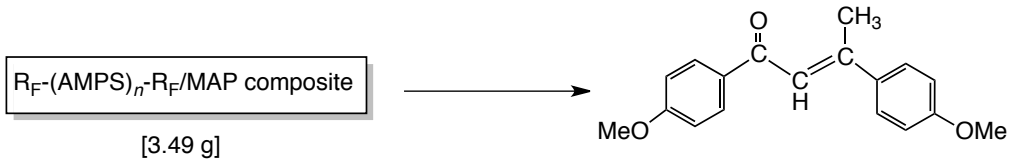


Scheme 4-2 Formation of homoaldol condensation product of MAP from $R_F$-$(AMPS)_n$-$R_F$/MAP composite

UV-vis spectra of the methanol solution of the product from the $R_F$-$(AMPS)_n$-$R_F$/MAP composite exhibited a clear absorption peak around 327 nm, of whose peak is quite different from that ($\lambda_{max}$: 270 nm) of the original MAP (see Fig. 4-1).

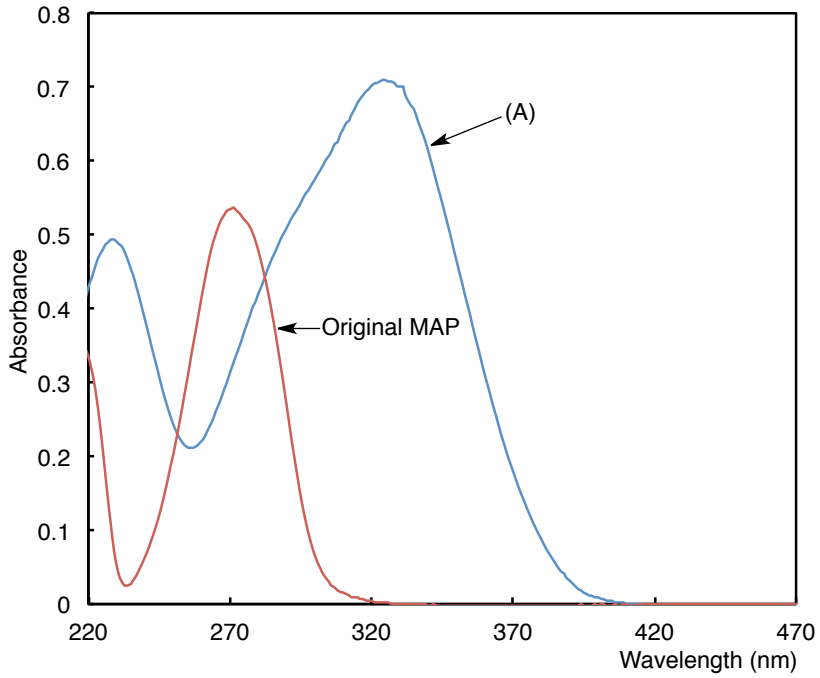


Fig. 4-1 UV-vis spectra of the homoaldol condensation product of MAP [(A): 167 $mgdm^{-3}$] from the $R_F$-$(AMPS)_n$-$R_F$/MAP composite in methanol and the original MAP (26.4 $\mu moldm^{-3}$).

$^1H$ NMR spectra of the obtained product show the formation of homoaldol comdensation product of MAP (see Fig. 4-2).

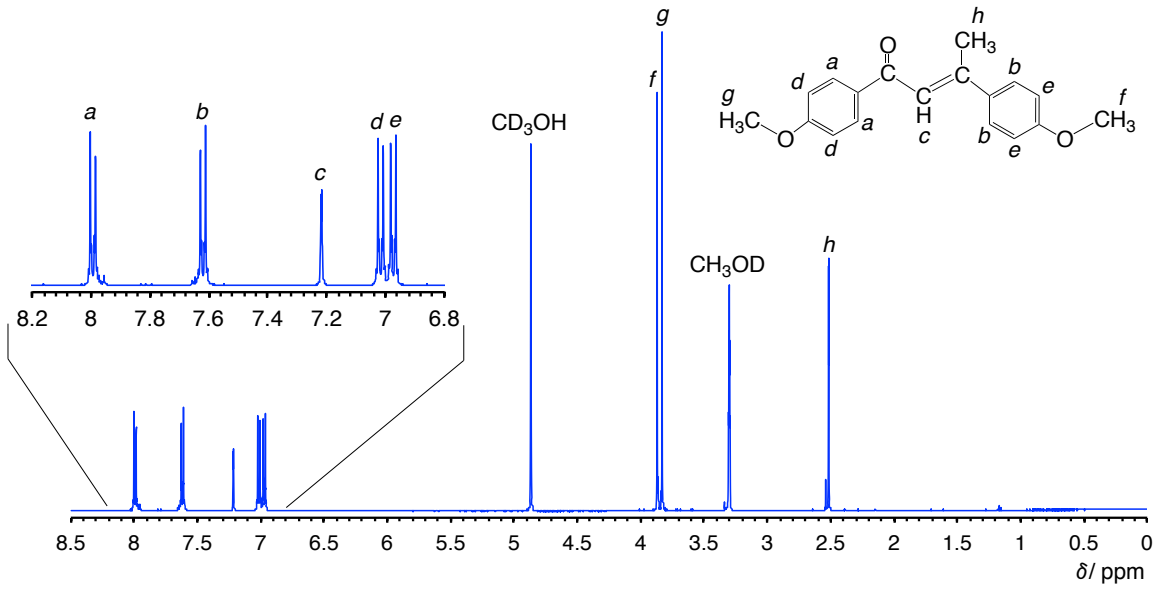


Fig. 4-2 $^{1}$H NMR spectra of homoaldol condensation product of MAP from the $R_F$-(AMPS)$_n$-$R_F$/MAP composite in $CD_3OD$

GC-MS spectra also exhibited the formation of the expected homoaldol product [$M^+$: 282]. Interestingly, $^{1}$H NMR spectra of the reaction product depicted the only *trans* form. Hitherto, there have been numerous reports on the photoisomerization of α,β-unsaturated ketones such as chalcones from the developmental viewpoints of novel photochromic materials.[38 ~ 41] Thus, in order to clarify the trans product formation, the photoisomerization of the homoaldol product have been studied under UV light irradiation ($\lambda_{max}$: 365 nm) at 25 °C by using $^{1}$H NMR specrtra and UV-vis spectra measurements. These results were show in Figs. 4-3 and 4-4.

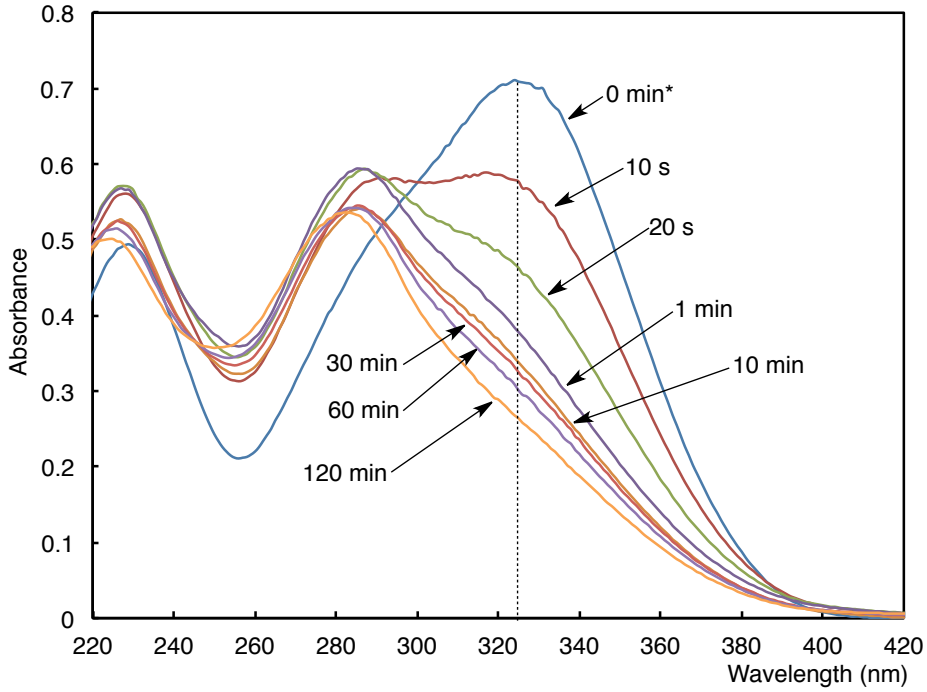


Fig. 4-3 Changes in the UV-vis spectra of the methanol solution of the homoaldol condensation product of MAP (167 mgdm$^{-3}$) from the $R_F$-$(AMPS)_n$-$R_F$/MAP composite under the UV irradiation ($\lambda_{max}$ = 365 nm) at 25 °C: *UV irradiation time

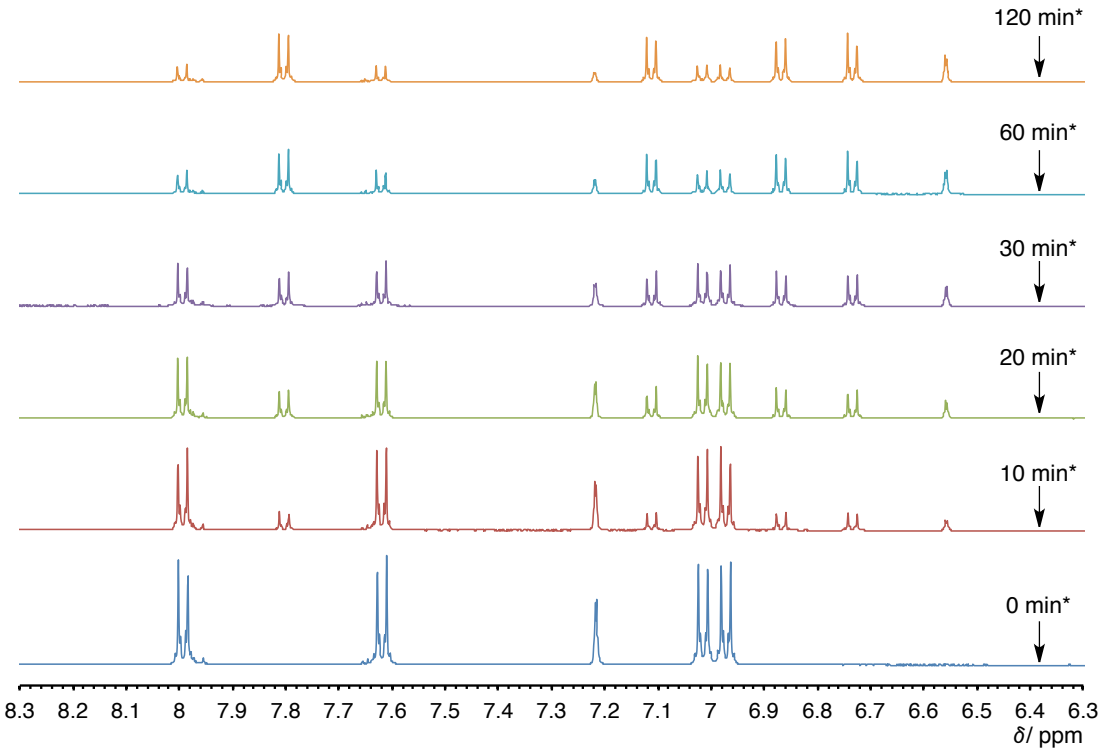


Fig. 4-4 Changes in the $^1$H NMR spectra of the homoaldol condensation product of MAP from the $R_F$-$(AMPS)_n$-$R_F$/MAP composite under UV (lmax = 365 nm) irradiation in $CD_3OD$ at 25 °C.
*UV irradiation time

UV-vis spectra and $^1$H NMR specrtra show that the photoisomerization of the homoaldol product from *trans* to *cis* form can proceed smoothly under UV light irradiation, indicating that the $R_F$-$(AMPS)_n$-$R_F$ oligomer should give selectively *trans*-homoaldol product of MAP.

### 4.3.2. Homoaldol condensation of AP, ABP and AMN in the presence of $R_F$-$(AMPS)_n$-$R_F$ oligomer

The homoaldol reaction products, which were obtained from the $R_F$-$(AMPS)_n$-$R_F$/AP composite (see Scheme 4-1) have been studied by the use of UV-vis spectra and 1H NMR spectra measurements, and the results are shown in Scheme 4-3, Figs. 4-5 and 4-6.

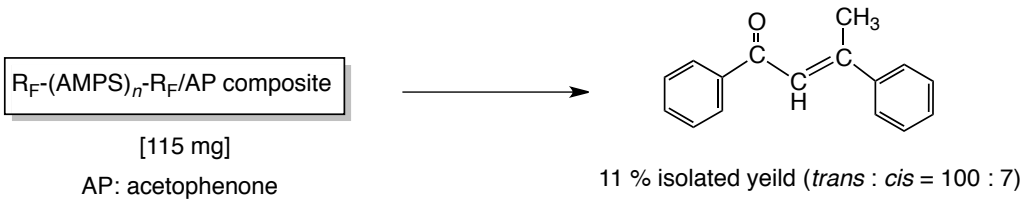


Scheme 4-3 Formation of homoaldol condensation product of AP from $R_F$-$(AMPS)_n$-$R_F$/AP composite

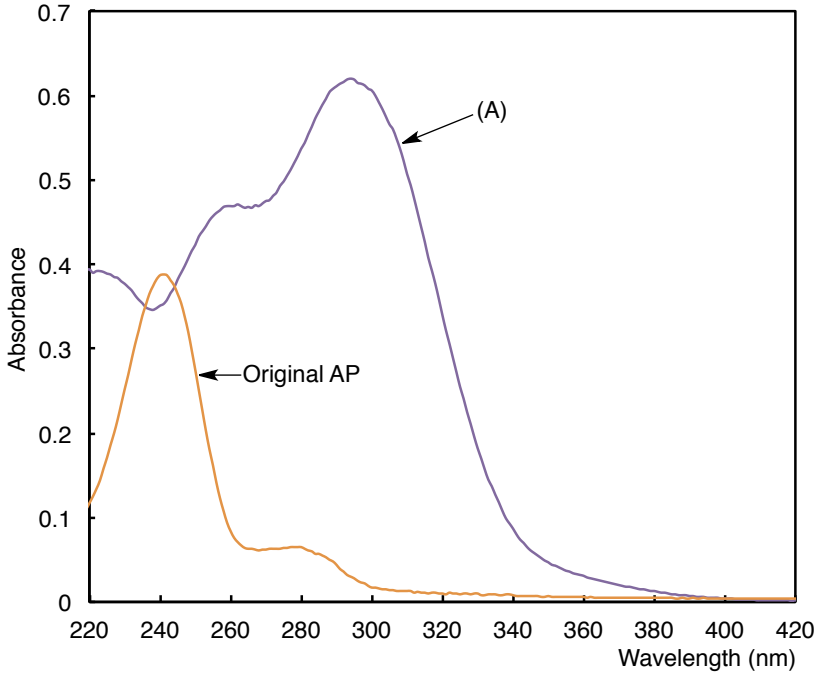


Fig. 4-5 UV-vis spectra of the homoaldol condensation product of AP [(A): 100 mgdm$^{-3}$] from the $R_F$-$(AMPS)_n$-$R_F$/AP composite in methanol and the original AP (26.4 μmoldm$^{-3}$).

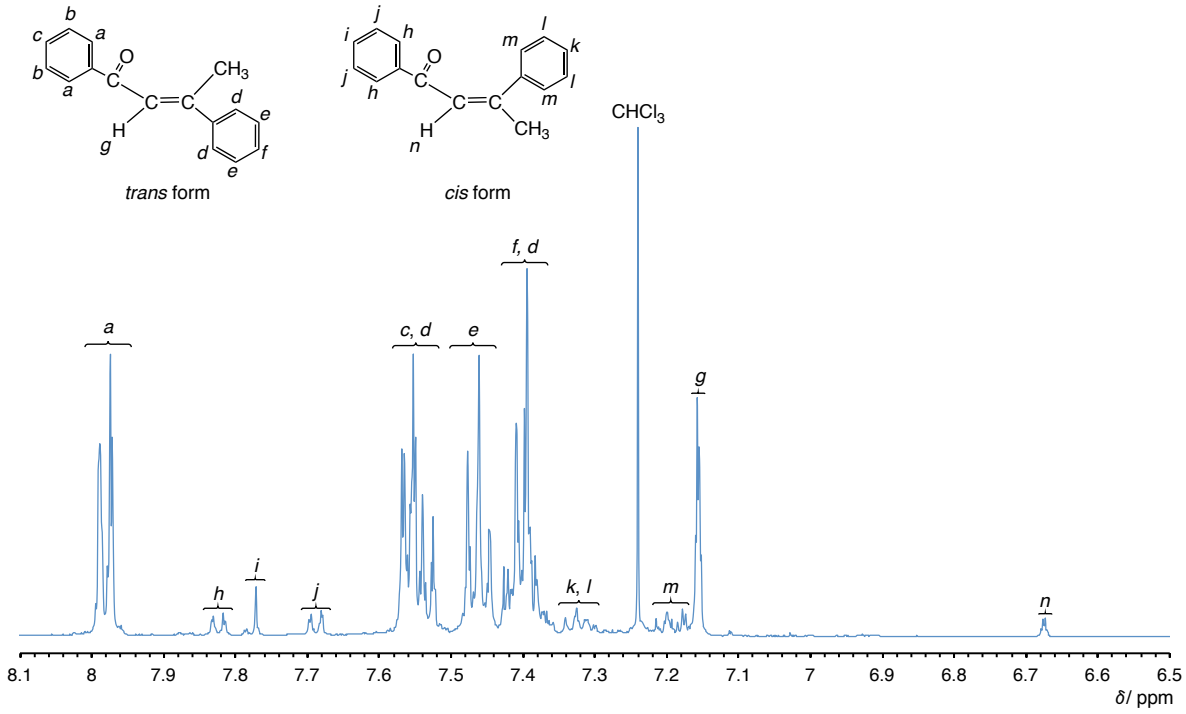


Fig. 4-6 $^1$H NMR spectra of homoaldol condensation product of AP from the $R_F$-$(AMPS)_n$-$R_F$/AP composite in $CDCl_3$

UV-vis spectra of the homoaldol condensation product of AP in methanol can exhibit clear absorption peaks around 294 and 259 nm related to the formation of the expected reaction products, of whose peaks are quit different from that ($\lambda_{max}$: 241 nm) of the original AP (see Fig. 4-5). These two peaks would be due to the formation of the *trans*- and *cis*-homoaldol products, respectively.

$^1$H NMR spectra show that the $R_F$-(AMPS)$_n$-$R_F$/AP composite can give the homoaldol condensation product of AP (see Fig. 4-6). The trans homoaldol product was preferentially obtained, and the product distribution (*trans*/*cis*) was 100/7 based on the $^1$H NMR spectra in Fig. 4-6.

In addition, the reaction products from $R_F$-(AMPS)$_n$-$R_F$/4-acetylbiphenyl (ABP), and /2-acetyl-6-methoxynaphthalne (AMN) composites have been studied by using UV-vis spectra measurement (see Scheme 4-4, Fig. 4-7 and Fig. 4-8).

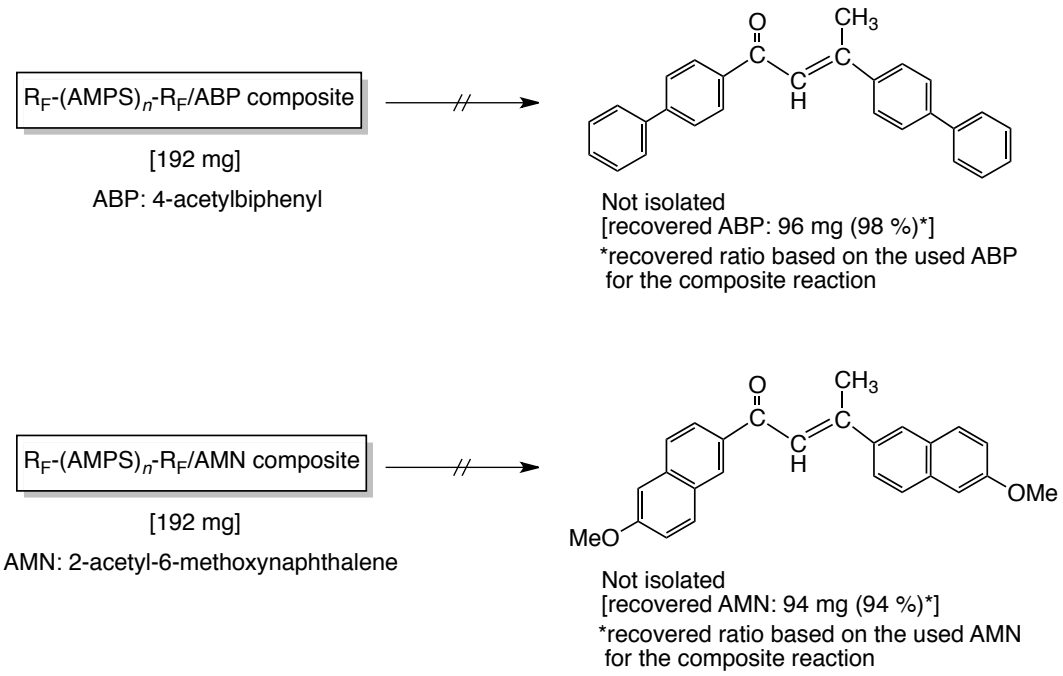


Scheme 4-4 Schemmatic illustration for the homoaldol condensation products of ABP and AMN from $R_F$-(AMPS)$_n$-$R_F$/ABP and /AMN composites.

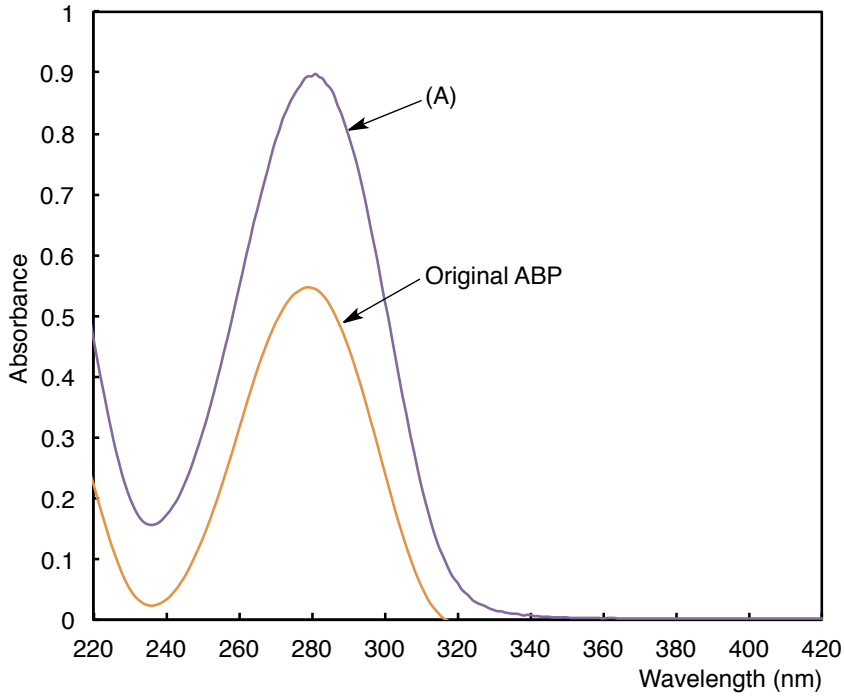


Fig. 4-7 UV-vis spectra of the methanol solutions of the extractive [(A): 10 mgdm$^{-3}$] from the $R_F$-(AMPS)$_n$-$R_F$/ABP composite and the original ABP (33.0 μmoldm$^{-3}$).

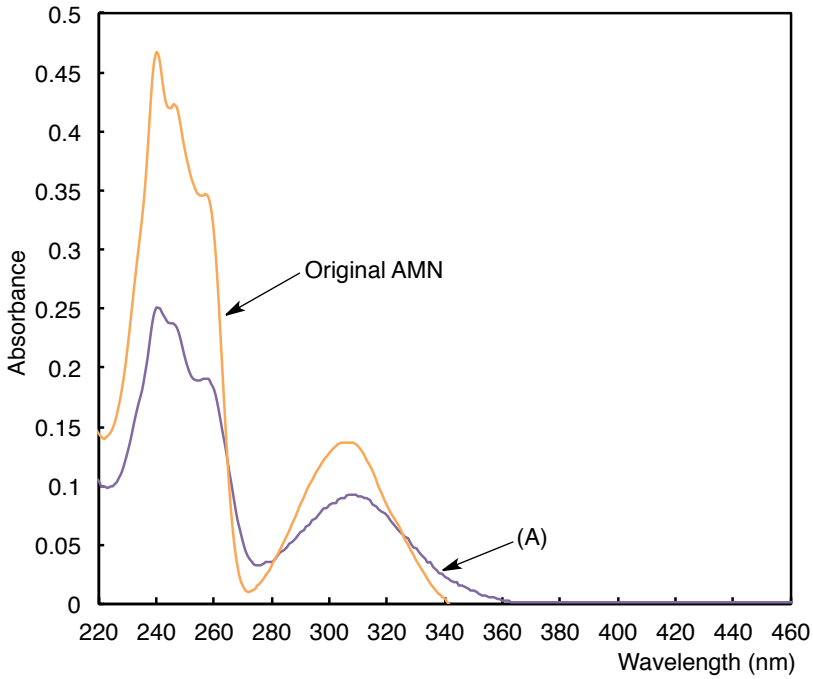


Fig. 4-8 UV-vis spectra of the methanol solutions of the extractive [(A): 1 mgdm$^{-3}$] from the $R_F$-$(AMPS)_n$-$R_F$/AMN composite and the original AMN (33.0 μmoldm$^{-3}$).

As shown in Figs. 4-7 and 4-8, any absorption peaks related to the homoaldol condensation products cannot be detected, and each clear absorption peak corresponding to the recovered starting ketones was observed. The recovered yields of ABP and AMN were 98 and 94 %, respectively (see Scheme 4-4). In addition, $^1$H NMR spectra (data not shown) of the extractives from the aqueous phase exhibited the presence of recovered $R_F$-$(AMPS)_n$-$R_F$ oligomer.

### 4.3.3. Interaction of MAP with -(AMPS)$_n$- oligomer, and sulfuric acid

The homoaldol condensation products of MAP, which are prepared from the corresponding non-fluorinated AMPS oligomer/MAP composite and sulfuric acid/MAP composite, was studied as shown in Scheme 4-5.

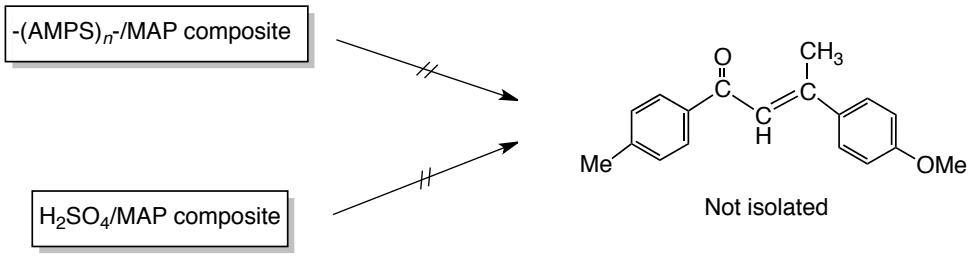


Scheme 4-5 Formation of the homoaldol condensation product of MAP from -(AMPS)$_n$-/MAP composite and $H_2SO_4$/MAP composite [MAP: 4'-methoxyacetophenone].

However, any absorption peaks related to the formation of the homoaldol products of MAP around 327 nm could not be detected at all as illustrated Fig. 4-1, and a clear absorption peak related to the recovered MAP was observed in each case (see Fig. 4-9).

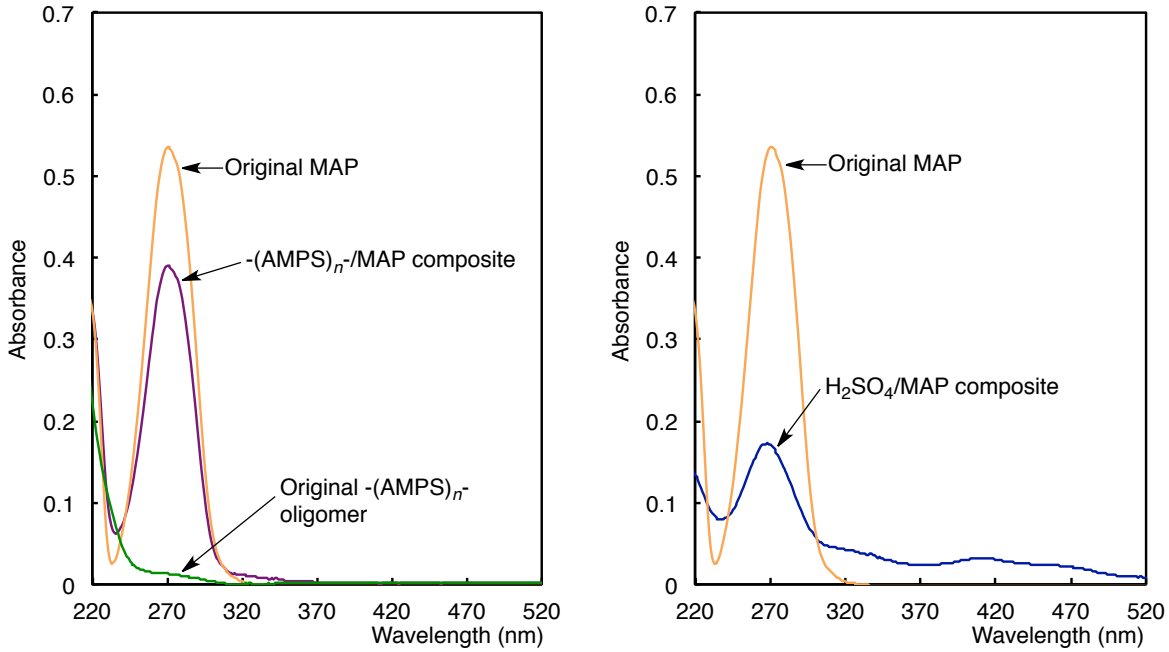


Fig. 4-9 UV-vis spectra of the methanol solutions of -(AMPS)$_n$-/MAP composite (0.01 gdm$^{-3}$), $H_2SO_4$/MAP composite (50 mgdm$^{-3}$), original -(AMPS)$_n$- oligomer (0.01 gdm$^{-3}$), and original MAP (26.4 μmoldm$^{-3}$).

α,β-Unsaturated ketones such as dypnone have been prepared coventionally by the action of Lewis acid catalysts such as aluminum chloride on acetophenone.[42 ~ 44] Recently, there have been some reports on the homoaldol condensation of aromatic ketones such as acetophenone to replace the conventional Lewis acids catalysts with enviromentally friendly solid acid catalysts such as zeolite.[45] However, studies on the homoaldol reactions of aromatic ketones catalyzed by Brønsted acid have been hitherto very limited due to its poor reactivity. In fact, as shown in Scheme 4-5 and Fig. 4-9, sulfuric acid is not a suitable acid catalyst for the homoaldol condensation of MAP. Similarly, non-fluorinated AMPS oligomer was unable to give the expected homoaldol products at all.

The pH values of $H_2SO_4$, the $R_F$-$(AMPS)_n$-$R_F$ oligomer, and the -$(AMPS)_n$- oligomer were measured at 25 °C as followings:

| $H_2SO_4$ | $R_F$-$(AMPS)_n$-$R_F$ | -$(AMPS)_n$- |
|---|---|---|
| 2.28* | 2.86** | 3.21** |

*Concentration of acid catalyst: 4.8 mmoldm$^{-3}$.
**Concentration of oligomer based on monomer unit: 4.8 mmoldm$^{-3}$.

The acidity of -$(AMPS)_n$- oligomer was lower than that of $R_F$-$(AMPS)_n$-$R_F$, indicating that this oligomer could not interact with MAP to give the homoaldol product. Because, the -$(AMPS)_n$- oligomer is unable to provide the corresponding oligomeric aggregate cores to interact with guest molecules due to the absence of terminal fluoroalkyl groups. The present $R_F$-$(AMPS)_n$-$R_F$ oligomer can act as a typical Brønsted acid catalyst for the present homoaldol reaction, and the expected homoaldol products of aromatic ketones such as MAP and AP have been obtained under mild conditions. The acidity of $R_F$-$(AMPS)_n$-$R_F$ oligomer was lower than that of $H_2SO_4$; however, this fluorinated oligomer can afford the homoaldol products, quite different from $H_2SO_4$. This suggests that MAP or AP is likely to interact with the sulfobetaine-type segments [-NH(C=O)$CMe_2CH_2SO_3H$] in gel network cores to produce the homoaldol products.

In this way, it was verified that the specific $R_F$-$(AMPS)_n$-$R_F$ oligomeric gel network cores enable these aromatic ketones to afford the homoaldol condensation products through the effective interaction of these ketones with sulfobetaine-type segments in the fluorinated

oligomer. On the other hand, unexpectedlly, the expected homoaldol products of ABP and AMN cannot be isolated at all as shown in Scheme 4-4, Figs. 4-6 and 4-7, indicating that since such aromatic ketones possess more bulky substituents such as biphenyl and naphthalene units compared to the benzene ring in MAP or AP, these ketones could not be smoothly encapsulated into these fluorinated oligomeric gel network cores to give the expected homoaldol products due to their bulkiness.

## 4.4. Conclusion

Fluoroalkyl end-capped AMPS oligomer [$R_F$-(AMPS)$_n$-$R_F$]/aromatic ketones composites were prepared by heating the mixtures of the corresponding oligomer with ketones in methanol at 80 °C for 3 h. In these composites, $R_F$-(AMPS)$_n$-$R_F$/MAP and /AP composites were found to give the homoaldol condensation products of MAP and AP, respectively. However, $R_F$-(AMPS)$_n$-$R_F$/ABP and /AMN composites could not give the corresponding homoaldol condensation products at all under similar conditions, indicating that these bulky aromatic ketones, compared to MAP or AP, could not be smoothly encapsulated as guest molecules into the fluorinated AMPS oligomeric gel network cores due to their bulkiness. Furthermore, the corresponding non-fluorinted AMPS oligomer [-(AMPS)$_n$-]/MAP and sulfuric acid/MAP composites could not give the homoaldol condensation product of MAP at all under similar conditions. In this way, it was clarified that the fluorinated AMPS oligomeric gel network cores can provide a suitable host moiety to interact with aromatic ketones such as MAP and AP to give the homoaldol condensation products of ketones.

**References**


1) W. R. Dolbier Jr., *J. Fluorine Chem.*, **126**, 157 (2005).

2) J. Scheirs, Ed., "*Modern Fluoropolymers*", Wiley, Chichester (1997).

3) B. Ameduri, *Macromolecules*, **44**, 2394 (2011).

4) K. Johns and G. Stead, *J. Fluorine Chem.*, **104**, 5 (2000).

5) S. Yano, N. Okubo, and K. Takahashi, *Macromol. Symp.*, **108**, 279 (1996).

6) P. Fabbri, M. Messori, M. Montecchi, S. Nannarone, L. Pasquali, F. Pilati, C. Tonelli, and M. Toselli, *Polymer*, **47**, 1055 (2006).

7) B. Ameduri, *Chem. Rev.*, **109**, 6632 (2009).

8) Y.-C. Chen, C.-C. Tsai, and Y.-D. Lee, *J. Polym. Sci. Part A: Polym. Chem.*, **42**, 1789 (2004).

9) T. Imae, *Curr. Opin. Colloid Interface Sci.*, **8**, 307 (2003).

10) K. Johns and G. Stead, *J. Fluorine Chem.*, **104**, 5 (2000).

11) B. Ameduri and B. Boutevin, *J. Fluorine Chem.*, **104**, 53 (2000).

12) B. Ameduri, B. Boutevin, Well-Architectured Fluoropolymers: Synthesis, Properties and Applications; Amsterdam: Elsevier, 231 (2004).

13) J.-F. Berret, D. Calvet, A. Collet, and M. Viguier, *Curr. Opin. Colloid Interface Sci.*, **8**,

296 (2003).

14) T. Imae, H. Tabuchi, K. Funayama, A. Sato, T. Nakamura, and N. Amaya, *Colloid Sufaces A: Physicochem. Eng. Aspects*, **167**, 73 (2000).

15) P. Lebreton, B. Ameduri, B. Boutevin, and J. M. Corpart, *Macromol. Chem. Phys.*, **203**, 522 (2002).

16) M. J. Monteiro, M. M. Adamy, B. J. Leeuwen, A. M. Van Herk, and M. Destarac, *Macromolecules*, **38**, 1538 (2005).

17) A. E. Feiring, E. R. Wonchoba, F. Davdson, V. Percec, and B. Barboiu, *J. Polym. Sci. Part A: Polym. Chem.*, **38**, 3313 (2000).

18) M. Destarac, K. Matyjaszewski, E. Silverman, B. Ameduri, and B. Boutevin, *Macromolecules*, **33**, 4613 (2000).

19) Z. Shi and S. Holdcroft, *Macromolecules*, **38**, 4193 (2005).

20) K. Jankova and S. Hvilsted, *J. Fluorine Chem.*, **126**, 241 (2005).

21) G. Laruelle, E. Nicol, B. Ameduri, J.-F. Tassin, and N. Ajellal, *J. Polym. Sci. Part A: Polym. Chem.*, **49**, 3960 (2011).

22) Y. Patil and B. Ameduri, *Polym. Chem.*, **4**, 2783 (2013).

23) F. Boschet, G. Kostov, B. Ameduri, A. Jackson, and B. Boutevin, *Polym. Chem.*, 3, 217 (2012).

24) H. Sawada, *Chem. Rev.*, **96**, 1779 (1996).

25) H. Sawada and T. Kawase, *Kobunshi Ronbunshu*, **58**, 147 (2001).

26) H. Sawada and T. Kawase, *Kobunshi Ronbunshu*, **58**, 255 (2001).

27) H. Sawada, *J. Fluorine Chem.*, **105**, 219 (2000).

28) H. Sawada, *Prog. Polym. Sci.*, **32**, 509 (2007).

29) H. Sawada, *Polym. Chem.*, **3**, 46 (2012).

30) H. Sawada, S. Katayama, Y. Nakamura, T. Kawase, Y. Hayakawa, and M. Baba, *Polym.*, **39**, 743 (1998).

31) H. Sawada, S. Katayama, A. Ariyoshi, T. Kawase, Y. Hayakawa, T. Tomita, and M. Baba, *J. Mater. Chem.*, **8**, 1517 (1998).

32) M. Mugisawa, K. Ueno, K. Hamazaki, and H. Sawada, *Macromol. Rapid Commun.*, **28**, 733 (2007).

33) M. Mugisawa, K. Ohnishi, and H. Sawada, *Langmuir*, **23**, 5848 (2007).

34) H. Sawada, T. Kijima, and M. Mugisawa, *Polym. J.*, **42**, 494 (2010).

35) M. Mugisawa and H. Sawada, *Langmuir*, **24**, 9215 (2008).

36) T. Kijima, I. Javakhishvili, K. Jankova, S. Hvilsted, S. Kodama, M. Sugiya, and H. Sawada, *Colloid Polym. Sci.*, **290**, 589 (2012).

37) T. Kijima, M. Nishida, H. Fukaya, M. Yoshida, and H. Sawada, *J. Polym. Sci. Part A:*

*Polym. Chem.*, **51**, 2555 (2013).

38) H.Wunscher, G. Haucke, and P. Czerney, *J. Photochem.Photobiol. A: Chemiistry*, **152**, 61 (2002).

39) M. C. Moncada, F. Pina, A. Roque, A. J. Parola, M. Maestri, and V. Balzani, *Eur. J. Org. Chem.*, 304 (2004).

40) A. Roque, C. Lodeiro, F. Pina, M. Maestri, S. Dumas, P. passaniti, and V. Balazani, *J. Am. Chem. Soc.*, **125**, 987 (2003).

41) F. Pina, M. Joao Melo, M. Maestri, P. passaniti, and V. Balazani, *J. Am. Chem. Soc.*, **122**, 4496 (2000).

42) R. C. Elderfield and T. P. King, *J. Am. Chem. Soc.*, **76**, 5437 (1954).

43) N. O. Calloway and L. D. Green, *J. Am. Chem. Soc.*, **59**, 809 (1937).

44) S. Nagahara, L. Kawade, and K. Tomizawa, *J. Technology Education*, **13**, 77 (2006).

45) C. Venkatesan and A. P. Singh, *J. Mol. Catal. A: Chem.*, **181**, 179 (2002).

## Conclusions

The results obtained from this study are summarized as follows.

1. New crosslinked fluoroalkyl end-capped co-oligomeric nanocomposite-encapsulated magnetic nanoparticles, through the deprotecting reactions of corresponding fluorinated co-oligomers containing oxime-blocked segments in the presence of magnetic nanoparticles, were prepared in the nanometer-scale diameters (with diameters in the range of 154 ~ 192 nm). These nanoparticles were found to exhibit good dispersibility in traditional organic solvents. These nanopartilces were applied to the surface modification of poly(methyl methacrylate), resulting in good oleophobicity imparted by the fluorine and magnetic properties arising from the encapsulated magnetic nanoparticles. Fluoroalkyl end-capped 2-acrylamido-2-methylpropanesulfonic acid co-oligomers containing adamantane segments form nanometer-sized controlled fine particles in methanol and can interact with magnetic nanoparticles to form the fluorinated betaine-type co-oligomeric nanocomposite-encapsulated magnetic nanoparticles (with an average particle size of 25 ~ 183 nm). These fluorinated betaine-type nanocomposites-encapsulated magnetic nanoparticles were found to exhibit the lower critical solution temperature (LCST) characteristic in organic media such as *t*-butyl

alcohol, and were able to effectively decrease the LCST through the encapsulation of magnetic nanoparticles in fluorinated co-oligomeric nanoparticle cores. Interestingly, transmission electron microscopy images show that magnetic nanoparticles can be encapsulated inside the crosslinked fluorinated co-oligomeric nanocomposite cores; in contrast, magnetic nanoparticles are adsorbed on the surface of the fluorinated betaine-type co-oligomeric nanocomposite cores.

2. Fluoroalkyl end-capped betaine-type cooligomeric nanocomposites-immobilized palladium nanoparticles were prepared by the reactions of palladium chloride with sodium acetate in the presence of sodium chloride and the corresponding fluorinated cooligomers. Outer blocks of poly(2,3,4,5,6-pentafluorostyrene)-containing ABA-triblock copolymeric nanocomposites-immobilized palladium nanoparticles were also prepared by the use of the corresponding block copolymers under similar conditions. TEM images showed that palladium nanoparticles can be immobilized outside the fluorinated cooligomeric nanocomposite cores; in contrast, palladium nanoparticles can be effectively immobilized inside these fluorinated ABA-triblock copolymeric nanocomposite cores. Thus, these two different fluorinated copolymers were able to afford the controlled immobilization of palladium nanoparticles in the fluorinated nanocomposite cores. These fluorinated

nanocomposites-immobilized palladium nanoparticles were also applied to the catalysts for Suzuki-Miyaura cross-coupling reaction, and the different reactivity between these nanocomposites was observed.

3. A reddish-brown fluoroalkyl end-capped 2-acrylamido-2-methylpropanesulfonic acid (AMPS) oligomer [$R_F$-(AMPS)$_n$-$R_F$]/acetone composite was prepared by heating the white oligomer powder with acetone at 80 °C for 3 h. The color was not observed in the corresponding non-fluorinated AMPS oligomer/acetone composite. The coloring was probably caused by the formation of acetone polyaldol condensation products in the fluorinated oligomeric gel network cores. The colored $R_F$-(AMPS)$_n$-$R_F$/acetone composite powders were stable and did not exhibit any color change after 2 years in natural light at room temperature. The colored composite powders dissolved in methanol to give a reddish-brown solution at room temperature. However, the retro-polyaldol condensation decolored the solution after 1 day at room temperature. This is the first example of the retro-aldol polycondensation of acetone under mild conditions. The decoloration increased by between 38- and 70-fold under UV irradiation, compared with that in dark conditions. The coloring–decoloring behavior was consistent and repeatable; therefore our fluorinated oligomer/acetone composites are promising candidates for new fluorinated coloring materials.

4. Aromatic ketones such as 4'-methoxyacetophenone (MAP), acetophenone (AP), 4-acetylbiphenyl (ABP) and 2-acetyl-6-methoxynaphthalne (AMN) interacted with fluoroalkyl end-capped 2-acrylamido-2-methylpropanesulfonic acid oligomer [$R_F$-$(AMPS)_n$-$R_F$] at 80 °C for 3 h to give the corresponding fluorinated oligomer/aromatic ketones composites. In these composites, the $R_F$-$(AMPS)_n$-$R_F$/MAP and /AP composites were found to give the homoaldol condensation products of MAP and AP, respectively. In contrast, the corresponding non-fluorinated AMPS oligomer/MAP and sulfuric acid/MAP composites could not give the homoaldol products at all under similar conditions. This suggested that the $R_F$-$(AMPS)_n$-$R_F$ oligomer could provide the suitable fluorinated oligomeric gel network cores to interact with MAP or AP as a guest molecule, and the homoaldol condensation of encapsulated MAP and AP should procced smoothly in the fluorinated oligomeric gel network cores. The $R_F$-$(AMPS)_n$-$R_F$/ABP and /AMN composites could not give the homoaldol products at all under similar conditions, indicating that the more bulky aromatic ketones than MAP or AP are not likely to be encapsulated as guest molecules into the fluorinated AMPS oligomeric gel network cores.

**Publications**

1) H. Sawada, T. Kijima, and M. Mugisawa, "Selective Preparation of Novel Fluoroalkyl End-capped Co-oligomeric Nanocomposite-encapsulated Magnetites and Magnetite-adsorbing Co-oligomeric Nanoparticles", *Polym. J.*, **42**, 494 ~ 500 (2010).

2) T. Kijima, I. Javakhishvili, K. Jankova, S. Hvilsted, S. Kodama, M. Sugiya, and H. Sawada, "Controlled Immobilization of Palladium Nanoparticles in Two Different Fluorinated Polymeric Aggregate Cores and Their Application in Catalysis", *Colloid Polym. Sci.*, **290**, 589 ~ 597 (2012).

3) T. Kijima, M. Nishida, H. Fukaya, M. Yoshida, and H. Sawada, "Coloring-Decoloring Behavior of Fluoroalkyl End-Capped 2-Acrylamido-2-methylpropanesulfonic Acid Oligomer/Acetone Composite in Methanol", *J. Polym. Sci. Part A: Polym. Chem.*, **51**, 2555 ~ 2564 (2013).

4) T. Kijima, M. Nishida, H. Fukaya, M. Yoshida, and H. Sawada, " Homoaldol Condensation of Aromatic Ketones in Fluoroalkyl End-Capped 2-Acrylamido-2-methylpropanesulfonic Acid

Oligomeric Gel Network Cores ", *Polym. Adv. Technol.*, DOI: 10.1002/pat.3229.

(not described in this thesis)

5) H. Sawada, T. Tsuzuki-ishi, T. Kijima, J. Kawakami, M. Iizuka, and M. Yoshida, "Controlling Photochromism between Fluoroalkyl End-Capped Oligomer/Polyaniline and /*N*,*N'*-diphenyl-1,4-phenylenediamine Nanocomposites Induced by UV-Light-Responsive Titanium Oxide Nanoparticles", *J. Colloid Interface Sci.*, **359**, 461 ~ 466 (2011).

6) H. Sawada, T. Tsuzuki-ishi, T. Kijima, M. Iizuka, and M. Yoshida, "Preparation of Novel Fluoroalkyl End-Capped Oligomers/Polyaniline and /*N*,*N*'-diphenyl-1,4-phenylenediamine Nanocomposites", *Colloid Polym. Sci.*, **289**, 1103 ~ 1110 (2011).

**Acknowledgements**

The author would like to express his sincerest gratitude to Professor Hideo Sawada for his inspired supervision and valuable discussions.

He deeply thanks to Prof. Atsushi Yoshizawa, Prof. Masaaki Okazaki, Prof. Isoshi Nukatsuka and Prof. Toshiyuki Abe for their kind advice and discussions. He also deeply thanks to Prof. Katja Jankova on Technical University of Denmark, Mr. Shun Kodama and Dr. Masashi Sugiya on Nippon Chemical Industrial Co., Ltd., Dr. Masakazu Nishida and Dr. Haruhiko Fukaya on National Institution of Advanced Industrial Science and Technology, Prof. Masato Yoshida on Shimane University for their kind advice and discussions, respectively. He wishes to extend his thanks to all students of a laboratory for their cooperation and great advice.

Finally, he would like to specially thank to his parents and sister.